

Timelike and gravitational anomalous entanglement from the inner horizon

Qiang Wen^{1*}, Mingshuai Xu^{1◦} and Haocheng Zhong^{1†}

¹ Shing-Tung Yau Center and School of Physics, Southeast University, Nanjing 210096, China

* wenqiang@seu.edu.cn, ◦ xumingshuai@seu.edu.cn, † zhonghaocheng@outlook.com

Abstract

In the context of the $\text{AdS}_3/\text{CFT}_2$, the boundary causal development and the entanglement wedge of any boundary spacelike interval can be mapped to a thermal CFT_2 and a Rindler AdS_3 respectively via certain boundary and bulk Rindler transformations. Nevertheless, the Rindler mapping is not confined in the entanglement wedges. While the outer horizon of the Rindler AdS_3 is mapped to the RT surface, we also identify the pre-image of the inner horizon in the original AdS_3 , which we call the inner RT surface. In this paper we give some new physical interpretation for the inner RT surface. Firstly, the inner RT surface breaks into two pieces which anchor on the two tips of the causal development. Furthermore, we can take the two tips as the end points of a certain timelike interval and the inner RT surface is exactly the spacelike geodesic that represents the real part of the so-called holographic timelike entanglement entropy (HTEE). We also identify a timelike geodesic at boundary of the extended entanglement wedge, which represents the imaginary part of the HTEE. Secondly, in the duality between the topologically massive gravity (TMG) and gravitational anomalous CFT_2 , the entanglement entropy and the mixed state correlation that is dual to the entanglement wedge cross-section (EWCS) receive correction from the Chern-Simons term in the TMG. We find that, the correction to the holographic entanglement entropy can be reproduced by the area of the inner RT surface with a proper regulation, while the mixed state correlation can be represented by the saddle geodesic chord connecting with the two pieces of the inner RT surface of the mixed state we consider, which we call the inner EWCS. The equivalence between the twist on the RT surface and the length of inner RT surface is also discussed.

Contents

1	Introduction	2
2	Timelike entanglement entropy from the inner horizon	5
2.1	A brief introduction to the Rindler method in $\text{AdS}_3/\text{CFT}_2$	5
2.2	Pre-image of the inner horizon	8
3	Partial entanglement entropy, modular slice and entanglement wedge	11
3.1	Partial entanglement entropy	11
3.2	Modular slice, entanglement wedge and holographic PEE	12
3.2.1	Modular Hamiltonian slice	12
3.2.2	Modular momentum slice	16

4	Topological massive gravity and holographic entanglement entropy with gravitational anomaly	21
4.1	CFT ₂ with gravitational anomaly and topological massive gravity	21
4.2	Bulk description with gravitational anomaly	23
4.3	Gravitational anomalous entanglement from the inner RT surface	24
5	BPE and EWCS with gravitational anomaly	25
5.1	A brief introduction to the BPE with gravitational anomaly	25
5.2	A case study of non-adjacent intervals	28
5.2.1	BPE ⁿ (A, B) and the EWCS	28
5.2.2	BPE ^a (A, B) and the inner EWCS	30
6	Reproducing the twist description from the partner geodesic chord on the IRT surfaces	32
7	Summary and discussions	35
A	The IRT surface in the global AdS₃	37
B	Spacelike and null geodesics in the Poincaré AdS₃	39
C	A trick for locating the partner point \widehat{H} on $\widehat{\mathcal{E}}$	41
D	Replica trick for the CFT₂ with gravitational anomaly	42
E	The regulated geodesic chord on the inner RT surface and its flat limit	42
F	The equality between the two sides of (120)	46
	References	47

1 Introduction

It has long been known that, black holes in classical gravity satisfy thermodynamic laws and the area of the outer horizon A plays the role of the black hole entropy [1–3], which is called the Bekenstein-Hawking entropy,

$$S_{BH} = \frac{\text{Area}(A)}{4G}. \quad (1)$$

Since then, understanding the microscopic origin of the black hole entropy is believed to be an important window to explore the quantum theory of gravity, and many fruitful steps have been taken towards this task, see [4–6] for an incomplete list.

In the context of the AdS/CFT [7–9], the Bekenstein-Hawking formula is generalized to the Ryu-Takayanagi (RT) formula [10–12] for the entanglement entropy of regions in the dual boundary field theory. More explicitly, consider a static region \mathcal{A} in the boundary CFT, the RT formula gives a holographic formula for the entanglement entropy $S_{\mathcal{A}}$,

$$S_{\mathcal{A}} = \frac{\text{Area}(\mathcal{E})}{4G} \quad (2)$$

where \mathcal{E} is the (minimal) extremal surface in the AdS bulk homologous to the boundary region \mathcal{A} . At first, the RT formula was understood for the static spherical regions on the AdS boundary [13], where we can find a Rindler transformation that maps the entanglement wedge $\mathcal{W}_{\mathcal{A}}$ to a Rindler $\widetilde{\text{AdS}}_3$ black hole, then the entanglement entropy equals to the thermal entropy of the Rindler black hole that is captured by the outer horizon of the Rindler black hole [13]¹. Later, the general case of the RT formula was proved by the Lewkowycz-Maldacena prescription [17], which directly computes the holographic entanglement entropy by applying the replica trick in the gravity side.

Essentially, both the Bekenstein-Hawking and the RT formula are quantum information interpretations for the outer horizon of the black holes, while the analogous aspects associated to the inner horizon are much less understood. So far it is not clear which type of micro-states the inner horizon counts. Nevertheless, there have been observations that strongly indicate that the inner horizon has quantum information interpretation which deserves further investigation:

- It has been observed that the variation of the area of the inner horizon also satisfies a “first law” of thermodynamics for a large class of black holes² [18–20].
- It appears that the product of the inner and outer horizon areas only depend on the quantized charges and is independent of the mass of the black hole [18, 21–25].
- In the topological massive gravity [26, 27], the entropy of AdS black holes receives a correction from the Chern-Simons term, which is proportional to the area of the inner horizon [28–31].
- More importantly, in the flat limit of the non-extremal BTZ black holes, the outer horizon is pushed to infinity, hence only the inner horizon is left in the bulk, which is called the flat cosmological horizon. In this configuration the asymptotic symmetries are governed by the 3d Bondi-Metzner-Sachs (BMS₃) group and the correspondence between the 3d asymptotic flat spacetime and the BMS symmetric field theory (flat₃/BMSFT) was proposed [32, 33]. In this context the thermal entropy of the BMS field theory can be calculated by a Cardy-like formula and it matches to the area of the flat cosmological horizon [34, 35]. Also, the analogue of the RT formula in this holography has been derived [16] (see also [36]) which introduces two novel null geodesics for the geometric picture of the holographic entanglement entropy.

In this paper we will mainly discuss the inner horizon in the Rindler $\widetilde{\text{AdS}}_3$. The core of the Rindler method is the construction of the Rindler transformations that map the causal development $\mathcal{D}_{\mathcal{A}}$ of a boundary subregion \mathcal{A} to a boundaryless thermal Rindler space. Since the Rindler transformations are the symmetry transformations of the boundary QFT, the entanglement entropy of \mathcal{A} equals to the thermal entropy of the Rindler space. In holography, these Rindler transformations can be extended into the AdS bulk, which maps the entanglement wedge $\mathcal{W}_{\mathcal{A}}$ of \mathcal{A} to a Rindler $\widetilde{\text{AdS}}_3$. In this case, the Bekenstein-Hawking entropy, given by the area of the outer horizon of the Rindler $\widetilde{\text{AdS}}_3$, gives the entanglement entropy $S_{\mathcal{A}}$. Also we can read the modular flow from the Rindler transformations, which is a geometric flow generated by the modular Hamiltonian and is very useful in our discussions.

As we know that, the inverse Rindler transformations exactly map the outer horizon of the Rindler $\widetilde{\text{AdS}}_3$ to the RT surface $\mathcal{E}_{\mathcal{A}}$ in the original AdS spacetime. Then it is very interesting to ask what is the image of the inner horizon in the original AdS spacetime. For any spacelike

¹This is called the Rindler method to compute the holographic entanglement entropy, see also [14–16] for further progress on the Rindler method applied to holography beyond AdS/CFT.

²Such a “first law” for the inner horizons has negative energy or temperature.

interval \mathcal{A} , there is a unique timelike interval $\widehat{\mathcal{A}}$ that connects the two tips of $\mathcal{D}_{\mathcal{A}}$. Recently, the holographic entanglement entropy associated with timelike intervals has been studied in [37, 38]. The geometric picture includes two spacelike geodesics anchored on the endpoints of the timelike interval whose length makes the real part of the holographic timelike entanglement entropy, while the imaginary part is given by the length of a timelike geodesic connects the spacelike one at the null infinities. We identify the image of the Rindler inner horizon in the original AdS spacetime, and show that it coincides with the spacelike geodesics in the geometric picture of the holographic timelike entanglement entropy for $\widehat{\mathcal{A}}$. We also find the timelike geodesic that represents the geometric picture of the imaginary part is the boundary of the extended entanglement wedge, which is mapped to the exterior of the inner horizon in the Rindler $\widetilde{\text{AdS}}_3$.

Considering the correction to holographic entanglement entropy due to higher-order curvature terms in the bulk is also interesting. Two typical higher order corrections to the Hilbert-Einstein action are Gauss-Bonnet term [39] and Chern-Simons term [26, 27]. In this paper, we mainly focus on the Chern-Simons term, which is the low energy effective action of string theory. The Chern-Simons term, which explicitly depends on the connection, is not manifestly diffeomorphism invariant (up to a boundary term). This leads to unequal central charges c_L and c_R in the dual conformal field theory. Such a theory is called the conformal field theory with gravitational anomaly. In [40], the authors give a bulk description of the holographic entanglement entropy with gravitational anomaly, which is a spinning particle with a worldline action. However, the worldline action is not a pure geometric quantity, which is the main motivation of this work.

The paper is organized as follows. In Sec.2, we give a brief introduction of the Rindler method and give the explicit Rindler mapping. Then we identify the pre-image of the inner horizon in the original AdS_3 , which we call the inner RT (IRT) surface. In Sec.3 we briefly introduce the partial entanglement entropy (PEE) and the slicing structure of the entanglement wedge and extended entanglement wedge. Based on the fine structure we established the partnership between the points in the causal development and the points on the RT and the inner RT surfaces, based on which we further establish the duality between the PEE (or timelike PEE) and the geodesic chords on the RT (or inner RT) surfaces. In Sec.4, in the context of the correspondence between the topological massive gravity (TMG) and the gravitational anomalous CFT_2 , we give the bulk geometric description of the holographic entanglement entropy, which is the length of a geodesic chord on the IRT surface. This result is consistent with the one obtained by measuring the “twist” of the RT surface introduced in [40]. In Sec.5, we give the geometric picture for the gravitational anomalous correction to the balanced partial entanglement entropy (BPE), which was proposed to be the mixed state correlation dual to the EWCS. The geometric picture is just the saddle geodesic connecting the two pieces of the IRT surface of the mixed state region, and gives the same result as the one obtained by measuring the twist of the EWCS [41]. In Sec.6, we construct the PEE in the twist description based on the fine structure, and the result is consistent with the length of the partner geodesic chord on the IRT surface. We summarize our results and give discussion in the last section. In the appendix, we give details of some calculations and the comparison between our geometric description and the swing surface prescription [16, 42, 43] when taking the flat limit.

Through out this paper, we will put a tilde sign on the top of all the quantities in the Rindler $\widetilde{\text{AdS}}_3$, and put a hat sign on the top of all the quantities associated to the inner RT surface.

2 Timelike entanglement entropy from the inner horizon

2.1 A brief introduction to the Rindler method in AdS₃/CFT₂

The key point of the Rindler method is to construct a Rindler transformation, which maps the entanglement entropy to the thermal entropy by a symmetry transformation, such that the calculation of the entanglement entropy is equivalent to calculating the corresponding thermal entropy. Comparing with the entanglement entropy, the calculation of thermal entropy which we already have tools to evaluate is much easier. For example, the Cardy formula [44, 45] for the field theory side, and the Bekenstein-Hawking formula for the gravity side. The general strategy to construct a Rindler transformation by the symmetries of the boundary field theory and its bulk extension by holographic dictionary is summarized in Sec.2 of [16]. Here we only list some key points of the Rindler method applied to the AdS₃/CFT₂ correspondence. Firstly, we consider a spatial interval \mathcal{A} in the vacuum CFT₂ on the plane,

$$\mathcal{A} : (-l_U/2, -l_V/2) \rightarrow (l_U/2, l_V/2), \quad (l_U, l_V > 0), \quad (3)$$

where U and V are the light-cone coordinates,

$$U = \frac{x+t}{2}, \quad V = \frac{x-t}{2}. \quad (4)$$

In this paper, we set the AdS radius $\ell = 1$. The vacuum CFT₂ on the plane is dual to the Poincaré AdS₃ with the metric given by³,

$$ds^2 = 2\rho dUdV + \frac{d\rho^2}{4\rho^2}, \quad (7)$$

The causal development $\mathcal{D}_{\mathcal{A}}$ of the interval \mathcal{A} is a diamond shape region,

$$\mathcal{D}_{\mathcal{A}} = \left\{ (U, V) \mid -\frac{l_U}{2} < U < \frac{l_U}{2}, -\frac{l_V}{2} < V < \frac{l_V}{2} \right\}. \quad (8)$$

The bulk Rindler transformation maps the Poincaré AdS₃ (7) to a Rindler $\widetilde{\text{AdS}}_3$,

$$ds^2 = T_{\tilde{U}}^2 d\tilde{U}^2 + 2\tilde{\rho} d\tilde{U}d\tilde{V} + T_{\tilde{V}}^2 d\tilde{V}^2 + \frac{d\tilde{\rho}^2}{4(\tilde{\rho}^2 - T_{\tilde{U}}^2 T_{\tilde{V}}^2)}, \quad (9)$$

and the explicit transformation is given by [16, 46],

$$\begin{aligned} \tilde{U} &= \frac{1}{4T_{\tilde{U}}} \log \left[\frac{(2 - (l_U + 2U)(l_V - 2V)\rho)(2 + (l_U + 2U)(l_V + 2V)\rho)}{(2 - (l_U - 2U)(l_V + 2V)\rho)(2 + (l_U - 2U)(l_V - 2V)\rho)} \right], \\ \tilde{V} &= \frac{1}{4T_{\tilde{V}}} \log \left[\frac{(2 - (l_V + 2V)(l_U - 2U)\rho)(2 + (l_V + 2V)(l_U + 2U)\rho)}{(2 - (l_V - 2V)(l_U + 2U)\rho)(2 + (l_V - 2V)(l_U - 2U)\rho)} \right], \\ \tilde{\rho} &= \frac{T_{\tilde{U}} T_{\tilde{V}} (4 + 16UV\rho + (l_U^2 - 4U^2)(l_V^2 - 4V^2)\rho^2)}{4\rho l_U l_V}. \end{aligned} \quad (10)$$

³Under the following coordinate transformation,

$$U = \frac{x+t}{2}, \quad V = \frac{x-t}{2}, \quad \rho = \frac{2}{z^2} \quad (5)$$

the metric (7) can be rewritten in the Poincaré coordinate,

$$ds^2 = \frac{-dt^2 + dx^2 + dz^2}{z^2}. \quad (6)$$

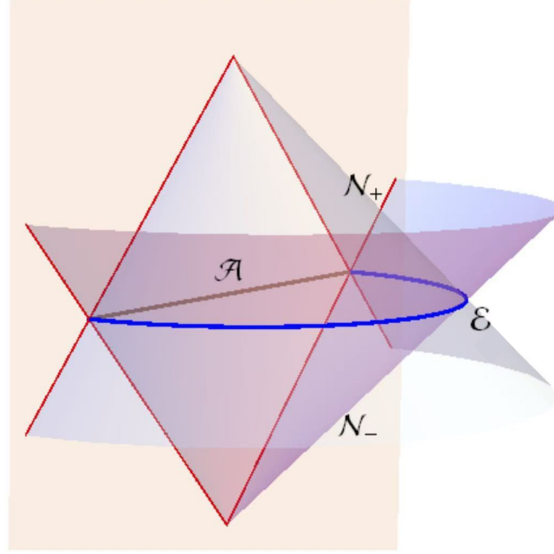


Figure 1: The figure is extracted from [46]. The pink surfaces represent the null hypersurfaces \mathcal{N}_\pm , and the blue curve represents the RT surface \mathcal{E} .

where $T_{\tilde{U}}$ and $T_{\tilde{V}}$ are the parameters characterizing the size of a thermal circle of the outer horizon,

$$\text{outer horizon: } (\tilde{U}, \tilde{V}) \sim (\tilde{U} + i\frac{\pi}{T_{\tilde{U}}}, \tilde{V} - i\frac{\pi}{T_{\tilde{V}}}), \quad (11)$$

The bulk Rindler transformation (10) reduces to the boundary Rindler transformation at the asymptotic boundary $\rho \rightarrow \infty$,

$$\tilde{U} = \frac{\beta_{\tilde{U}}}{\pi} \operatorname{arctanh}\left(\frac{2U}{l_U}\right), \quad \tilde{V} = \frac{\beta_{\tilde{V}}}{\pi} \operatorname{arctanh}\left(\frac{2V}{l_V}\right), \quad (12)$$

where $\beta_{\tilde{U}} = \pi/T_{\tilde{U}}$ and $\beta_{\tilde{V}} = \pi/T_{\tilde{V}}$. Similarly, the boundary Rindler transformation maps the vacuum CFT_2 on the plane to a thermal CFT_2 . Following the logic of the Rindler method, the entanglement entropy of the interval \mathcal{A} (3) is mapped to the thermal entropy of the thermal CFT_2 , which can be evaluated holographically. According to the bulk Rindler transformation (10), the outer horizon $\tilde{\rho} = T_{\tilde{U}}T_{\tilde{V}}$ of Rindler AdS_3 is mapped from two null hypersurfaces \mathcal{N}_\pm in the original AdS_3 space,

$$\mathcal{N}_+ : \rho = \frac{2}{(l_U + 2U)(l_V - 2V)}, \quad \mathcal{N}_- : \rho = \frac{2}{(l_U - 2U)(l_V + 2V)}, \quad (13)$$

whose intersection is precisely the RT surface \mathcal{E} ,

$$\mathcal{E} : \rho = \frac{2l_V}{l_U(l_V^2 - 4V^2)}, \quad U = \frac{l_U}{l_V}V. \quad (14)$$

See Fig.1 for an illustration. The length parameter τ of the RT surface \mathcal{E} is given by,

$$\tau(V) = \operatorname{arctanh}\left(\frac{2V}{l_V}\right), \quad (15)$$

where we set the center point of \mathcal{E} to be the origin for the length parameter. The entanglement wedge $\mathcal{W}_{\mathcal{A}}$ [47] is the bulk region enclosed by $\mathcal{D}_{\mathcal{A}}$ and \mathcal{N}_\pm , which is mapped to the exterior

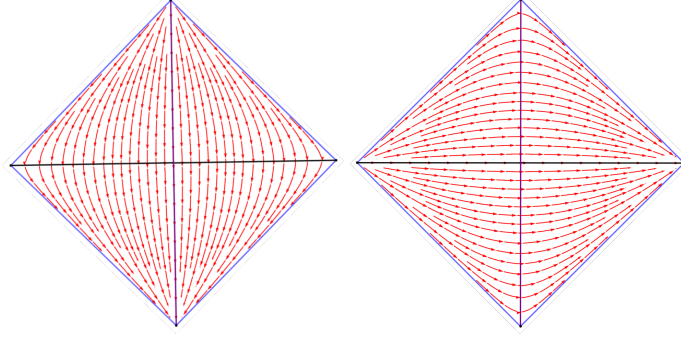


Figure 2: The left and the right figures show the modular flow lines of k_t^α and k_t^β in the causal development $\mathcal{D}_{\mathcal{A}}$, respectively. The black line represent the interval \mathcal{A} , and the purple line represent its partner interval $\widehat{\mathcal{A}}$.

of the outer horizon of Rindler $\widetilde{\text{AdS}}_3$ (9) under the bulk Rindler transformation⁴. Therefore, the thermal entropy of the boundary thermal CFT₂ equals to the Bekenstein-Hawking entropy of the outer horizon in Rindler $\widetilde{\text{AdS}}_3$ space. Now we denote the image of boundary interval \mathcal{A} (3) under the Rindler transformation (12) as $\tilde{\mathcal{A}}$. Due to the divergence of the entanglement entropy, we need to introduce cutoffs to regulate the interval \mathcal{A} ,

$$\mathcal{A}^{\text{reg}} : (-l_U/2 + \epsilon_U, -l_V/2 + \epsilon_V) \rightarrow (l_U/2 - \epsilon_U, l_V/2 - \epsilon_V). \quad (16)$$

Here, ϵ_U and ϵ_V are two infinitesimal constants of the same order⁵. After performing the Rindler transformation (12), the image of this regularized interval \mathcal{A}^{reg} is,

$$\begin{aligned} \tilde{\mathcal{A}}^{\text{reg}} : (-\Delta\tilde{U}/2, -\Delta\tilde{V}/2) &\rightarrow (\Delta\tilde{U}/2, \Delta\tilde{V}/2) \\ \Delta\tilde{U} = \frac{1}{T_{\tilde{U}}} \log\left(\frac{l_U}{\epsilon_U}\right), \quad \Delta\tilde{V} = \frac{1}{T_{\tilde{V}}} \log\left(\frac{l_V}{\epsilon_V}\right). \end{aligned} \quad (17)$$

The proper length on the outer horizon in the Rindler $\widetilde{\text{AdS}}_3$ is $ds^2 = (T_{\tilde{U}}d\tilde{U} + T_{\tilde{V}}d\tilde{V})^2$. Integration along the proper length gives the length of the outer horizon,

$$\ell_{\text{outer horizon}} = T_{\tilde{U}}\Delta\tilde{U} + T_{\tilde{V}}\Delta\tilde{V} = \log\left(\frac{l_U l_V}{\epsilon_U \epsilon_V}\right), \quad (18)$$

Therefore, the holographic entanglement entropy of the interval \mathcal{A} is given by,

$$S_{\mathcal{A}} = \frac{1}{4G} \log\left(\frac{l_U l_V}{\epsilon_U \epsilon_V}\right), \quad (19)$$

which exactly matches the result evaluated by the RT formula [10–12]. On the other hand, a useful byproduct of the Rindler method is the modular flow that manifests the replica symmetry. More explicitly, the Rindler transformation $\tilde{x} = f(x)$ is invariant under imaginary identification of the Rindler coordinates $\tilde{x}^i \sim \tilde{x}^i + i\beta_{\tilde{x}^i}$, which can be referred to as the thermal circle in the Rindler space. With the thermal circle, the modular flow k_t along the thermal circle in the Rindler space can be rewritten as $k_t = \beta_{\tilde{x}^i} \partial_{\tilde{x}^i}$. For example, for the thermal circle of the outer horizon (11), the corresponding bulk modular flow, which is also called the bulk modular Hamiltonian flow, is given by,

$$\begin{aligned} k_t^{\alpha, \text{bulk}} &= \beta_{\tilde{U}} \partial_{\tilde{U}} - \beta_{\tilde{V}} \partial_{\tilde{V}} \\ &= \frac{\pi}{2} \left(l_U - \frac{4U^2}{l_U} - \frac{2}{l_V \rho} \right) \partial_U - \frac{\pi}{2} \left(l_V - \frac{4V^2}{l_V} - \frac{2}{l_U \rho} \right) \partial_V + 4\pi \left(\frac{U}{l_U} - \frac{V}{l_V} \right) \rho \partial_\rho. \end{aligned} \quad (20)$$

⁴This can be seen clearly in Sec.3.2, where we introduce the concept of modular slice.

⁵The symbols ϵ_U, ϵ_V in this paper all represent two infinitesimal constants of the same order.

where the negative sign in the first line comes from the negative sign in the thermal circle (11). The superscript α is used to distinguish it from a new bulk modular flow $k_t^{\beta, \text{bulk}}$, which we propose in the next subsection. Interestingly, the null hypersurfaces \mathcal{N}_\pm , which are mapped to the outer horizon in Rindler $\widetilde{\text{AdS}}_3$, is just the Killing horizon of the bulk modular Hamiltonian flow $k_t^{\alpha, \text{bulk}}$. Furthermore, the RT surface \mathcal{E} is precisely the fixed points of $k_t^{\alpha, \text{bulk}}$ (or the bulk replica symmetry),

$$k_t^{\alpha, \text{bulk}}|_{\mathcal{E}} = 0. \quad (21)$$

Asymptotically, we have the boundary modular flow k_t^α ,

$$k_t^\alpha = \left(\frac{\pi l_U}{2} - \frac{2\pi U^2}{l_U} \right) \partial_U - \left(\frac{\pi l_V}{2} - \frac{2\pi V^2}{l_V} \right) \partial_V, \quad (22)$$

See the left figure of Fig.2 for the boundary modular Hamiltonian flow lines generated by k_t^α . In fact, we can also define the temporal and the spatial coordinates in the Rindler $\widetilde{\text{AdS}}_3$,

$$\begin{aligned} \text{Rindler time: } \tilde{t} &:= \pi \left(\frac{\tilde{U}}{\beta_{\tilde{U}}} - \frac{\tilde{V}}{\beta_{\tilde{V}}} \right) = \frac{1}{4} \log \left(\frac{((l_U + 2U)(l_V - 2V)\rho - 2)^2}{((l_U - 2U)(l_V + 2V)\rho - 2)^2} \right), \\ \text{Rindler space: } \tilde{x} &:= \pi \left(\frac{\tilde{U}}{\beta_{\tilde{U}}} + \frac{\tilde{V}}{\beta_{\tilde{V}}} \right) = \frac{1}{4} \log \left(\frac{((l_U + 2U)(l_V + 2V)\rho + 2)^2}{((l_U - 2U)(l_V - 2V)\rho + 2)^2} \right). \end{aligned} \quad (23)$$

where we have used the bulk Rindler transformation (10). In this Rindler coordinate system (\tilde{t}, \tilde{x}) , the thermal circle of the outer horizon (11) is just $\tilde{t} \sim \tilde{t} + 2\pi i$, and the modular Hamiltonian flow $k_t^{\alpha, \text{bulk}}$ can be rewritten as,

$$k_t^{\alpha, \text{bulk}} = 2\pi \partial_{\tilde{t}}. \quad (24)$$

In other words, the modular Hamiltonian flow $k_t^{\alpha, \text{bulk}}$ is precisely the generator of the time translation in the Rindler $\widetilde{\text{AdS}}_3$, which is also why it is called the modular Hamiltonian flow, whose modular flow lines are just the Rindler temporal coordinate lines when mapped to the Rindler $\widetilde{\text{AdS}}_3$.

2.2 Pre-image of the inner horizon

In the last subsection, we indicated that the outer horizon $\tilde{\rho} = T_{\tilde{U}} T_{\tilde{V}}$ in the Rindler $\widetilde{\text{AdS}}_3$ is mapped from the null hypersurfaces \mathcal{N}_\pm (13), whose intersection line is the RT surface \mathcal{E} (14). Furthermore, the region outside the outer horizon in the Rindler $\widetilde{\text{AdS}}_3$ is mapped from the entanglement wedge $\mathcal{W}_{\mathcal{A}}$ in the original Poincaré AdS_3 . Since the bulk Rindler transformation is not confined within the entanglement wedge⁶, and there are indeed two horizons, it is also interesting to study the properties of the inner horizon. For example, what is the physical significance of the pre-image of the inner horizon in the original Poincaré AdS_3 , and can we construct another modular flow associated with the inner horizon? In this subsection, we aim to answer these two questions.

Firstly, there is another thermal circle for the inner horizon $\tilde{\rho} = -T_{\tilde{U}} T_{\tilde{V}}$,

$$\text{inner horizon: } (\tilde{U}, \tilde{V}) \sim \left(\tilde{U} + i \frac{\pi}{T_{\tilde{U}}}, \tilde{V} + i \frac{\pi}{T_{\tilde{V}}} \right), \quad (25)$$

⁶We will return to this point in Sec.3.2.2.

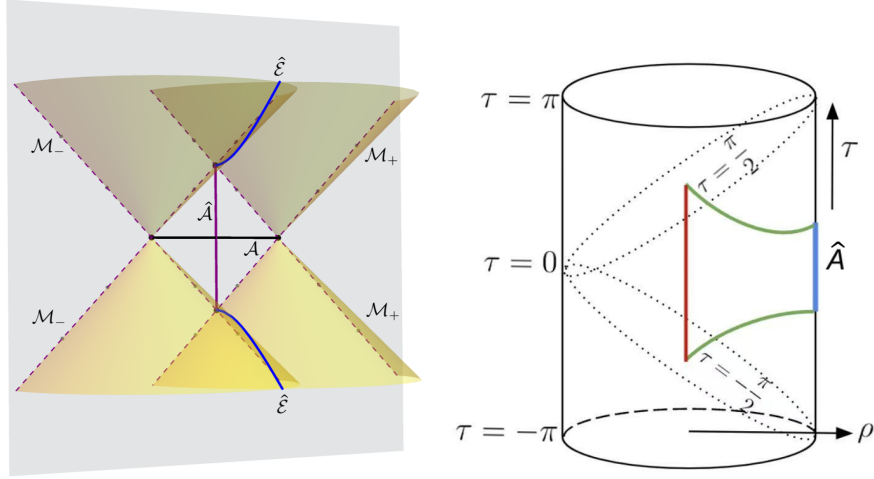


Figure 3: The right figure is extracted from [37]. The left figure: the blue curve is the IRT surface that is the intersection line between the two null hypersurfaces \mathcal{M}_\pm . The right figure: the green solid line represents the real part of the timelike entanglement entropy, and the red solid line represents the imaginary part, which correspond to the spacelike geodesic and the timelike geodesic respectively.

which generates another bulk modular flow $k_t^{\beta,\text{bulk}}$, whose Killing horizon is just the inner horizon,

$$\begin{aligned} k_t^{\beta,\text{bulk}} &= \beta_{\tilde{v}} \partial_{\tilde{v}} + \beta_{\tilde{v}} \partial_{\tilde{v}} \\ &= \frac{\pi}{2} \left(l_U - \frac{4U^2}{l_U} + \frac{2}{l_V \rho} \right) \partial_U + \frac{\pi}{2} \left(l_V - \frac{4V^2}{l_V} + \frac{2}{l_U \rho} \right) \partial_V + 4\pi \left(\frac{U}{l_U} + \frac{V}{l_V} \right) \rho \partial_\rho. \end{aligned} \quad (26)$$

Similarly, the positive sign in the first line comes from the positive sign in the thermal circle (25). The difference between $k_t^{\alpha,\text{bulk}}$ and $k_t^{\beta,\text{bulk}}$ is that l_V is replaced with $-l_V$, i.e.

$$V \leftrightarrow -V \Leftrightarrow t \leftrightarrow x \quad (27)$$

Asymptotically, we have the boundary modular flow k_t^β ,

$$k_t^\beta = \left(\frac{\pi l_U}{2} - \frac{2\pi U^2}{l_U} \right) \partial_U + \left(\frac{\pi l_V}{2} - \frac{2\pi V^2}{l_V} \right) \partial_V. \quad (28)$$

See the right figure of Fig.2 for the boundary modular flow lines generated by k_t^β . The physical significance of $k_t^{\beta,\text{bulk}}$ can be understood more clearly in the Rindler coordinate system (\tilde{t}, \tilde{x}) , where the modular flow $k_t^{\beta,\text{bulk}}$ can be rewritten as:

$$k_t^{\beta,\text{bulk}} = 2\pi \partial_{\tilde{x}}, \quad (29)$$

i.e. the bulk modular flow $k_t^{\beta,\text{bulk}}$ is the generator of the spatial translations in the Rindler AdS_3 , hence we refer to it as the bulk modular momentum flow. In the Rindler coordinate system (\tilde{t}, \tilde{x}) , the thermal circle of the inner horizon (25) is $\tilde{x} \sim \tilde{x} - 2\pi i$.

Secondly, solving the equation $\tilde{\rho} = -T_{\tilde{U}} T_{\tilde{V}}$ can also give us two null hypersurfaces \mathcal{M}_\pm , which are mapped to the inner horizon under the bulk Rindler transformation (10),

$$\mathcal{M}_+ : \rho = -\frac{2}{(l_U - 2U)(l_V - 2V)}, \quad \mathcal{M}_- : \rho = -\frac{2}{(l_U + 2U)(l_V + 2V)}, \quad (30)$$

and their interaction line is $\widehat{\mathcal{E}}$ which we refer to as the inner Ryu-Takayanagi (IRT) surface in this paper,

$$\widehat{\mathcal{E}}: \rho = -\frac{2l_V}{l_U(l_V^2 - 4V^2)}, \quad U = -\frac{l_U}{l_V}V, \quad (31)$$

see the left figure of Fig.3 for an illustration. The length parameter $\widehat{\tau}$ of the IRT surface $\widehat{\mathcal{E}}$ is given by,

$$\widehat{\tau} = \frac{1}{2} \log \left(\frac{2V - l_V}{2V + l_V} \right), \quad (32)$$

where we set the null infinity (i.e. $V = \infty$) to be the origin for the length parameter. One can easily verify that $k_t^{\beta, \text{bulk}}$ is vanishing on $\widehat{\mathcal{E}}$. Furthermore, the IRT surface $\widehat{\mathcal{E}}$ intersects with the asymptotic boundary at the endpoints of a boundary timelike interval $\widehat{\mathcal{A}}$, which connects the two tips of the causal development $\mathcal{D}_{\mathcal{A}}$ and is referred to as the *partner interval* of \mathcal{A} in this paper,

$$\widehat{\mathcal{A}}: (-l_U/2, l_V/2) \rightarrow (l_U/2, -l_V/2). \quad (33)$$

If we consider a case when \mathcal{A} is a static spacelike interval of length L , i.e. $l_U = l_V = L/2$, then the corresponding partner interval $\widehat{\mathcal{A}}$ is a pure timelike interval⁷ of the same length (which means the time difference) L . Under the (t, x, z) coordinates (5), the corresponding IRT surface $\widehat{\mathcal{E}}$ (31) is given by,

$$\widehat{\mathcal{E}}: t^2 - z^2 = \frac{L^2}{4}. \quad (34)$$

Recently, the authors in [37,38] defined the so-called timelike entanglement entropy (TEE) through the analytical continuation of the entropy formula for spacelike intervals. Specifically, consider a pure timelike interval $\widehat{\mathcal{A}}$ with the length L , the TEE $S_{\widehat{\mathcal{A}}}^{(T)}$ of this pure timelike interval $\widehat{\mathcal{A}}$ can be evaluated via the analytical continuation for the spacelike entanglement entropy, i.e.,

$$S_{\widehat{\mathcal{A}}}^{(T)} = \frac{c}{3} \log \left(\frac{\sqrt{-L^2}}{\epsilon} \right) = \frac{c}{3} \log \left(\frac{L}{\epsilon} \right) + \frac{c\pi i}{6}. \quad (35)$$

Here, ϵ represents the UV cutoff, and $\sqrt{-L^2}$ denotes $\sqrt{-ds^2}$ for the pure timelike interval $\widehat{\mathcal{A}}$. And c is the central charge that equals to $3/2G$. Accordingly, the geometric picture of the real part of the TEE, can be derived through analytical continuation (i.e. Wick rotation) for the RT surface and aligns exactly with the IRT surface $\widehat{\mathcal{E}}$ (34). This strongly implies that the key to understanding the timelike entanglement lies within the modular momentum associated with the inner horizon, rather than the modular Hamiltonian⁸. Furthermore, the difference between

⁷Here “pure timelike” refers to the fact that $\widehat{\mathcal{A}}$ is located at the $x = 0$ slice.

⁸In fact, we may define the TEE based on the modular momentum, which is similar to the method used to define entanglement entropy based on the modular Hamiltonian. More explicitly, the modular Hamiltonian and the modular momentum operators $H_{\text{mod}}, P_{\text{mod}}$ are derived by substituting the classical generators L_i, \bar{L}_i in k_t^α, k_t^β with their quantum counterparts, which are the generators $\mathcal{L}_i, \bar{\mathcal{L}}_i$ of the Virasoro algebra (D.2),

$$\begin{aligned} H_{\text{mod}} &= \frac{\pi l_U}{2} \mathcal{L}_{-1} - \frac{2\pi}{l_U} \mathcal{L}_1 - \frac{\pi l_V}{2} \bar{\mathcal{L}}_{-1} + \frac{2\pi}{l_V} \bar{\mathcal{L}}_1, \\ P_{\text{mod}} &= \frac{\pi l_U}{2} \mathcal{L}_{-1} - \frac{2\pi}{l_U} \mathcal{L}_1 + \frac{\pi l_V}{2} \bar{\mathcal{L}}_{-1} - \frac{2\pi}{l_V} \bar{\mathcal{L}}_1. \end{aligned} \quad (36)$$

The entanglement entropy $S_{\mathcal{A}}$ can be expressed as a function of H_{mod} according to its definition, i.e. $H_{\text{mod}} = -\log \rho_{\mathcal{A}}$,

$$S_{\mathcal{A}} = -\text{Tr}(\rho_{\mathcal{A}} \log \rho_{\mathcal{A}}) = \text{Tr}(H_{\text{mod}} e^{-H_{\text{mod}}}). \quad (37)$$

Similarly, the TEE may be defined as,

$$S_{\widehat{\mathcal{A}}}^{(T)} = \text{Tr}(P_{\text{mod}} e^{-P_{\text{mod}}}). \quad (38)$$

Similarly, the timelike entanglement entropy should also enjoy a thermodynamic first law analogue to the one associated to the inner horizon.

the covariant RT surface (14) and the covariant IRT surface (31) is also simply $l_V \leftrightarrow -l_V$ or equivalently $l_t \leftrightarrow l_x$. In other words, the covariant IRT surface (31) can also be obtained by applying a Wick rotation to the covariant RT surface (14), and thus aligns with the result obtained by covariantizing the static case.

The geometric picture of the imaginary part, referred to as $\widehat{\mathcal{E}}_{\text{im}}$, is a timelike geodesic that connects the endpoints of the two pieces of the spacelike geodesics $\widehat{\mathcal{E}}$ at the past and future null infinities, such that $\widehat{\mathcal{E}} \cup \widehat{\mathcal{E}}_{\text{im}}$ remains connected. See the right figure of Fig.3. Interestingly, the length of this timelike geodesic reproduces the imaginary part of the TEE obtained from the analytical continuation. However, unlike the real part, the imaginary part is independent of the length L of the timelike interval $\widehat{\mathcal{A}}$, which comes from the property of timelike geodesics, i.e. the proper lengths between the past and future null infinities for all timelike geodesics are the same.

Later, various principles have been proposed to determine the geometric picture for the holographic TEE. For example, in [48], the authors generalize the RT formula by extending the concept of the area of homologous surfaces to include complex values. Specifically, the area of the timelike part is considered imaginary, while that of the spacelike part remains real. When comparing the complex-valued areas of homologous surfaces, the imaginary part is dominant. In [49], the authors claimed that the first order derivative of the timelike part and that of the spacelike part should be equal at the merging point. In this way, when we extremalize the area of the timelike part of the homologous surface, the spacelike part will also be extremalized at the same time due to this requirement. Also in [50], the authors proposed that, the holographic timelike entanglement entropy is captured by the boundary-anchored extremal surfaces in the analytic continuation of the holographic spacetimes with complex coordinates.

In this paper, we interpret the spacelike geodesic that represents the real part of the TEE as the IRT surface $\widehat{\mathcal{E}}$, which is the set of the fixed points of the bulk modular momentum flow. We also interpret the timelike geodesic that represents the imaginary part of the TEE as the boundary of the extended entanglement wedge, see the discussions around (70). We find that the points on this timelike geodesic are not the fixed points of the modular momentum flow, which makes their role in the analogue replica story [17] of the extended entanglement wedge unclear. Nevertheless, we omit the imaginary part of the TEE temporarily.

3 Partial entanglement entropy, modular slice and entanglement wedge

3.1 Partial entanglement entropy

In this paper, we mainly focus on the two-dimensional system, and x denotes the spatial coordinate. The *entanglement contour* $s_{\mathcal{A}}(x)$ [51] is a function for the region \mathcal{A} , which is conjectured to capture the contribution from each site x inside \mathcal{A} to the entanglement entropy $S_{\mathcal{A}}$. In other words, it is the density function of the entanglement entropy $S_{\mathcal{A}}$ which satisfies,

$$S_{\mathcal{A}} = \int_{\mathcal{A}} s_{\mathcal{A}}(x) dx. \quad (39)$$

The *partial entanglement entropy* (PEE) [46, 52–56] which describes the contribution from a subset $\mathcal{A}_i \subset \mathcal{A}$ to the entanglement entropy $S_{\mathcal{A}}$ can be obtained by the integration of the entanglement contour $s_{\mathcal{A}}(x)$ for the region \mathcal{A}_i ,

$$s_{\mathcal{A}}(\mathcal{A}_i) = \int_{\mathcal{A}_i} s_{\mathcal{A}}(x) dx. \quad (40)$$

The PEE $s_{\mathcal{A}}(\mathcal{A}_i)$ describes certain type of the correlation between the subset \mathcal{A}_i and the region $\bar{\mathcal{A}}$ that purifies \mathcal{A} , hence it is useful to rewrite the PEE as,

$$s_{\mathcal{A}}(\mathcal{A}_i) \equiv \mathcal{I}(\mathcal{A}_i, \bar{\mathcal{A}}). \quad (41)$$

The PEE should satisfy a set of requirements [51, 52] including all the requirements satisfied by the mutual information $I(A, B)$ ⁹ and an additional key requirement of additivity according to its physical significance, see [41, 57–68] for recent progresses on PEE. Suppose A, B, C are three non-overlapping regions on a Cauchy surface, we list the physical requirements satisfied by the PEE in the following,

1. Additivity: $\mathcal{I}(A, B \cup C) = \mathcal{I}(A, B) + \mathcal{I}(A, C)$;
2. Permutation symmetry: $\mathcal{I}(A, B) = \mathcal{I}(B, A)$;
3. Normalization¹⁰: $\mathcal{I}(A, B)|_{B \rightarrow \bar{\mathcal{A}}} = S_A$;
4. Positivity: $\mathcal{I}(A, B) > 0$;
5. Upper bounded: $\mathcal{I}(A, B) \leq \min\{S_A, S_B\}$;
6. $\mathcal{I}(A, B)$ should be invariant under any local unitary transformations inside A or B ;
7. Symmetry: For any symmetry transformation \mathcal{T} under which $\mathcal{T}A = A'$ and $\mathcal{T}B = B'$, we have $\mathcal{I}(A, B) = \mathcal{I}(A', B')$.

Up to now, there are many prescriptions to construct the PEE. We mainly focus on two of them in this paper, one is the additive linear combination (ALC) proposal [42, 46, 56] in two-dimensional system¹¹, consider an interval \mathcal{A} which is partitioned into three sub-intervals $\mathcal{A}_1 \cup \mathcal{A}_2 \cup \mathcal{A}_3$ where \mathcal{A}_2 is the middle one and $\mathcal{A}_1(\mathcal{A}_3)$ denotes the left (right) sub-interval of \mathcal{A}_2 , the proposal claims that

$$s_{\mathcal{A}}(\mathcal{A}_2) = \frac{1}{2} (S_{\mathcal{A}_1 \cup \mathcal{A}_2} + S_{\mathcal{A}_2 \cup \mathcal{A}_3} - S_{\mathcal{A}_1} - S_{\mathcal{A}_3}). \quad (42)$$

The other one is the geometric construction applied to the holographic theories with a local modular Hamiltonian [42, 46], which claims there is an one-to-one correspondence between the points in the region \mathcal{A} and the points on the RT surface \mathcal{E} , hence gives a natural contour function for \mathcal{A} . We will introduce this geometric construction in detail in the next subsection. The PEEs evaluated by these two proposals are highly consistent with each other [42, 46, 69].

3.2 Modular slice, entanglement wedge and holographic PEE

3.2.1 Modular Hamiltonian slice

The concept of modular (Hamiltonian) slice is proposed to provide a natural slicing of the entanglement wedge [46], which we call the fine structure of the entanglement wedge. This slicing is natural in the Rindler $\widehat{\text{AdS}}_3$ where there are translational symmetries along the Rindler coordinate (\tilde{t}, \tilde{x}) , and modular slices are exactly the 2-dimensional spacetime slices with fixed

⁹One should be careful not to confuse the PEE $\mathcal{I}(A, B)$ and the mutual information $I(A, B)$.

¹⁰Note that the normalization requirement is subtle as we need to match between two infinitely large quantities. In fact this requirement should only be imposed to special regions to make sure the existence of the solution for the whole set of requirements. For example, in the Poincaré AdS_{d+1} , the normalization requirement can only be imposed to spherical regions on the boundary [66, 68]

¹¹In higher dimension, the ALC proposal only applies to the situation when all degrees of freedom settle in a unique order (for example a line or a circle).

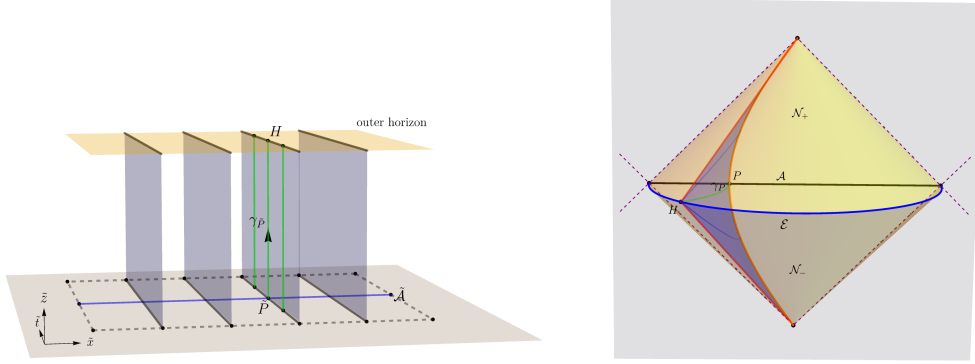


Figure 4: The left figure shows the modular Hamiltonian slices in the Rindler $\widetilde{\text{AdS}}_3$, i.e. the spacetime slices with fixed \tilde{x} coordinates shaded in gray blue. The green lines represent the $\tilde{\rho}$ coordinate lines, with the one indicated by an arrow being the specific line that passes through the boundary point \tilde{P} , denoted as $\gamma_{\tilde{P}}$. The right figure shows the modular Hamiltonian slice that passes through P in the original Poincaré AdS_3 , and the orange curve represents the modular Hamiltonian flow \mathcal{L}_H . The red curves represent the intersection lines between the modular Hamiltonian slice and the null hypersurface \mathcal{N}_{\pm} .

\tilde{x} coordinates, and the slicing respects the spatial translational symmetry. Also due to the translational symmetry, the entanglement contour of the Rindler boundary CFT is flat, which can be mapped to the entanglement contour for the original interval via the inverse Rindler transformations. Also the modular slices in the Rindler $\widetilde{\text{AdS}}_3$ can be mapped to certain spacetime slices in the entanglement wedge \mathcal{W}_A , hence we obtain the slicing structure in the entanglement wedge.

We can also identify the modular slices in the entanglement wedge without referring to the Rindler $\widetilde{\text{AdS}}_3$ by the following prescription:

- Firstly, given an arbitrary point P in the causal development \mathcal{D}_A , we can identify a saddle geodesic γ_P that connects P to the RT surface \mathcal{E} (or IRT surface $\tilde{\mathcal{E}}$) with the minimal length. Note that, the saddle geodesic γ_P intersects with \mathcal{E} vertically, and we call the intersection point H on the RT surface the partner point of P . See the right figure of Fig.4.
- Secondly, we let the point P move along the boundary modular flow line that passes through P , then the saddle geodesic γ_P moves accordingly and sweeps out a 2-dimensional hypersurface \mathcal{P}_H in the entanglement wedge, which is exactly the modular slice defined in [46].

The above construction maps the modular slices in the original space exactly to the modular slices with fixed \tilde{x} coordinate in the Rindler $\widetilde{\text{AdS}}_3$. Let us consider the boundary point $P = (U_1, V_1)$ ¹² and its image point $\tilde{P} = (\tilde{U}_1, \tilde{V}_1)$ on the Rindler boundary, one can find that the saddle geodesic γ_P maps to the line $\gamma_{\tilde{P}}$ that emanates from \tilde{P} , moving along $\tilde{\rho}$ direction and ending on the outer horizon $\tilde{\rho} = T_{\tilde{U}}T_{\tilde{V}}$ (see the green lines in the left figure of Fig.4), i.e.

$$\gamma_{\tilde{P}} : \tilde{t} = \tilde{t}_{\tilde{P}}, \quad \tilde{x} = \tilde{x}_{\tilde{P}}, \quad \tilde{\rho} \geq T_{\tilde{U}}T_{\tilde{V}}, \quad (43)$$

where

$$\tilde{t}_{\tilde{P}} = \frac{1}{2} \log \left(\frac{(l_U + 2U_1)(l_V - 2V_1)}{(l_U - 2U_1)(l_V + 2V_1)} \right), \quad \tilde{x}_{\tilde{P}} = \frac{1}{2} \log \left(\frac{(l_U + 2U_1)(l_V + 2V_1)}{(l_U - 2U_1)(l_V - 2V_1)} \right), \quad (44)$$

¹²From now on, if we omit the ρ coordinate of a point, then this is a boundary point, i.e. $\rho = \infty$.

represent the Rindler temporal and spatial coordinates of \tilde{P} respectively. It is obvious that, $\gamma_{\tilde{P}}$ is the saddle geodesic connecting \tilde{P} and the outer horizon $\tilde{\rho} = T_{\tilde{U}} T_{\tilde{V}}$.

We can obtain the pre-image γ_P in the original Poincaré AdS₃ of $\gamma_{\tilde{P}}$ by using the mapping (23) and then solving the following equations:

$$\begin{aligned} \frac{1}{4} \log \left(\frac{((l_U + 2U)(l_V - 2V)\rho - 2)^2}{((l_U - 2U)(l_V + 2V)\rho - 2)^2} \right) &= \tilde{t}_{\tilde{P}}, \\ \frac{1}{4} \log \left(\frac{((l_U + 2U)(l_V + 2V)\rho + 2)^2}{((l_U - 2U)(l_V - 2V)\rho + 2)^2} \right) &= \tilde{x}_{\tilde{P}}. \end{aligned} \quad (45)$$

Note that, there are two solutions for this equation: one is a spacelike geodesic (46) that corresponds to the $\gamma_{\tilde{P}}$ (43) outside the horizon, and the other is a timelike geodesic (60) that corresponds to the extension of $\gamma_{\tilde{P}}$ inside the horizon. Then the saddle geodesic γ_P is given by the spacelike solution,

$$\gamma_P: \quad \rho(V) = \frac{2\tilde{l}_V}{\tilde{l}_U (\tilde{l}_V^2 - 4(V - V_0)^2)}, \quad U(V) = \frac{\tilde{l}_U}{\tilde{l}_V} (V - V_0) + U_0, \quad (46)$$

where the parameters $(\tilde{l}_U, \tilde{l}_V, V_0, U_0)$ read,

$$\tilde{l}_U = \frac{-l_U^2 + 4U_1^2}{4U_1}, \quad \tilde{l}_V = \frac{-l_V^2 + 4V_1^2}{4V_1}, \quad V_0 = \frac{l_V^2 + 4V_1^2}{8V_1}, \quad U_0 = \frac{l_U^2 + 4U_1^2}{8U_1}. \quad (47)$$

see the green line in the right figure of Fig.4. Compared with (31), it is easy to find that γ_P is part of the RT surface for the interval with extension \tilde{l}_U and \tilde{l}_V and the center point (U_0, V_0) . One can further check that, γ_P is normal to the RT surface \mathcal{E} , hence is the saddle geodesic. We can also identify the intersection point H between γ_P (46) and the RT surface \mathcal{E} , whose coordinate is given by

$$U_H = \frac{l_U}{l_V} V_H, \quad V_H = \frac{l_V (l_V U_1 + l_U V_1)}{l_U l_V + 4U_1 V_1}. \quad (48)$$

Consider an arbitrary point $H = (U_H, V_H)$ on the RT surface \mathcal{E} . We can also obtain a boundary curve by fixing V_H in (48), which we denote as \mathcal{L}_H .

$$\mathcal{L}_H: \quad U(V) = \frac{l_U l_V (V_H - V)}{l_V^2 - 4V V_H}. \quad (49)$$

One can easily verify that all points on this curve have the same partner point $H = (U_H, V_H)$. More importantly, this curve is precisely the boundary modular Hamiltonian flow line of k_t^α . The curve \mathcal{L}_H is mapped to a boundary line $\tilde{\mathcal{L}}_H$ along the \tilde{t} direction in the Rindler AdS₃, see the black lines on the Rindler boundary in the left figure of Fig.4. Consider the boundary point $P = (U_1, V_1)$ that lies within this modular flow line \mathcal{L}_H , i.e., it satisfies the following equation,

$$U_1 = \frac{l_U l_V (V_H - V_1)}{l_V^2 - 4V_1 V_H}. \quad (50)$$

On the other hand, each point on \mathcal{L}_H (49) determines a corresponding saddle geodesic, and the set of all these saddle geodesics forms the modular Hamiltonian slice \mathcal{P}_H , see the blue surface in the right figure of Fig.4,

$$\begin{aligned} \mathcal{P}_H: \quad \rho &= \frac{2\tilde{l}_V}{\tilde{l}_U (\tilde{l}_V^2 - 4(V - V_0)^2)}, \quad U = \frac{\tilde{l}_U}{\tilde{l}_V} (V - V_0) + U_0, \\ &(V_H < V < V_1, -l_V/2 < V_1 < l_V/2) \end{aligned} \quad (51)$$

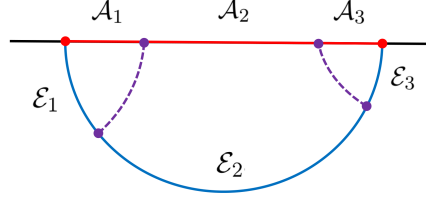


Figure 5: The figure is extracted from [61]. The PEEs $s_{\mathcal{A}}(\mathcal{A}_i)$ are captured by the length of \mathcal{E}_i . The purple lines are the saddle geodesics that are normal to the RT surface \mathcal{E} . Although the figure looks static, we should consider it to be a covariant configuration.

where the parameters $(\tilde{l}_U, \tilde{l}_V, U_0, V_0)$ in the above expression are given by (47) and (50). Also we can check that, all the points on \mathcal{P}_H maps to points on the modular slice with fixed \tilde{x} coordinate in the Rindler AdS_3 ,

$$\tilde{x} = \frac{1}{2} \log \left(\frac{l_V + 2V_H}{l_V - 2V_H} \right). \quad (52)$$

Note that, the saddle geodesics for different points on $\tilde{\mathcal{L}}_H$ intersect with the outer horizon at different points (see the green lines in the left figure of Fig.4), but all these intersection points are mapped to the only point H on the RT surface \mathcal{E} via the inverse Rindler transformations. In summary, we come up with the following conclusions:

- All points on the modular flow line \mathcal{L}_H have the same partner point H on \mathcal{E} .
- The points (e.g. H) on \mathcal{E} , the modular flow lines (e.g. \mathcal{L}_H) and the modular slices (e.g. \mathcal{P}_H) are in one-to-one correspondence.
- The construction of modular slice gives a natural slicing for the entanglement wedge,

$$\mathcal{W}_{\mathcal{A}} = \left\{ \mathcal{P}_H \mid -\frac{l_V}{2} < V_H < \frac{l_V}{2} \right\}. \quad (53)$$

One motivation to introduce the above fine structure of the entanglement wedge is to compute the PEE $s_{\mathcal{A}}(\mathcal{A}_i)$ [46, 53], where \mathcal{A}_i is any sub-interval of \mathcal{A} . Based on the partner relation between the points in $\mathcal{D}_{\mathcal{A}}$ and those on \mathcal{E} , we obtain the correspondence between any sub-interval \mathcal{A}_i of \mathcal{A} and the geodesic chord \mathcal{E}_i on \mathcal{E} . Here the points in \mathcal{A}_i has partner points on \mathcal{E} , which are exactly the points that make the geodesic chord \mathcal{E}_i . It has been argued in [46, 53] that the PEE $s_{\mathcal{A}}(\mathcal{A}_i)$ is captured by the length of the partner sub-interval \mathcal{E}_i on \mathcal{E} , i.e.

$$s_{\mathcal{A}}(\mathcal{A}_i) = \frac{\text{Length}(\mathcal{E}_i)}{4G}, \quad (54)$$

see Fig.5 for an illustration. For later convenience, we define the length parameter λ along the RT surface \mathcal{E} , and establish the relation between any boundary point, for example $P = (U_1, V_1)$, and the length parameter of its partner point H (48) on \mathcal{E} ,

$$\lambda(P) \equiv \frac{1}{2} \log \left(\frac{(l_U + 2U_1)(l_V + 2V_1)}{(l_U - 2U_1)(l_V - 2V_1)} \right). \quad (55)$$

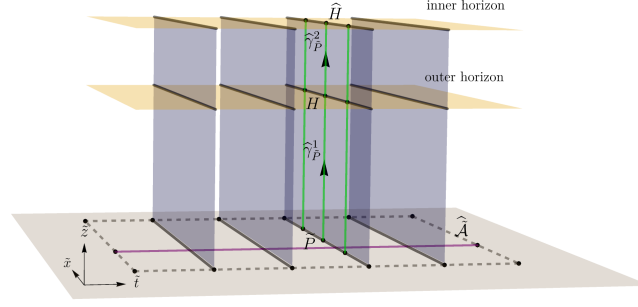


Figure 6: The gray blue surfaces are the spacetime slices with fixed \tilde{t} coordinate, which are also the modular momentum slices. The green lines represent the $\tilde{\rho}$ coordinate lines, with the one indicated by an arrow being the specific line that passes through the boundary point \tilde{P} , denoted as $\hat{\gamma}_{\tilde{P}}$, which is further divided into two parts $\hat{\gamma}_{\tilde{P}}^1$ and $\hat{\gamma}_{\tilde{P}}^2$. The purple line $\hat{\mathcal{A}}$ represents the partner interval of $\tilde{\mathcal{A}}$.

Then for any sub-interval \mathcal{A}_i with the following two endpoints,

$$\mathcal{A}_i : P = (U_1, V_1) \rightarrow Q = (U_2, V_2), \quad (56)$$

the PEE $s_{\mathcal{A}}(\mathcal{A}_i)$ is just given by,

$$s_{\mathcal{A}}(\mathcal{A}_i) = \frac{\lambda(Q) - \lambda(P)}{4G} = \frac{1}{8G} \log \left(\frac{(l_U - 2U_1)(l_V - 2V_1)(l_U + 2U_2)(l_V + 2V_2)}{(l_U + 2U_1)(l_V + 2V_1)(l_U - 2U_2)(l_V - 2V_2)} \right). \quad (57)$$

This result aligns exactly with the result evaluated by the ALC proposal (42).

We point out that, the PEE $s_{\mathcal{A}}(\mathcal{A}_i)$ is invariant under the modular flow, which means that, any sub-interval that intersects with the same class of modular flow lines or modular slices, has the same PEE [53]. More explicitly, if the endpoints of the sub-intervals \mathcal{A}_i and \mathcal{A}'_i are in the same pair of modular flow lines, then $s_{\mathcal{A}}(\mathcal{A}_i) = s_{\mathcal{A}}(\mathcal{A}'_i)$, as their partner geodesic chords coincide. On the other hand, one can compute the PEE using the ALC proposal, and the requirement of modular invariance is sufficient to determine the boundary modular flow lines (see [53] for various examples).

3.2.2 Modular momentum slice

Now we want to define a similar fine structure which is invariant under the modular momentum flow k_t^β . In this prescription, the coordinates \tilde{t} and \tilde{x} exchange their role, such that the \tilde{x} direction becomes timelike, hence $\partial_{\tilde{x}}$ plays the role of the Hamiltonian in the region between the outer and the inner horizon. Also, the bulk modular momentum flow $k_t^{\beta, \text{bulk}}$ vanishes on the IRT surface $\hat{\mathcal{E}}$. In this subsection, we follow a similar prescription to construct the modular momentum slices.

The bulk modular momentum flow represents the bulk replica symmetry for the timelike interval $\hat{\mathcal{A}}$, whose image interval is a line along the \tilde{t} direction in the Rindler AdS_3 . And in the Rindler AdS_3 , the modular momentum flow lines are the \tilde{x} coordinate lines, hence the modular momentum slices are just the spacetime slices with fixed \tilde{t} coordinate, see Fig.6. Note that, unlike the modular (Hamiltonian) slices, the modular momentum slice here is normal to the \tilde{t} direction, rather than the \tilde{x} direction. Now we start from an arbitrary point \tilde{P} , which is the image of a point P in $\mathcal{D}_{\mathcal{A}}$, and search for a saddle curve $\hat{\gamma}_{\tilde{P}}$ connecting \tilde{P} and the inner horizon. This is again the line along the $\tilde{\rho}$ direction (see the green lines in Fig.6), i.e.,

$$\hat{\gamma}_{\tilde{P}} : \tilde{t} = \tilde{t}_P, \quad \tilde{x} = \tilde{x}_P, \quad \tilde{\rho} \geq -T_{\tilde{U}} T_{\tilde{V}}. \quad (58)$$

Since $\widehat{\gamma}_{\tilde{p}}$ transitions from spacelike to timelike when passing through the outer horizon, we divide it into the following two parts,

$$\begin{aligned}\widehat{\gamma}_{\tilde{p}}^1: \tilde{t} = \tilde{t}_p, \quad \tilde{x} = \tilde{x}_p, \quad \tilde{\rho} \geq T_{\tilde{U}} T_{\tilde{V}}, \\ \widehat{\gamma}_{\tilde{p}}^2: \tilde{t} = \tilde{t}_p, \quad \tilde{x} = \tilde{x}_p, \quad -T_{\tilde{U}} T_{\tilde{V}} \leq \tilde{\rho} \leq T_{\tilde{U}} T_{\tilde{V}}.\end{aligned}\quad (59)$$

When mapping back to the original Poincaré AdS₃, $\widehat{\gamma}_p^1$ is the spacelike solution of (45), which is precisely γ_p as given by (46). And $\widehat{\gamma}_p^2$ is the timelike solution of (45), which is given by,

$$\widehat{\gamma}_p^2: \rho(V) = C_1 C_2 (-1 + \cos[2 \operatorname{arccot}(2C_2(C_4 - V))]), \quad U(V) = C_3 + \frac{C_2(V - C_4)}{C_1}, \quad (60)$$

where the parameters (C_1, C_2, C_3, C_4) read,

$$C_1 = \frac{l_U^2 + 4U_1^2}{l_U(l_U^2 - 4U_1^2)}, \quad C_2 = -\frac{l_V^2 + 4V_1^2}{l_V(l_V^2 - 4V_1^2)}, \quad C_3 = \frac{2l_U^2 U_1}{l_U^2 + 4U_1^2}, \quad C_4 = \frac{2l_V^2 V_1}{l_V^2 + 4V_1^2}. \quad (61)$$

Since $\widehat{\gamma}_p$ intersects with both the outer and the inner horizons, P has partner points on both the RT and the IRT surfaces. Again we denote the partner point on \mathcal{E} as H and the partner point on $\widehat{\mathcal{E}}$ as \widehat{H} . Given the coordinate of $P = (U_1, V_1)$, H can again be specified by (48), while the partner \widehat{H} is given by the intersection point between $\widehat{\gamma}_p^2$ and $\widehat{\mathcal{E}}^{\text{13}}$, i.e.

$$\widehat{H} = \widehat{\gamma}_p^2 \cap \widehat{\mathcal{E}}, \quad V_{\widehat{H}} = -\frac{l_V(l_U l_V - 4U_1 V_1)}{4(l_V U_1 - l_U V_1)}. \quad (62)$$

One can see that, when P is on the interval \mathcal{A} , its partner on $\widehat{\mathcal{E}}$ goes to infinity, and when P approaches one of the tips of $\mathcal{D}_{\mathcal{A}}$, its partner point also approaches the same tip. Similarly, for an arbitrary point $\widehat{H} = (U_{\widehat{H}}, V_{\widehat{H}})$ on $\widehat{\mathcal{E}}$, the corresponding modular momentum flow line can be also given by fixing $V_{\widehat{H}}$ in (62), which we denote as $\widehat{\mathcal{L}}_{\widehat{H}}$,

$$\widehat{\mathcal{L}}_{\widehat{H}}: U(V) = \frac{l_U(l_V^2 - 4V V_{\widehat{H}})}{4l_V(V - V_{\widehat{H}})}, \quad (63)$$

Also, one can easily verify that all points on $\widehat{\mathcal{E}}$ associated with the modular momentum flow $\widehat{\mathcal{L}}_{\widehat{H}}$ has the same partner point $\widehat{H} = (U_{\widehat{H}}, V_{\widehat{H}})$. Note that, the points on $\widehat{\mathcal{L}}_{\widehat{H}}$ have different partner points on the RT surface \mathcal{E} . When we move $P = (U_1, V_1)$ along $\widehat{\mathcal{L}}_{\widehat{H}}$, which satisfies,

$$U_1 = \frac{l_U(l_V^2 - 4V_1 V_{\widehat{H}})}{4l_V(V_1 - V_{\widehat{H}})}, \quad (64)$$

its saddle geodesics $\widehat{\gamma}_p^1$ and $\widehat{\gamma}_p^2$ sweep out two spacetime slices, $\widehat{\mathcal{P}}_{\widehat{H}}^1$ and $\widehat{\mathcal{P}}_{\widehat{H}}^2$, respectively. See the two blue surfaces in the left and the right figure of Fig.7. Then the modular momentum slice $\widehat{\mathcal{P}}_{\widehat{H}}$ associated to $\widehat{\mathcal{L}}_{\widehat{H}}$ is defined as the union of these two slices,

$$\begin{aligned}\widehat{\mathcal{P}}_{\widehat{H}}^1: \rho = \frac{2\tilde{l}_V}{\tilde{l}_U(\tilde{l}_V^2 - 4(V - V_0)^2)}, \quad U = \frac{\tilde{l}_U}{\tilde{l}_V}(V - V_0) + U_0, \\ (V_1 < V < V_H, -l_V/2 < V_1 < l_V/2),\end{aligned}\quad (65)$$

$$\begin{aligned}\widehat{\mathcal{P}}_{\widehat{H}}^2: \rho = C_1 C_2 (-1 + \cos[2 \operatorname{arccot}(2C_2(C_4 - V))]), \quad U = C_3 + \frac{C_2(V - C_4)}{C_1}, \\ (V_{\widehat{H}} < V < V_H, -l_V/2 < V_1 < l_V/2),\end{aligned}$$

¹³In appendix C, we also present a trick for locating the partner point \widehat{H} on $\widehat{\mathcal{E}}$ using the null hypersurface.

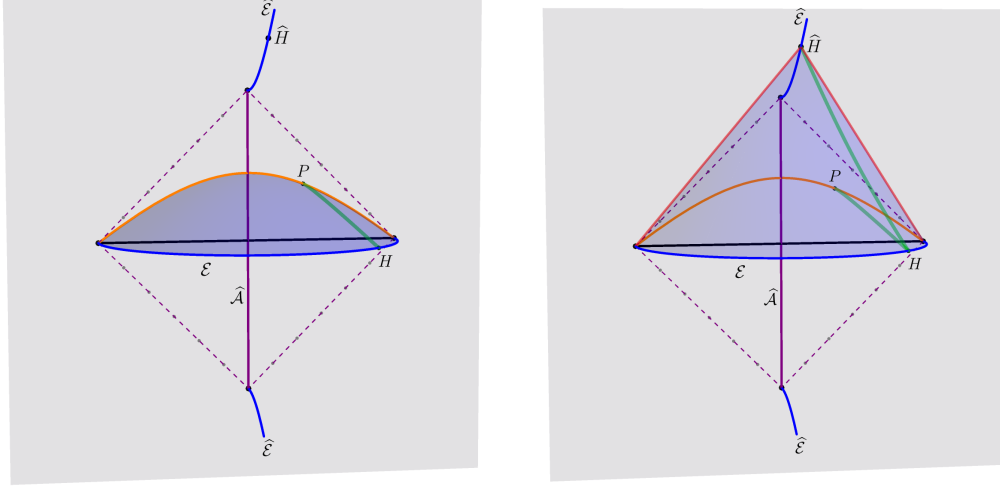


Figure 7: The orange curve is the boundary modular momentum flow line $\widehat{\mathcal{L}}_{\widehat{H}}$. P is a boundary point on $\widehat{\mathcal{L}}_{\widehat{H}}$, with its partner points on \mathcal{E} and $\widehat{\mathcal{E}}$ denoted by H and \widehat{H} , respectively. The blue surfaces in the left figure and that in the right figure represent the hypersurfaces $\widehat{\mathcal{P}}_{\widehat{H}}^1$ and $\widehat{\mathcal{P}}_{\widehat{H}}^2$, respectively, and their union forms the modular momentum slice $\widehat{\mathcal{P}}_{\widehat{H}}$. The green curve in the left figure is the spacelike saddle geodesic $\widehat{\gamma}_P^1$. The two green curves in the right figure are the spacelike saddle geodesic $\widehat{\gamma}_P^1$ and the timelike saddle geodesic $\widehat{\gamma}_P^2$ respectively. The red lines are the intersection lines between $\widehat{\mathcal{P}}_{\widehat{H}}$ and \mathcal{M}_{\pm} .

The parameters $(C_1, C_2, C_3, C_4, \widetilde{l}_U, \widetilde{l}_V, U_0, V_0)$ in the above expression are given by (47), (61) and (64). As expected, $\widehat{\mathcal{P}}_{\widehat{H}}$ maps to a fixed \widetilde{t} slice in the Rindler AdS_3 ,

$$\widetilde{t} = \frac{1}{2} \log \left(\frac{2V_{\widehat{H}} - l_V}{2V_{\widehat{H}} + l_V} \right). \quad (66)$$

Again the modular momentum flow lines (e.g. $\widehat{\mathcal{L}}_{\widehat{H}}$), the points (e.g. \widehat{H}) on the IRT surface $\widehat{\mathcal{E}}$ and the modular momentum slices (e.g. $\widehat{\mathcal{P}}_{\widehat{H}}$) are in one-to-one correspondence.

As we have shown that the entanglement wedge $\mathcal{W}_{\mathcal{A}}$ is the union of all the modular Hamiltonian slices, and covers the region outside the outer horizon in the Rindler AdS_3 . Now we define the extended entanglement wedge $\widehat{\mathcal{W}}_{\mathcal{A}}$, which is the union of all the modular momentum slices and is mapped to the region outside the inner horizon in the Rindler AdS_3 correspondingly, i.e.,

$$\widehat{\mathcal{W}}_{\mathcal{A}} = \left\{ \widehat{\mathcal{P}}_{\widehat{H}} \mid |V_{\widehat{H}}| > \frac{l_V}{2} \right\}. \quad (67)$$

The extended entanglement wedge $\widehat{\mathcal{W}}_{\mathcal{A}}$ contains the entanglement wedge $\mathcal{W}_{\mathcal{A}}$ as a sub-region. As $|V_{\widehat{H}}|$ increases, the modular momentum slice goes deeper into the bulk. It is also interesting to note that, when $V_{\widehat{H}} \rightarrow \pm\infty$, the union of these two corresponding modular momentum slice $\widehat{\mathcal{P}}_{\widehat{H}}^2$ makes a smooth timelike hypersurface, which is given by,

$$\begin{aligned} \widehat{\mathcal{P}}_{\infty}^2 &\equiv \lim_{V_{\widehat{H}} \rightarrow \infty} \widehat{\mathcal{P}}_{\widehat{H}}^2 \cup \lim_{V_{\widehat{H}} \rightarrow -\infty} \widehat{\mathcal{P}}_{\widehat{H}}^2 \\ &= \left\{ \rho = \frac{2l_V (l_V^2 + 4V_1^2)}{l_U (l_V^4 + 4l_V^2 (V^2 - 4VV_1 + V_1^2) + 16V^2V_1^2)}, U = l_U \left(\frac{4l_V V_1}{l_V^2 + 4V_1^2} - \frac{V}{l_V} \right) \right\} \quad (68) \\ & \quad (-\infty < V < \infty, -l_V/2 < V_1 < l_V/2). \end{aligned}$$

See the blue surface in the left figure of Fig.8. Therefore, the extended entanglement wedge $\widehat{\mathcal{W}}_{\mathcal{A}}$ is the region bounded by the null hypersurfaces \mathcal{M}_{\pm} , the causal development $\mathcal{D}_{\mathcal{A}}$ and the timelike hypersurface $\widehat{\mathcal{P}}_{\infty}^2$. According to (63), in the limit $\widehat{H} \rightarrow \infty$, the modular momentum flow line $\widehat{L}_{\widehat{H}}$ becomes \widehat{L}_{∞} , which is precisely the boundary straight line overlapping with the interval \mathcal{A} . In other words, the timelike hypersurface $\widehat{\mathcal{P}}_{\infty}^2$ is the modular momentum slice associated with the modular momentum flow line \widehat{L}_{∞} that overlaps with the interval \mathcal{A} . For convenience, we define two hypersurfaces $\Xi_{\mathcal{A}}$ and $\Xi_{\widehat{\mathcal{A}}}$ as the spacetime slices where \mathcal{A} and $\widehat{\mathcal{A}}$ are located, respectively,

$$\Xi_{\mathcal{A}} : Ul_U - Vl_V = 0, \quad \Xi_{\widehat{\mathcal{A}}} : Ul_U + Vl_V = 0. \quad (69)$$

It is well known that the RT surface \mathcal{E} is a boundary of the intersection surface between the entanglement wedge and the hypersurface $\Xi_{\mathcal{A}}$. Similarly, we can also study the intersection surface between the extended entanglement wedge $\widehat{\mathcal{W}}_{\mathcal{A}}$ and the hypersurface $\Xi_{\widehat{\mathcal{A}}}$. The intersection line between $\widehat{\mathcal{P}}_{\infty}^2$ and $\Xi_{\widehat{\mathcal{A}}}$ is denoted as $\widehat{\gamma}_{\infty}^2$, which is a timelike geodesic,

$$\widehat{\gamma}_{\infty}^2 : \rho = \frac{2l_V}{l_U(l_V^2 + 4V^2)}, \quad U = -\frac{l_U}{l_V}V, \quad (70)$$

see the red line in Fig.8. Therefore, the intersection surface between the extended entanglement wedge $\widehat{\mathcal{W}}_{\mathcal{A}}$ and the spacetime slice $\Xi_{\widehat{\mathcal{A}}}$ is a co-dimension one region bounded by the timelike interval $\widehat{\mathcal{A}}$, the IRT surface $\widehat{\mathcal{E}}$ and the timelike geodesic $\widehat{\gamma}_{\infty}^2$, see the gray region in the right figure of Fig.8. Hence the timelike geodesic $\widehat{\gamma}_{\infty}^2$ gives a natural geometric interpretation for the imaginary part of the TEE $S_{\widehat{\mathcal{A}}}^{(T)}$ (35), and connects the two parts of the IRT surface $\widehat{\mathcal{E}}$ at the past and the future null infinities. As expected, the absolute value of the length of $\widehat{\gamma}_{\infty}^2$ is π , i.e.,

$$\ell_{\widehat{\gamma}_{\infty}^2} = \int_{-\infty}^{\infty} \frac{2l_V}{l_V^2 + 4V^2} dV = \pi. \quad (71)$$

In particular, if we consider the case when \mathcal{A} is a static spacelike interval of length L , i.e. $l_U = l_V = L/2$. Under the (t, x, z) coordinates (5), the corresponding timelike geodesic $\widehat{\gamma}_{\infty}^2$ (70) is given by,

$$\widehat{\gamma}_{\infty}^2 : t^2 - z^2 = -\frac{L^2}{4}, \quad x = 0. \quad (72)$$

One can easily verify that the asymptotic behavior (when $t \rightarrow \pm\infty$) at the null infinity of $\widehat{\gamma}_{\infty}^2$ is the same as that of the IRT surface $\widehat{\mathcal{E}}$ (34) at the first order derivative level, i.e.

$$\widehat{\gamma}_{\infty}^2 : z \sim t, \quad \widehat{\mathcal{E}} : z \sim t \quad (73)$$

which explains why the requirement that the first order derivatives of the timelike geodesic and the spacelike geodesic should be equal at the merging point, which is proposed in [49], is reasonable. More interestingly, when we embed the Poincaré AdS₃ into the global AdS₃, the IRT surface can be extended to the asymptotic boundary, with the anchor points being the two tips of the causal development of the complement $\mathcal{B} = \bar{\mathcal{A}}$. Thus, the extended part can be referred to as the IRT surface of \mathcal{B} . In this situation, the IRT surface of \mathcal{A} and that of its complement \mathcal{B} are not the same one. See Fig.14 and appendix A for the details. Also note that, the timelike geodesic $\widehat{\gamma}_{\infty}^2$ is not the set of fixed points of the modular momentum flow $k_t^{\beta, \text{bulk}}$, hence does not play the similar role as the IRT surface $\widehat{\mathcal{E}}$ in the bulk replica story.

Similarly, we can also define the length parameter $\widehat{\lambda}$ on $\widehat{\mathcal{E}}$ and establish the function $\widehat{\lambda}(P)$, between any boundary point $P = (U_1, V_1)$ and the length parameter of its partner point \widehat{H} (62) on $\widehat{\mathcal{E}}$, i.e.,

$$\widehat{\lambda}(P) \equiv \frac{1}{2} \log \left(\frac{(l_U + 2U_1)(l_V - 2V_1)}{(l_U - 2U_1)(l_V + 2V_1)} \right). \quad (74)$$

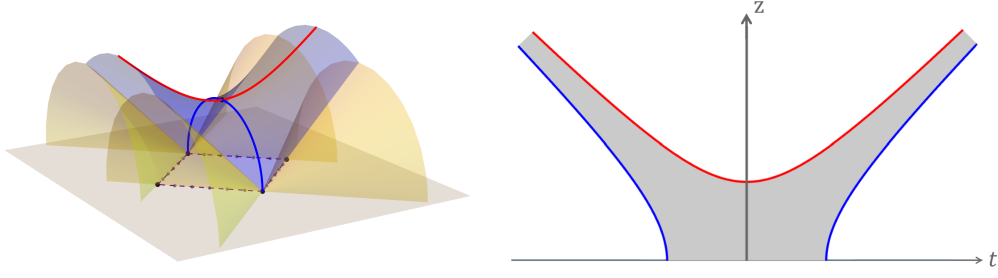


Figure 8: In the left figure, the blue surface is the modular momentum slice $\widehat{\mathcal{P}}_\infty^2$. The extended entanglement wedge $\widehat{\mathcal{W}}_{\mathcal{A}}$ is the bulk region bounded by \mathcal{M}_\pm (the yellow surfaces), $\mathcal{D}_{\mathcal{A}}$ and $\widehat{\mathcal{P}}_\infty^2$. The red curves in the left and the right figures represent the intersection line between $\widehat{\mathcal{P}}_\infty^2$ and $\Xi_{\widehat{\mathcal{A}}}$, which we denote as $\widehat{\gamma}_\infty^2$. In the right figure, the blue curve represents the IRT surface $\widehat{\mathcal{E}}$. And the shadow region is the intersection surface between $\widehat{\mathcal{W}}_{\mathcal{A}}$ and $\Xi_{\widehat{\mathcal{A}}}$.

As any boundary point in $\mathcal{D}_{\mathcal{A}}$ has a partner point on $\widehat{\mathcal{E}}$ according to (62), in the same sense any sub-interval $\widehat{\mathcal{A}}_i$ of the timelike interval $\widehat{\mathcal{A}}$ (33) corresponds to a geodesic chord $\widehat{\mathcal{E}}_i$ on the IRT surface $\widehat{\mathcal{E}}$. Similar to (54), the timelike partial entanglement entropy (TPEE) $s_{\widehat{\mathcal{A}}}^{(T)}(\widehat{\mathcal{A}}_i)$ that captures the contribution from the sub-interval $\widehat{\mathcal{A}}_i$ (56) to the TEE $S_{\widehat{\mathcal{A}}}^{(T)}$ is also given by the length of its partner geodesic chord $\widehat{\mathcal{E}}_i$. More explicitly, consider the sub-interval $\widehat{\mathcal{A}}_i$ with the following two endpoints,

$$\widehat{\mathcal{A}}_i : P = (U_1, V_1) \rightarrow Q = (U_2, V_2), \quad (75)$$

we should have,

$$\begin{aligned} s_{\widehat{\mathcal{A}}}^{(T)}(\widehat{\mathcal{A}}_i) &= \frac{\text{Length}(\widehat{\mathcal{E}}_i)}{4G} = \frac{\widehat{\lambda}(Q) - \widehat{\lambda}(P)}{4G} \\ &= \frac{1}{8G} \log \left(\frac{(l_U - 2U_1)(l_V + 2V_1)(l_U + 2U_2)(l_V - 2V_2)}{(l_U + 2U_1)(l_V - 2V_1)(l_U - 2U_2)(l_V + 2V_2)} \right). \end{aligned} \quad (76)$$

We can also use the TPEE $s_{\widehat{\mathcal{A}}}^{(T)}(\widehat{\mathcal{A}}^{\text{reg}})$, where $\widehat{\mathcal{A}}^{\text{reg}}$ is the following regularized timelike interval of $\widehat{\mathcal{A}}$, to regulate the timelike entanglement entropy $S_{\widehat{\mathcal{A}}}^{(T)}$,

$$\widehat{\mathcal{A}}^{\text{reg}} : (-l_U/2 + \epsilon_U, l_V/2 - \epsilon_V) \rightarrow (l_U/2 - \epsilon_U, -l_V/2 + \epsilon_V). \quad (77)$$

The partner points of the left and the right endpoints of $\widehat{\mathcal{A}}^{\text{reg}}$ on $\widehat{\mathcal{E}}$ are denoted by \widehat{H}_1 and \widehat{H}_2 , respectively. These points are given by,

$$V_{\widehat{H}_1} = \frac{l_V}{2} + \frac{\epsilon_U \epsilon_V}{l_U}, \quad V_{\widehat{H}_2} = -\frac{l_V}{2} - \frac{\epsilon_U \epsilon_V}{l_U}, \quad (78)$$

where we ignore the higher order terms $\mathcal{O}(\epsilon^3)$. One can easily find that \widehat{H}_1 approaches to the lower tip of $\mathcal{D}_{\mathcal{A}}$, while \widehat{H}_2 approaches to the upper tip of $\mathcal{D}_{\mathcal{A}}$. Therefore, the timelike entanglement entropy $S_{\widehat{\mathcal{A}}}^{(T)}$ is given by,

$$S_{\widehat{\mathcal{A}}}^{(T)} = s_{\widehat{\mathcal{A}}}^{(T)}(\widehat{\mathcal{A}}^{\text{reg}}) = \frac{\text{Length}(\widehat{\mathcal{E}}^{\text{reg}})}{4G} = \frac{1}{4G} \log \left(\frac{l_U l_V}{\epsilon_U \epsilon_V} \right), \quad (79)$$

where $\widehat{\mathcal{E}}^{\text{reg}}$ is the partner geodesic chord of $\widehat{\mathcal{A}}^{\text{reg}}$ on $\widehat{\mathcal{E}}$, and we ignore the higher order terms $\mathcal{O}(\epsilon)$. The result aligns exactly with $S_{\mathcal{A}}$ (19).

Before ending up this section, we also point out that, one can also use the null geodesics on \mathcal{M}_\pm to identify the one-to-one correspondence between the boundary modular momentum flow line $\widehat{\mathcal{L}}_{\widehat{H}}$, the point \widehat{H} on $\widehat{\mathcal{E}}$ and the modular slice $\widehat{\mathcal{P}}_{\widehat{H}}$ (65). This prescription looks more similar to the previous work [42, 46]. Let us denote the bulk modular flow lines on the null hypersurfaces \mathcal{M}_\pm (30) as $\widehat{\mathcal{L}}_{\widehat{H}}^\pm$. Hence, \widehat{H} , $\widehat{\mathcal{L}}_{\widehat{H}}$ and $\widehat{\mathcal{L}}_{\widehat{H}}^\pm$ are in one-to-one correspondence,

$$\widehat{H} \leftrightarrow \widehat{\mathcal{L}}_{\widehat{H}} \leftrightarrow \widehat{\mathcal{L}}_{\widehat{H}}^\pm, \quad (80)$$

where $\widehat{\mathcal{L}}_{\widehat{H}}^\pm$ are also the null geodesics since \mathcal{M}_\pm are the Killing horizons of $k_t^{\beta, \text{bulk}}$. More explicitly, $\widehat{\mathcal{L}}_{\widehat{H}}^\pm$ are the intersection lines between $\widehat{\mathcal{P}}_{\widehat{H}}$ and \mathcal{M}_\pm , i.e. the null geodesics connecting the endpoints of \mathcal{A} with \widehat{H} ,

$$\widehat{\mathcal{L}}_{\widehat{H}}^\pm : \rho(V) = -\frac{2l_V(l_V \mp 2V_{\widehat{H}})}{l_U(l_V \mp 2V)^2(l_V \pm 2V_{\widehat{H}})}, \quad U(V) = \frac{l_U(l_V(V - 2V_{\widehat{H}}) \pm 2VV_{\widehat{H}})}{l_V(l_V \mp 2V_{\widehat{H}})}, \quad (81)$$

see the red lines in Fig.7. In other words, \widehat{H} , $\widehat{\mathcal{L}}_{\widehat{H}}$ and $\widehat{\mathcal{L}}_{\widehat{H}}^\pm$ are respectively the intersections of $\widehat{\mathcal{P}}_{\widehat{H}}$ with the IRT surface $\widehat{\mathcal{E}}$, the asymptotic boundary and the null hypersurfaces \mathcal{M}_\pm .

4 Topological massive gravity and holographic entanglement entropy with gravitational anomaly

4.1 CFT₂ with gravitational anomaly and topological massive gravity

In this paper, the quantum field theory we study is the two-dimensional CFT with gravitational anomaly [70] in the vacuum on the plane. We will denote the CFT₂ with gravitational anomaly as CFT₂^a. Such theories are described by two copies of the Virasoro algebra with two unequal central charges c_L and c_R , and there is a breakdown of energy-momentum conservation at the quantum level [70]. Consider the same boundary spatial interval \mathcal{A} as described in (3). The entanglement entropy $S_{\mathcal{A}}$ for the interval \mathcal{A} can be obtained using the replica method [40], as we reviewed in appendix D,

$$\begin{aligned} S_{\mathcal{A}} &= \frac{c_L}{6} \log\left(\frac{l_U}{\epsilon_U}\right) + \frac{c_R}{6} \log\left(\frac{l_V}{\epsilon_V}\right) \\ &= \frac{c_L + c_R}{12} \log\left(\frac{l_U l_V}{\epsilon_U \epsilon_V}\right) + \frac{c_L - c_R}{12} \log\left(\frac{l_U l_V}{\epsilon_U \epsilon_V}\right). \end{aligned} \quad (82)$$

where ϵ_U and ϵ_V are the cutoffs along the U direction and V direction, respectively.

The asymptotic symmetry algebra of Einstein gravity has two equal central charges. In order to incorporate the effect of gravitational anomaly, we should consider the topological massive gravity (TMG) [27, 71] whose action includes an additional Chern-Simons (CS) term, namely

$$I_{\text{TMG}} = \frac{1}{16\pi G} \int d^3x \sqrt{-g} \left(R + \Lambda + \frac{1}{2\mu} \varepsilon^{\alpha\beta\gamma} \left(\Gamma^\rho_{\alpha\sigma} \partial_\beta \Gamma^\sigma_{\gamma\rho} + \frac{2}{3} \Gamma^\rho_{\alpha\sigma} \Gamma^\sigma_{\beta\eta} \Gamma^\eta_{\gamma\rho} \right) \right) \quad (83)$$

where $\Lambda = -2$ is the cosmological constant with a AdS₃ radius $\ell = 1$ and μ is the coupling constant that characterizes the interaction strength between the CS term and the Einstein-Hilbert term. We denote this correspondence as TMG₃/CFT₂^a correspondence. The Einstein

gravity can be recovered in the limit $\mu \rightarrow \infty$. Compared with the Einstein gravity, the left and the right central charges of the boundary CFT_2 of the TMG are not equal any more [72],

$$c_L = \frac{3}{2G} \left(1 + \frac{1}{\mu}\right), \quad c_R = \frac{3}{2G} \left(1 - \frac{1}{\mu}\right), \quad (84)$$

and the equation of motion is influenced by the CS term [40],

$$R_{\mu\nu} - \frac{1}{2}(R + 2)g_{\mu\nu} = -\frac{1}{\mu}C_{\mu\nu} \quad (85)$$

where $C_{\mu\nu}$ is the Cotton tensor. Therefore, the TMG also admits the locally AdS_3 solutions in the case that the Cotton tensor is vanishing. For example, the BTZ black hole solutions,

$$ds^2 = T_U^2 dU^2 + 2\rho dUdV + T_V^2 dV^2 + \frac{d\rho^2}{4(\rho^2 - T_U^2 T_V^2)}, \quad (86)$$

which can be written in the ADM form,

$$\begin{aligned} ds^2 &= -\frac{(r^2 - r_-^2)(r^2 - r_+^2)}{r^2} dt^2 + \frac{r^2}{(r^2 - r_-^2)(r^2 - r_+^2)} dr^2 + r^2 \left(d\varphi + \frac{r_+ r_-}{r^2} dt \right)^2 \\ &= -\left(r^2 + \frac{J^2}{4r^2} - M \right) dt^2 + \frac{1}{\left(r^2 + \frac{J^2}{4r^2} - M \right)} dr^2 + r^2 \left(d\varphi + \frac{J}{2r^2} dt \right)^2, \end{aligned} \quad (87)$$

by the following coordinate transformations,

$$\begin{aligned} U &= \frac{\varphi + t}{2}, \quad V = \frac{\varphi - t}{2}, \quad \rho = 2r^2 - r_-^2 - r_+^2, \\ T_U &= r_+ + r_-, \quad T_V = r_+ - r_-, \end{aligned} \quad (88)$$

and M, J are the physical conserved charges in the Einstein gravity,

$$M = r_+^2 + r_-^2, \quad J = 2r_+ r_-. \quad (89)$$

However, due to the presence of the CS term, the physical conserved charges in the TMG get shifted [72, 73],

$$\mathcal{M} = M + \frac{J}{\mu}, \quad \mathcal{J} = J + \frac{M}{\mu}. \quad (90)$$

The black hole entropy in such theories is derived in [31] based on the Wald formula [74–76], and the result shows that the correction of the thermal entropy for the outer horizon from the CS term is proportional to the area (or the length) of the inner horizon [28–31],

$$S_{\text{outer}} = \frac{\ell_{\text{outer horizon}}}{4G} + \frac{\ell_{\text{inner horizon}}}{4G\mu} \quad (91)$$

where the length of the horizons comes from the integration for their induced metrics. As we reviewed in Sec.2.1, the entanglement entropy of the interval \mathcal{A} (3) is mapped to the thermal entropy of the outer horizon of Rindler AdS_3 (9). The length of the inner horizon of the Rindler AdS_3 (9) is given by,

$$\ell_{\text{inner horizon}} = T_{\tilde{U}} \Delta \tilde{U} - T_{\tilde{V}} \Delta \tilde{V} = \log \left(\frac{l_U \epsilon_V}{l_V \epsilon_U} \right), \quad (92)$$

where $\Delta\tilde{U}$ and $\Delta\tilde{V}$ are the lengths of $\tilde{\mathcal{A}}^{\text{reg}}$ along the U direction and the V direction, as described in (16). Substituting (18), (92) into (91), we obtain the (regulated) holographic entanglement entropy with gravitational anomaly,

$$S_{\mathcal{A}} = S_{\mathcal{A}}^n + S_{\mathcal{A}}^a = \frac{1}{4G} \log\left(\frac{l_U l_V}{\epsilon_U \epsilon_V}\right) + \frac{1}{4\mu G} \log\left(\frac{l_U \epsilon_V}{l_V \epsilon_U}\right), \quad (93)$$

which is exactly the same as the result (82) evaluated by the replica method with the central charges (84). Here, the first term $S_{\mathcal{A}}^n$ represents the contribution from the Einstein-Hilbert action, while the second term $S_{\mathcal{A}}^a$ represents the correction from the CS term, which we refer to as the normal part and the anomalous part of the entanglement entropy respectively. In [40], the authors set the cutoffs to be $\epsilon_U = \epsilon_V = \epsilon$, then the entanglement entropy $S_{\mathcal{A}}$ is given by,

$$S_{\mathcal{A}} = S_{\mathcal{A}}^n + S_{\mathcal{A}}^a = \frac{1}{4G} \log\left(\frac{l_U l_V}{\epsilon^2}\right) + \frac{1}{4\mu G} \log\left(\frac{l_U}{l_V}\right). \quad (94)$$

4.2 Bulk description with gravitational anomaly

In [40], the authors proposed a bulk description for the holographic entanglement entropy with gravitational anomaly by generalizing the LM prescription [17]. They claimed that the holographic entanglement entropy can be obtained by extremizing a worldline action for a spinning particle in the AdS_3 bulk, which we refer to as the *twist description* in this paper,

$$S_{\text{HEE}} = \frac{1}{4G} \int_C d\tau \left(\sqrt{g_{\mu\nu} \dot{X}^\mu \dot{X}^\nu} + \frac{1}{\mu} \tilde{\mathbf{n}} \cdot \nabla \mathbf{n} \right), \quad (95)$$

where C represents the worldline of a spinning particle, τ is the length parameter, \dot{X}^μ is the tangent vector to the worldline, $\tilde{\mathbf{n}}$ and \mathbf{n} are unit spacelike and timelike vectors respectively which are orthogonal to each other and also orthogonal to the tangent vector \dot{X}^μ , i.e.

$$\tilde{\mathbf{n}}^2 = 1, \quad \mathbf{n}^2 = -1, \quad \mathbf{n} \cdot \tilde{\mathbf{n}} = 0, \quad \tilde{\mathbf{n}} \cdot \dot{X} = 0, \quad \mathbf{n} \cdot \dot{X} = 0, \quad (96)$$

and ∇ presents the covariant derivative along the worldline,

$$\nabla \mathbf{n} := \dot{X}^\mu \nabla_\mu \mathbf{n}. \quad (97)$$

For the Poincaré AdS_3 , the solution to this worldline action is precisely the RT surface \mathcal{E}^{14} , hence the first term in (95) represents the length of the RT surface. The second term presents the correction from the CS term which we denote as S_{CS} . Interestingly, the integrand in S_{CS} can be rewritten as a total derivative [40],

$$\tilde{\mathbf{n}} \cdot \nabla \mathbf{n} = \partial_\tau \log((\mathbf{q} - \tilde{\mathbf{q}}) \cdot \mathbf{n}), \quad (98)$$

hence the value of S_{CS} only depends on the boundary,

$$S_{CS} = \frac{1}{4\mu G} \log\left(\frac{\mathbf{q}(\tau_f) \cdot \mathbf{n}_f - \tilde{\mathbf{q}}(\tau_f) \cdot \mathbf{n}_f}{\tilde{\mathbf{q}}(\tau_i) \cdot \mathbf{n}_i - \tilde{\mathbf{q}}(\tau_i) \cdot \mathbf{n}_i}\right), \quad (99)$$

where the subscripts f and i present the final and the initial points of the worldline respectively, and the two vectors \mathbf{q} and $\tilde{\mathbf{q}}$ determine a reference parallel transported normal frame satisfying,

$$\begin{aligned} \mathbf{q}^2 &= -1, & \tilde{\mathbf{q}}^2 &= 1, & \mathbf{q} \cdot \dot{X} &= 0, & \tilde{\mathbf{q}} \cdot \dot{X} &= 0, \\ \mathbf{q} \cdot \tilde{\mathbf{q}} &= 0, & \nabla \mathbf{q} &= 0, & \nabla \tilde{\mathbf{q}} &= 0. \end{aligned} \quad (100)$$

¹⁴When the bulk spacetime is not locally AdS_3 spacetime, there could be some non-geodesic solutions for the worldline action (95) [40]. One can consult [40, 77–79] for more discussions about the worldline action (95).

In this paper, we only focus on the locally AdS₃ spacetime, such that the solution to this worldline action is precisely the RT surface \mathcal{E} (14). And the explicit expressions of the reference normal frame $\{\mathbf{q}, \tilde{\mathbf{q}}\}$ are given by,

$$\begin{aligned}\mathbf{q} &= \frac{1}{\sqrt{2l_U l_V \rho}} (l_U \partial_U - l_V \partial_V), \\ \tilde{\mathbf{q}} &= \sqrt{\frac{2}{l_U l_V \rho}} \left(-\frac{l_U (U+V)}{l_U + l_V} \partial_U - \frac{l_V (U+V)}{l_U + l_V} \partial_V + 2\rho \partial_\rho \right),\end{aligned}\tag{101}$$

up to an overall sign depends on a choice of handedness. If taking the following boundary condition for \mathbf{n} ,

$$\mathbf{n}_i = \mathbf{n}_f \propto \partial_t,\tag{102}$$

where t is the temporal coordinate of the boundary CFT₂, it has been verified in [40] that S_{CS} for this boundary condition exactly matches the anomalous part $S_{\mathcal{A}}^a$ (94) with the cutoffs being $\epsilon_U = \epsilon_V = \epsilon$. Furthermore, in Sec.6, we point out that this boundary condition (102) of \mathbf{n} indeed comes from a specific regulation $\epsilon_U = \epsilon_V$, see (156). Nevertheless, although we have fixed the boundary condition for \mathbf{n} , the specific value of \mathbf{n} remains highly non-unique over the entire RT surface. More importantly, unlike the RT surface, the twist description is not purely geometric, which poses difficulties for calculating or even defining the anomalous part of the PEE, as well as the EWCS. One main purpose of this paper is to search for a purely geometric picture of the anomalous part such that $S_{\mathcal{A}}^a$ corresponds to the area (or length) of some newly-defined geometric quantity under a proper regulation, similarly to the case of the RT prescription.

4.3 Gravitational anomalous entanglement from the inner RT surface

According to (91), the correction of the thermal entropy for the outer horizon from the CS term is proportional to the length of the inner horizon, hence it is natural to think that the anomalous entropy, entanglement entropy and PEE could be represented by the area of certain sub-region on the inner horizon or the IRT surface $\hat{\mathcal{E}}$ (31), which we refer to as the *IRT description*. In this section, we realize this idea and find the same results as those obtained by using the normal frames (99). Again let us begin with the regularized interval, and its image in the Rindler AdS₃:

$$\mathcal{A}^{\text{reg}} : (-l_U/2 + \epsilon_U, -l_V/2 + \epsilon_V) \rightarrow (l_U/2 - \epsilon_U, l_V/2 - \epsilon_V),\tag{103}$$

$$\tilde{\mathcal{A}}^{\text{reg}} : (-\Delta\tilde{U}/2, -\Delta\tilde{V}/2) \rightarrow (\Delta\tilde{U}/2, \Delta\tilde{V}/2),\tag{104}$$

where $\Delta\tilde{U} = \frac{1}{T_{\tilde{U}}} \log\left(\frac{l_U}{\epsilon_U}\right)$, $\Delta\tilde{V} = \frac{1}{T_{\tilde{V}}} \log\left(\frac{l_V}{\epsilon_V}\right)$. As we have reviewed, after the Rindler transformation, the reduced density matrix $\rho_{\mathcal{A}}$ is mapped to a thermal state in the Rindler spacetime with translation symmetries along \tilde{x} and \tilde{t} directions, hence the entanglement contour for both the entanglement entropy and the timelike entanglement entropy is flat, and the two entanglement entropies satisfy the volume law. After the regulation, the length of $\tilde{\mathcal{A}}^{\text{reg}}$ is measurable, and we can compute the entanglement entropy by calculating the regulated lengths of its partner geodesic chords on the horizons, for example the normal part of the entanglement entropy is calculated by the length of its partner geodesic chord on the outer horizon (18), while the anomalous part of the entanglement entropy comes from the length of its partner on the inner horizon (92).

Firstly, let us consider the normal part of the entanglement entropy and ignore the anomalous contribution. Actually, what we are computing is the contribution to the entropy $S_{\tilde{\mathcal{A}}}^n$ of the Rindler AdS₃ from the regulated interval $\tilde{\mathcal{A}}^{\text{reg}}$, i.e. the PEE $s_{\tilde{\mathcal{A}}}^n(\tilde{\mathcal{A}}^{\text{reg}})|_{\tilde{\mathcal{A}}^{\text{reg}} \rightarrow \tilde{\mathcal{A}}}$. Here $\tilde{\mathcal{A}}$ is the

image of \mathcal{A} which has infinite length. Since the PEE structure is invariant under the Rindler transformations, which are symmetries of the CFT, we should have

$$s_{\tilde{\mathcal{A}}}^n(\tilde{\mathcal{A}}^{\text{reg}})|_{\tilde{\mathcal{A}}^{\text{reg}} \rightarrow \tilde{\mathcal{A}}} = s_{\mathcal{A}}^n(\mathcal{A}^{\text{reg}})|_{\mathcal{A}^{\text{reg}} \rightarrow \mathcal{A}} = S_{\mathcal{A}}^n. \quad (105)$$

The next step is to identify the partner geodesic chord \mathcal{E}^{reg} of \mathcal{A}^{reg} on the RT surface \mathcal{E} , hence we can compute the PEE using the correspondence (54) between the PEE and geodesic chords on the RT surface \mathcal{E} . The computation is now straightforward by replacing the \mathcal{A}_i in (56) and (57) by \mathcal{A}^{reg} (103). After we ignore the higher order terms $\mathcal{O}(\epsilon^2)$, we get

$$S_{\mathcal{A}}^n = \frac{1}{4G} \log \left(\frac{l_U l_V}{\epsilon_U \epsilon_V} \right). \quad (106)$$

Then we compute the anomalous part of the entanglement entropy using the same prescription,

$$s_{\tilde{\mathcal{A}}}^a(\tilde{\mathcal{A}}^{\text{reg}})|_{\tilde{\mathcal{A}}^{\text{reg}} \rightarrow \tilde{\mathcal{A}}} = s_{\mathcal{A}}^a(\mathcal{A}^{\text{reg}})|_{\mathcal{A}^{\text{reg}} \rightarrow \mathcal{A}} = S_{\mathcal{A}}^a. \quad (107)$$

Since the anomalous part of the thermal entropy for the Rindler $\widetilde{\text{AdS}}_3$ is proportional to the area of the inner horizon with a coefficient $1/(4\mu G)$, the correspondence between the anomalous PEE (*APEE*) $s_{\mathcal{A}}^a(\mathcal{A}_i)$ and the area of the partner geodesic chord should be modified accordingly,

$$\begin{aligned} s_{\mathcal{A}}^a(\mathcal{A}^{\text{reg}}) &= \frac{\text{Length}(\hat{\mathcal{E}}^{\text{reg}})}{4G\mu} = \frac{\hat{\lambda}(Q) - \hat{\lambda}(P)}{4G} \\ &= \frac{1}{4\mu G} \log \left(\frac{l_U \epsilon_V}{l_V \epsilon_U} \right) \end{aligned} \quad (108)$$

where P and Q are the left and the right endpoints of \mathcal{A}^{reg} , and we have replaced $\hat{\mathcal{A}}_i$ in (76) with \mathcal{A}^{reg} (103), and ignore the higher order terms $\mathcal{O}(\epsilon^2)$. Finally we get the entanglement entropy (93) for intervals in gravitational anomalous CFT_2 , which coincides with the results obtained in [41].

One can also identify the partner geodesic chord of \mathcal{A}^{reg} on the IRT surface using a prescription similar to the so-called swing surface prescription using null geodesics emanating from the endpoints of \mathcal{A} . This prescription indeed uses the intersection lines (which are null lines) between the modular momentum slices and the inner horizon in the Rindler $\widetilde{\text{AdS}}_3$. Nevertheless, in the original AdS_3 , the image of these null lines all anchor on the boundary at the endpoints of \mathcal{A} , we need further input to clarify which null line gives the correspondence between the endpoints of \mathcal{A}^{reg} and their partner points on $\hat{\mathcal{E}}$. When taking the flat limit, we recover the swing surface picture proposed in [16], see appendix E for more details.

5 BPE and EWCS with gravitational anomaly

5.1 A brief introduction to the BPE with gravitational anomaly

In general, the balanced partial entanglement entropy (BPE) is a special PEE that satisfies the certain balanced conditions and is claimed to be dual to the EWCS [61, 62]. In [61, 62], it was shown that the BPE exactly captures the same type of mixed state correlations as the reflected entropy, and is conjectured to be purification independent. These conjectures have passed various tests [41, 57, 61, 62, 65, 67].

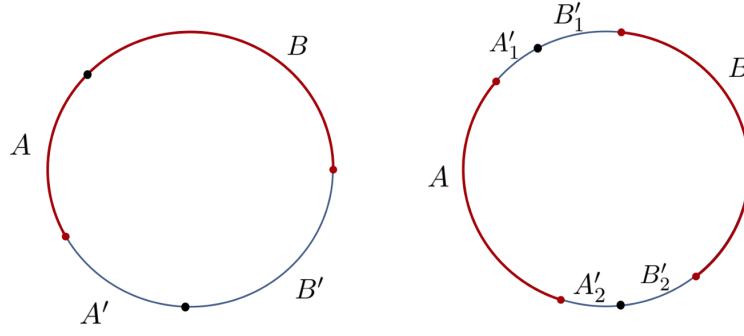


Figure 9: The figures are extracted from [61]. The region $A'B'$ serves as an auxiliary system to purify the bipartite system ρ_{AB} . The left figure represents the adjacent case. While the right figure represents the non-adjacent case, where we need to make a further separation, $A' = A'_1 \cup A'_2$ and $B' = B'_1 \cup B'_2$.

Consider a bipartite system $\mathcal{H}_A \otimes \mathcal{H}_B$ with the density matrix ρ_{AB} , we can introduce an auxiliary system $A'B'$ to purify it such that the whole system $ABA'B'$ is in a pure state $|\psi\rangle$, and satisfies $\text{Tr}_{A'B'} = \rho_{AB}$. Then the BPE between A and B is defined as,

$$\text{BPE}(A, B) = s_{AA'}(A) |_{\text{balanced}} \quad (109)$$

where the subscript “balanced” means that the partition of the auxiliary system $A'B'$ should satisfy the balance conditions, which are listed in the following:

1. When A and B are adjacent, the balance condition is¹⁵,

$$s_{AA'}(A) = s_{BB'}(B). \quad (110)$$

2. When A and B are non-adjacent, we need to further decompose the disconnected regions, $A' = A'_1 \cup A'_2$ and $B' = B'_1 \cup B'_2$. In this case, we have two balance conditions,

$$s_{AA'}(A) = s_{BB'}(B), \quad s_{AA'}(A'_1) = s_{BB'}(B'_1). \quad (111)$$

See Fig.9 for an illustration. The partition points in the auxiliary system $A'B'$ are called the balanced points which are determined by the balance conditions. When the gravitational anomaly is taken into account, the normal part and the anomalous part of the holographic entanglement entropy should satisfy the balance conditions independently [41, 80], for example in the adjacent cases we should have,

$$s_{AA'}^n(A) = s_{BB'}^n(B), \quad s_{AA'}^a(A) = s_{BB'}^a(B), \quad (112)$$

and the BPE can also be decomposed into two parts

$$\text{BPE}^n(A, B) = s_{AA'}^n(A) |_{\text{balanced}} \quad \text{BPE}^a(A, B) = s_{AA'}^a(A) |_{\text{balanced}} \quad (113)$$

For various covariant configurations in the gravitational anomalous CFT_2 , both the normal and the anomalous parts of the $\text{BPE}(A, B)$ have been carried out carefully using the ALC proposal (42) in [41]. For example, let us consider the configurations in the right figure of Fig.9, where A'_1 and A'_2 satisfy the balance condition. Using the ALC proposal, the $\text{BPE}^a(A, B)$ is,

$$\text{BPE}^a(A, B) = s_{A'_1 A'_2}^a(A) |_{\text{balanced}} = \frac{1}{2} \left(S_{A'_1 A}^a + S_{AA'_2}^a - S_{A'_1}^a - S_{A'_2}^a \right). \quad (114)$$

¹⁵In fact, the solution to the balance conditions may not be unique. In such cases, we choose the minimal one as our definition, which called the minimal condition [61].

Following our analysis on the fine structure of the extended entanglement wedge, the APEE $s_{A_1'AA_2'}^a(A)$ also has a geometric picture, which is the partner geodesic chord of A on the IRT surface $\widehat{\mathcal{E}}_{A_1'AA_2'}$ of $A_1'AA_2'$, we call this geodesic chord $\widehat{\mathcal{E}}_{A_1'AA_2'}(A)$. More explicitly, we have,

$$s_{A_1'AA_2'}^a(A) = \frac{\text{Length}(\widehat{\mathcal{E}}_{A_1'AA_2'}(A))}{4\mu G}. \quad (115)$$

The computation can be explicitly done by adapting this configuration to the formula (76). As we have shown, the ALC proposal and the geometric picture coincide, hence (115) and (114) give the same result. Since the BPE is a special PEE that satisfies the balanced condition (111), its anomalous part $\text{BPE}^a(A, B)$ has a natural geometric interpretation in terms of sub-regions of the inner horizon or IRT surface, which is the main topic in this section.

On the gravity side, the length of the EWCS is no longer enough to reproduce both of the normal and the anomalous parts of the $\text{BPE}(A, B)$. We can also decompose the gravity dual of the $\text{BPE}(A, B)$ into the normal part and the anomalous part, i.e.

$$E_W(A, B) = E_W^n(A, B) + E_W^a(A, B), \quad (116)$$

where the normal part is given by

$$E_W^n(A, B) = \frac{1}{4G} \text{Length}(\Sigma_{AB}), \quad (117)$$

with Σ_{AB} representing the EWCS of the entanglement wedge \mathcal{W}_{AB} . As in the non-anomalous configurations [61, 62], the length of the EWCS matches the normal part of the BPE (see also [41] for the covariant configurations)

$$E_W^n(A, B) = \text{BPE}^n(A, B) = \frac{1}{4G} \text{Length}(\Sigma_{AB}). \quad (118)$$

One the other hand, the anomalous part $E_W^a(A, B)$ is supposed to be the geometric picture for the anomalous part of the BPE. Since the normal part $E_W^n(A, B)$ matches the $\text{BPE}^n(A, B)$, we expect the anomalous part $E_W^a(A, B)$ to match $\text{BPE}^a(A, B)$. According to our previous discussion, the geometric picture for the anomalous part is just the geodesic chord on the IRT surface $\widehat{\mathcal{E}}_{A_1'AA_2'}(A)$, hence we should have

$$E_W^a(A, B) = \text{BPE}^a(A, B) = \frac{1}{4\mu G} \text{Length}(\widehat{\mathcal{E}}_{A_1'AA_2'}(A)). \quad (119)$$

Another construction for the geometric picture of $\text{BPE}^a(A, B)$ was given in [41] using the twist description [40]. Unlike the case for the RT surface, the end points of the EWCS are settled in the bulk, naively choosing the time direction as the normal vector in the normal frame is not well motivated, and furthermore the time direction is in general not normal to the EWCS. Interestingly, since the EWCS anchors on the RT surfaces of AB vertically, the authors of [41] proposed that, spacelike normal vector $\tilde{\mathbf{n}}$ can be chosen to be the tangent vector of the RT surfaces of AB . With the normal vectors $\tilde{\mathbf{n}}_i$ and $\tilde{\mathbf{n}}_f$ at the endpoints of the EWCS determined, we can compute the CS correction to the EWCS by (99), and the results exactly match the anomalous part of the BPE,

$$\text{BPE}^a(A, B) = \frac{1}{4\mu G} \log \left(\frac{\mathbf{q}(\tau_f) \cdot \mathbf{n}_f - \tilde{\mathbf{q}}(\tau_f) \cdot \mathbf{n}_f}{\tilde{\mathbf{q}}(\tau_i) \cdot \mathbf{n}_i - \tilde{\mathbf{q}}(\tau_i) \cdot \mathbf{n}_i} \right). \quad (120)$$

Both \mathbf{n}_i and \mathbf{n}_f can be determined up to an overall sign according to a choice of handedness. Here we only need to choose the signs to ensure that the term inside the logarithm is positive. This result also coincide with the reflected entropy [81] for gravitational anomalous CFT_2 [82].

In this section, we demonstrate that the geodesic chord $\widehat{\mathcal{E}}_{A_1 A_2}^a(A)$ is also the saddle geodesic connecting the two pieces of the IRT surface $\widehat{\mathcal{E}}_{AB}$ of $A \cup B$, which is exactly the same as the EWCS Σ_{AB} . Furthermore, in the next section, we discuss the geometric construction of the APEE in the twist description, based on the fine structure of the extended entanglement wedge. In that context, we point out that the right hand side of (120) indeed evaluates the APEE $s_{A_1 A_2}^a(A)$, which explains the equality between the two sides of (120), see appendix F for details.

5.2 A case study of non-adjacent intervals

5.2.1 BPEⁿ(A, B) and the EWCS

Let us give an explicit example of two non-adjacent intervals A and B with connected entanglement wedge \mathcal{W}_{AB} , where

$$A : (U_1, V_1) \rightarrow (U_2, V_2), \quad B : (U_3, V_3) \rightarrow (U_4, V_4) \quad (121)$$

Due to the conformal symmetry, the EWCS only depends on two conformal invariants η and $\bar{\eta}$,

$$\eta = \frac{(V_2 - V_1)(V_4 - V_3)}{(V_3 - V_1)(V_4 - V_2)}, \quad \bar{\eta} = \frac{(U_2 - U_1)(U_4 - U_3)}{(U_3 - U_1)(U_4 - U_2)}. \quad (122)$$

Therefore, without losing generality, we can fix three endpoints of the interval A, B , and set the parameters (U_4, V_4) free, for example,

$$U_1 = V_1 = 0, \quad U_2 = V_2 = \frac{1}{2}, \quad U_3 = V_3 = \frac{3}{2}. \quad (123)$$

Furthermore, it is convenient to rewrite the parameters (U_4, V_4) in terms of the conformal invariants $(\eta, \bar{\eta})$ which can simplify the calculation,

$$U_4 = \frac{3(\bar{\eta} - 1)}{2(3\bar{\eta} - 1)}, \quad V_4 = \frac{3(\eta - 1)}{2(3\eta - 1)}. \quad (124)$$

Since the the entanglement wedge is connected, the RT surface has two pieces $\mathcal{E}_{AB} = \mathcal{E}_1 \cup \mathcal{E}_2$, which are given by,

$$\begin{aligned} \mathcal{E}_1 : \rho(V) &= \frac{(\eta - 1)(3\bar{\eta} - 1)}{V(3\eta - 3 - 2V(3\eta - 1))(\bar{\eta} - 1)}, & U(V) &= \frac{(3\eta - 1)(\bar{\eta} - 1)}{(\eta - 1)(3\bar{\eta} - 1)}V, \\ \mathcal{E}_2 : \rho(V) &= -\frac{2}{3 + 4(-2 + V)V}, & U(V) &= V, \end{aligned} \quad (125)$$

where \mathcal{E}_1 and \mathcal{E}_2 are also the RT surfaces of $AA_2 B_2' B$ and $A_2' B_2'$, respectively, see Fig.10. As we discussed above, the Σ_{AB} is a type I spacelike geodesic¹⁶ connecting the RT surfaces \mathcal{E}_1 and \mathcal{E}_2 while satisfying the extremal condition,

$$\frac{\partial L(U_{H_1}, V_{H_1}, \rho_{H_1}, U_{H_2}, V_{H_2}, \rho_{H_2})}{\partial U_{H_1}} = \frac{\partial L(U_{H_1}, V_{H_1}, \rho_{H_1}, U_{H_2}, V_{H_2}, \rho_{H_2})}{\partial U_{H_2}} = 0, \quad (126)$$

where $L(U_{H_1}, V_{H_1}, \rho_{H_1}, U_{H_2}, V_{H_2}, \rho_{H_2})$ represents the proper distance (B.5) between H_1 and H_2 , and H_1 and H_2 are the points where Σ_{AB} anchors on \mathcal{E}_1 and \mathcal{E}_2 , see Fig.10. The solution of this extremal condition is given by,

$$V_{H_1} = \frac{3(\eta - 1)(3\bar{\eta} - 1)}{2 + 8\sqrt{\eta\bar{\eta}} - 6\bar{\eta} + 6\eta(3\bar{\eta} - 1)}, \quad V_{H_2} = \frac{1}{2} + \frac{1}{1 + 9\sqrt{\eta\bar{\eta}}}, \quad (127)$$

¹⁶Here ‘‘type I’’ means that Σ and its extension can be referred to as the RT surface of a certain boundary interval. See appendix B for details.

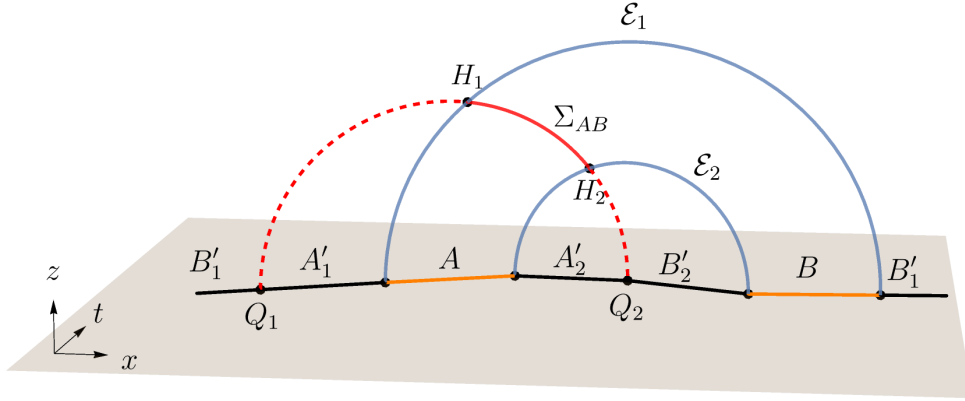


Figure 10: Extracted from [41]. Illustration for the EWCS in the non-adjacent case. The extension of the EWCS Σ_{AB} intersects with the asymptotic boundary at the two points Q_1 and Q_2 .

hence, we arrive at,

$$E_W^n(A, B) = \frac{1}{4G} \text{Length}(\Sigma_{AB}) = \frac{1}{8G} \log \frac{(\sqrt{\eta} + 1)(\sqrt{\bar{\eta}} + 1)}{(\sqrt{\eta} - 1)(\sqrt{\bar{\eta}} - 1)}. \quad (128)$$

Following [41], we can extend Σ_{AB} to an RT surface that anchors on the boundary at Q_1 and Q_2 . The RT surface corresponds to the boundary interval $A'_1 A A'_2$ shown in Fig.10. The equation of Σ_{AB} with its extension is¹⁷,

$$\rho(V) = \frac{2\tilde{l}_V}{\tilde{l}_U(\tilde{l}_V^2 - 4(V - V_0)^2)}, \quad U(V) = \frac{\tilde{l}_U}{\tilde{l}_V}(V - V_0) + U_0, \quad (129)$$

according to (B.3) and (127), the parameters $(\tilde{l}_U, \tilde{l}_V, V_0, U_0)$ are given by,

$$\tilde{l}_U = \frac{6\sqrt{\bar{\eta}}}{9\bar{\eta} - 1}, \quad \tilde{l}_V = \frac{6\sqrt{\eta}}{9\eta - 1}, \quad V_0 = \frac{3(1 - 3\eta)}{2(1 - 9\eta)}, \quad U_0 = \frac{3(1 - 3\bar{\eta})}{2(1 - 9\bar{\eta})}, \quad (130)$$

hence the extension of the Σ_{AB} intersects with the asymptotic boundary at the two points $Q_1 = (U_{Q_1}, V_{Q_1})$ and $Q_2 = (U_{Q_2}, V_{Q_2})$, see Fig.10,

$$\begin{aligned} U_{Q_1} &= -\frac{\tilde{l}_U}{2} + \tilde{y} = \frac{1}{2} - \frac{1}{3\sqrt{\bar{\eta}} - 1}, & V_{Q_1} &= -\frac{\tilde{l}_V}{2} + \tilde{x} = \frac{1}{2} - \frac{1}{3\sqrt{\eta} - 1} \\ U_{Q_2} &= \frac{\tilde{l}_U}{2} + \tilde{y} = \frac{1}{2} + \frac{1}{3\sqrt{\bar{\eta}} + 1}, & V_{Q_2} &= \frac{\tilde{l}_V}{2} + \tilde{x} = \frac{1}{2} + \frac{1}{3\sqrt{\eta} + 1}. \end{aligned} \quad (131)$$

Without loss of generality, we suppose that A have a smaller size than that of B , i.e.

$$U_4 - U_3 > U_2 - U_1, \quad V_4 - V_3 > V_2 - V_1 \Leftrightarrow \frac{1}{9} < \eta, \bar{\eta} < \frac{1}{3}, \quad (132)$$

such that the point Q_1 is on the left of the interval A . Otherwise, it would be on the right-hand side of B . The points Q_1, Q_2 and the endpoints of AB make a decomposition for the time slice

¹⁷We hope that the same symbols “ $(\tilde{l}_U, \tilde{l}_V, V_0, U_0)$ ” with different meanings in (46) and (129) do not cause any confusion.

where the bipartite system AB are settled on, see Fig.10. Given the partition points Q_1 and Q_2 , then A'_1, A'_2, B'_1 and B'_2 regions are also determined. In [41], the authors show that balance conditions (112) are satisfied by this partition. Therefore,

$$\begin{aligned} \text{BPE}^n(A, B) &= s_{A'_1 A'_2}^n(A) = s_{B'_1 B'_2}^n(B) = \frac{1}{8G} \log \frac{(\sqrt{\eta} + 1)(\sqrt{\bar{\eta}} + 1)}{(\sqrt{\eta} - 1)(\sqrt{\bar{\eta}} - 1)}, \\ \text{BPE}^a(A, B) &= s_{A'_1 A'_2}^a(A) = s_{B'_1 B'_2}^a(B) = \frac{1}{8\mu G} \log \frac{(\sqrt{\eta} - 1)(\sqrt{\bar{\eta}} + 1)}{(\sqrt{\eta} + 1)(\sqrt{\bar{\eta}} - 1)} \end{aligned} \quad (133)$$

where the PEEs and the APEEs are calculated by the ALC proposal. Hence, we conclude that,

$$E_W^n(A, B) = \frac{1}{4G} \text{Length}(\Sigma_{AB}) = s_{A'_1 A'_2}^n(A)|_{\text{balanced}} = \text{BPE}^n(A, B). \quad (134)$$

5.2.2 $\text{BPE}^a(A, B)$ and the inner EWCS

Given the partition points Q_1 and Q_2 (131), we can also compute the length of the partner geodesic chord $\widehat{\mathcal{E}}_{A'_1 A'_2}(A)$, and verify the coincidence between it and $\text{BPE}^a(A, B)$ (133). More explicitly, for an arbitrary boundary point $P = (U_p, V_p)$ in the casual development of the interval $A'_1 A'_2$, the function $\widehat{\lambda}(P)$ is given by (74),

$$\widehat{\lambda}(P) = \frac{1}{2} \log \left(\frac{[\widetilde{l}_U + 2(U_p - U_0)][\widetilde{l}_V - 2(V_p - V_0)]}{[\widetilde{l}_U - 2(U_p - U_0)][\widetilde{l}_V + 2(V_p - V_0)]} \right), \quad (135)$$

where the parameters $(\widetilde{l}_U, \widetilde{l}_V, V_0, U_0)$ are specified by (130). Therefore, the anomalous part $E_W^a(A, B)$ is,

$$\begin{aligned} E_W^a(A, B) &= \frac{\text{Length}(\widehat{\mathcal{E}}_{A'_1 A'_2}(A))}{4\mu G} = \frac{\widehat{\lambda}(P_2) - \widehat{\lambda}(P_1)}{4\mu G} \\ &= \frac{1}{8\mu G} \log \frac{(\sqrt{\eta} - 1)(\sqrt{\bar{\eta}} + 1)}{(\sqrt{\eta} + 1)(\sqrt{\bar{\eta}} - 1)}, \end{aligned} \quad (136)$$

where P_1 and P_2 are the left and the right endpoints of A respectively, as specified by (121). More importantly, the result aligns exactly with the $\text{BPE}^a(A, B)$ (133) evaluated by the ALC proposal.

More interestingly, we find that the partner geodesic chord $\widehat{\mathcal{E}}_{A'_1 A'_2}(A)$ is also the saddle geodesic that connecting the two pieces of the IRT surface $\widehat{\mathcal{E}}_{AB}$ of AB , which we call the inner EWCS (or IEWCS for short). In such a way, the calculation of $E_W^a(A, B)$ is also an optimization problem, which is the same as the calculation of $E_W^n(A, B)$. Since the entanglement wedge \mathcal{W}_{AB} is in the connected phase, and the RT surface $\mathcal{E}_{AB} = \mathcal{E}_1 \cup \mathcal{E}_2$, where \mathcal{E}_1 and \mathcal{E}_2 are also the RT surfaces of $AA'_2 B'_2 B$ and $A'_2 B'_2$, respectively. It is natural to take the IRT surface for AB to be,

$$\widehat{\mathcal{E}}_{AB} = \widehat{\mathcal{E}}_1 \cup \widehat{\mathcal{E}}_2, \quad (137)$$

which is the union of the two IRT surfaces of $AA'_2 B'_2 B$ and $A'_2 B'_2$, see Fig.11. More explicitly, we can write down the functions for these two IRT surfaces,

$$\begin{aligned} \widehat{\mathcal{E}}_1 : \rho(V) &= \frac{(\eta - 1)(3\bar{\eta} - 1)}{V(3 - 2V + 3(2V - 1)\eta)(\bar{\eta} - 1)}, \\ U(V) &= \frac{(3 - 2V + 3(2V - 1)\eta)(1 - \bar{\eta})}{2(\eta - 1)(3\bar{\eta} - 1)} \\ \widehat{\mathcal{E}}_2 : \rho(V) &= \frac{2}{3 + 4(-2 + V)V}, \\ U(V) &= 2 - V \end{aligned} \quad (138)$$

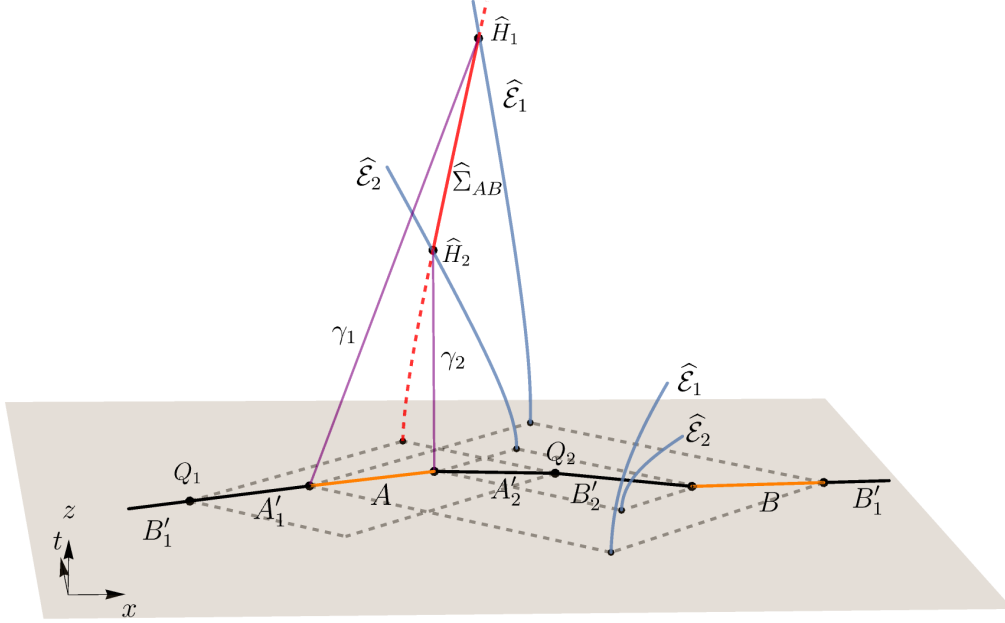


Figure 11: Illustration for the anomalous part $E_W^a(A, B)$ in the non-adjacent case. The dashed line represents the boundary of the causal development. The purple lines γ_1 and γ_2 represent the null geodesics. The IEWCS $\hat{\Sigma}_{AB}$ (the red solid line) and its extension (the red dashed line) can be referred to as the IRT surface of the interval $A'_1AA'_2$ whose endpoints are also Q_1 and Q_2 .

Similarly, the IEWCS $\hat{\Sigma}_{AB}$ is the saddle type II spacelike geodesic¹⁸ connecting the IRT surfaces $\hat{\mathcal{E}}_1$ and $\hat{\mathcal{E}}_2$. To calculate the IEWCS $\hat{\Sigma}_{AB}$, we also impose the extremal condition,

$$\frac{\partial L(U_{\hat{H}_1}, V_{\hat{H}_1}, \rho_{\hat{H}_1}, U_{\hat{H}_2}, V_{\hat{H}_2}, \rho_{\hat{H}_2})}{\partial U_{\hat{H}_1}} = \frac{\partial L(U_{\hat{H}_1}, V_{\hat{H}_1}, \rho_{\hat{H}_1}, U_{\hat{H}_2}, V_{\hat{H}_2}, \rho_{\hat{H}_2})}{\partial U_{\hat{H}_2}} = 0, \quad (139)$$

were we also take $L(U_{\hat{H}_1}, V_{\hat{H}_1}, \rho_{\hat{H}_1}, U_{\hat{H}_2}, V_{\hat{H}_2}, \rho_{\hat{H}_2})$ as (B.5), which represents the proper distance between \hat{H}_1 and \hat{H}_2 but may differ by a negative sign, depending on whether \hat{H}_1 and \hat{H}_2 are on the same sector of the type II spacelike geodesic, see appendix B for details. Nevertheless, the overall sign does not affect our discussion, since it does not affect the solution of this extremal condition. And \hat{H}_1 and \hat{H}_2 are the intersection points of $\hat{\Sigma}_{AB}$ with the IRT surfaces $\hat{\mathcal{E}}_{AA'_2B'_2B}$ and $\hat{\mathcal{E}}_{A'_2B'_2}$ respectively, see Fig.11. The solution of this extremal condition is given by,

$$V_{\hat{H}_1} = \frac{3(\eta-1)\sqrt{\eta}}{2(\sqrt{\eta}-\sqrt{\eta})(1+3\sqrt{\eta\eta})}, \quad V_{\hat{H}_2} = \frac{3}{2} + \frac{\sqrt{\eta}}{\sqrt{\eta}-\sqrt{\eta}}. \quad (140)$$

Interestingly, $\hat{\Sigma}_{AB}$ and its extension can also be referred to as the IRT surface $\hat{\mathcal{E}}_{A'_1AA'_2}$ of the interval $A'_1AA'_2$, whose equation is given by,

$$\hat{\mathcal{E}}_{A'_1AA'_2} : \rho(V) = -\frac{2\tilde{l}_V}{\tilde{l}_U(\tilde{l}_V^2 - 4(V-V_0)^2)}, \quad U(V) = -\frac{\tilde{l}_U}{\tilde{l}_V}(V-V_0) + U_0, \quad (141)$$

¹⁸Here “type II” means that $\hat{\Sigma}$ and its extension can be referred to as the IRT surface of a certain boundary interval. See appendix B for details.

see Fig.11 for an illustration. Here, the parameters $(\tilde{l}_U, \tilde{l}_V, V_0, U_0)$ are also given by (130). According to (32), the length parameter of the IRT surface $\hat{\mathcal{E}}_{A_1 A_2'}$ is,

$$\hat{\tau} = \frac{1}{2} \log \left(\frac{2(V - V_0) - \tilde{l}_V}{2(V - V_0) + \tilde{l}_V} \right). \quad (142)$$

Therefore, by substituting (140) into the above equation, the anomalous part $E_W^a(A, B)$ is given by the length of $\hat{\Sigma}_{AB}$ divided by $4\mu G$,

$$E_W^a(A, B) = \frac{\text{Length}(\hat{\Sigma}_{AB})}{4\mu G} = \frac{\hat{\tau}_{\hat{H}_2} - \hat{\tau}_{\hat{H}_1}}{4\mu G} = \frac{1}{8\mu G} \log \frac{(\sqrt{\eta} - 1)(\sqrt{\eta} + 1)}{(\sqrt{\eta} + 1)(\sqrt{\eta} - 1)}, \quad (143)$$

which coincides with (136) as we expected. Moreover, we emphasize that the IEWCS $\hat{\Sigma}_{AB}$ is precisely the partner geodesic chord of A on the IRT surface $\hat{\mathcal{E}}_{A_1 A_2'}$, which is $\hat{\mathcal{E}}_{A_1 A_2'}(A)$. This can be shown by demonstrating that the points \hat{H}_1 and \hat{H}_2 are the partner points corresponding to the left and right endpoints of A , respectively. In appendix C, we present a trick for locating the partner point \hat{H} on the IRT surface $\hat{\mathcal{E}}$ of the boundary point P . More explicitly, the partner point \hat{H} is the intersection point between the null hypersurface introduced by P and the IRT surface $\hat{\mathcal{E}}$, see Fig.15. Now, let us use this trick to indicate \hat{H}_1 and \hat{H}_2 are the partner points corresponding to the left and the right endpoints of A , respectively. For example, according to (B.12), the null hypersurface \mathcal{N}_1 introduced by the left endpoint (U_1, V_1) of the interval A is given by,

$$\mathcal{N}_1: \quad \rho = -\frac{1}{2UV}. \quad (144)$$

One can easily verify that the null hypersurface \mathcal{N}_1 intersects with the IRT surface $\hat{\mathcal{E}}_{A_1 A_2'}$ (141) at \hat{H}_1 (140). In other words, \hat{H}_1 is the partner point on $\hat{\mathcal{E}}_{A_1 A_2'}$ of the left endpoint of A according to the discussion in appendix C, and the geodesic connecting the left endpoint of A with \hat{H}_1 is a null geodesic, see Fig.11. A similar discussion applies to the right endpoints of A , which finishes our proof.

On the other hand, as the saddle geodesic connecting the two pieces of the IRT surface $\hat{\mathcal{E}}_{AB}$, the IEWCS $\hat{\Sigma}_{AB}$ also represents the timelike mixed state correlation between the timelike intervals \hat{A} and \hat{B} . In fact, as we mention above, both the EWCS and the IEWCS should be understood as the mixed state correlations between two causal developments, \mathcal{D}_A and \mathcal{D}_B , rather than just between the intervals A and B , or \hat{A} and \hat{B} , due to the Lorentz symmetry. Moreover, one can easily verify that the result (143) corresponding to the IEWCS can not be derived from the EWCS (128) through analytical continuation.

6 Reproducing the twist description from the partner geodesic chord on the IRT surfaces

In this section, we aim to construct the geometric picture of the anomalous partial entanglement entropy in the twist description, and the interval \mathcal{A} we consider is specified by (3). In Sec.3.2.2, we have analyzed the fine structure of the extended entanglement wedge using the modular momentum slices, and identified the partnership between points in the causal development \mathcal{D}_A and points on the RT and the IRT surfaces using two saddle geodesics $\hat{\gamma}_P^1$ (46) and $\hat{\gamma}_P^2$ (60), which are mapped to the curves along the $\tilde{\rho}$ direction in the Rindler AdS₃. For the boundary point $P = (U_1, V_1)$, the corresponding normalized tangent vectors at H (the partner

point of P on \mathcal{E}) for \mathcal{E} , $\widehat{\gamma}_P^1$, and $\widehat{\gamma}_P^2$ are denoted as $v_{\mathcal{E}}|_H$, $v_{\widehat{\gamma}_P^1}|_H$, and $v_{\widehat{\gamma}_P^2}|_H$, respectively, which are given by

$$\begin{aligned} v_{\mathcal{E}}|_H &= \frac{\xi_1 \xi_3}{2\xi_5^2} (l_U \partial_U + l_V \partial_V) + \frac{8(l_V U_1 + l_U V_1) \xi_5}{l_U l_V \xi_1 \xi_3} \partial_\rho, \\ v_{\widehat{\gamma}_P^1}|_H &= \frac{2l_U l_V}{\xi_5^2} (\xi_1 V_1 \partial_U + \xi_3 U_1 \partial_V) - \frac{4(l_U^2 l_V^2 - 16U_1^2 V_1^2)}{l_U l_V \xi_1 \xi_3} \partial_\rho, \\ v_{\widehat{\gamma}_P^2}|_H &= \frac{1}{2\xi_5^2} (-l_U \xi_1 \xi_4 \partial_U + l_V \xi_2 \xi_3 \partial_V) + \frac{8(l_U V_1 - l_V U_1) \xi_5}{l_U l_V \xi_1 \xi_3} \partial_\rho, \end{aligned} \quad (145)$$

where $(\xi_1, \xi_2, \xi_3, \xi_4, \xi_5)$ are,

$$\xi_1 = l_U^2 - 4U_1^2, \quad \xi_2 = l_U^2 + 4U_1^2, \quad \xi_3 = l_V^2 - 4V_1^2, \quad \xi_4 = l_V^2 + 4V_1^2, \quad \xi_5 = l_U l_V + 4U_1 V_1. \quad (146)$$

More interestingly, these tangent vectors satisfy the following property,

$$\begin{aligned} (v_{\widehat{\gamma}_P^1}|_H)^2 &= (v_{\mathcal{E}}|_H)^2 = 1, \quad (v_{\widehat{\gamma}_P^2}|_H)^2 = -1 \\ v_{\mathcal{E}}|_H \cdot v_{\widehat{\gamma}_P^1}|_H &= v_{\mathcal{E}}|_H \cdot v_{\widehat{\gamma}_P^2}|_H = v_{\widehat{\gamma}_P^1}|_H \cdot v_{\widehat{\gamma}_P^2}|_H = 0, \end{aligned} \quad (147)$$

which is exactly the same as (96). This gives a natural configuration for the normal vectors $\mathbf{n}, \tilde{\mathbf{n}}$ across the entire RT surface \mathcal{E} . More explicitly, consider an arbitrary boundary curve \mathcal{C} (not necessarily a straight line), which has the same endpoints with the interval \mathcal{A} , see Fig.12. Given any point P on \mathcal{C} , one can determine two corresponding saddle geodesics $\widehat{\gamma}_P^{1,2}$, as well as their tangent vectors $v_{\widehat{\gamma}_P^1}|_H$ and $v_{\widehat{\gamma}_P^2}|_H$ at the partner point H on \mathcal{E} . Then it is a natural choice to define these vectors as the values of the normal vectors $\mathbf{n}, \tilde{\mathbf{n}}$ at the point H . Since there is a one-to-one correspondence between the points on \mathcal{C} and points on \mathcal{E} , we can determine the normal vectors $\mathbf{n}, \tilde{\mathbf{n}}$ across the entire RT surface using the same prescription,

$$\tilde{\mathbf{n}}|_H := v_{\widehat{\gamma}_P^1}|_H, \quad \mathbf{n}|_H := v_{\widehat{\gamma}_P^2}|_H. \quad (148)$$

Although the RT surface for \mathcal{C} and \mathcal{A} are the same, the configuration of the normal vectors $\mathbf{n}, \tilde{\mathbf{n}}$ on the RT surface \mathcal{E} depends on the position of every point on \mathcal{C} . On the other hand, given a configuration of the normal vectors $\mathbf{n}, \tilde{\mathbf{n}}$ on \mathcal{E} , we can determine the boundary partner points of \mathcal{E} by shooting the spacelike geodesics to the boundary with the initial direction $\tilde{\mathbf{n}}^{19}$. Then the union of all the points where these geodesics anchor on the boundary form a unique spacelike curve \mathcal{C} homologous to \mathcal{E} . Therefore, the boundary curve \mathcal{C} and the configuration of the normal vectors $\mathbf{n}, \tilde{\mathbf{n}}$ are in one-to-one correspondence.

Given a configuration of the normal vectors $\mathbf{n}, \tilde{\mathbf{n}}$ on \mathcal{E} , the corresponding boundary curve is denoted as \mathcal{C} . In [40], the authors claimed that the anomalous part $S_{\mathcal{A}}^a$ is given by,

$$S_{\mathcal{A}}^a = \frac{1}{4\mu G} \int_{\mathcal{E}} d\tau \tilde{\mathbf{n}} \cdot \nabla \mathbf{n} = \frac{1}{4\mu G} \int_{\mathcal{E}} d \log((\mathbf{q} - \tilde{\mathbf{q}}) \cdot \mathbf{n}), \quad (149)$$

where the reference frame $\{\mathbf{q}, \tilde{\mathbf{q}}\}$ is given by (98). For arbitrary sub-region \mathcal{E}_i on \mathcal{E} , it determines a corresponding sub-curve \mathcal{C}_i based on the one-to-one correspondence between the points on \mathcal{C} and those on \mathcal{E} , see Fig.12 for the sub-curve \mathcal{C}_i . It is natural to interpret the part associated with \mathcal{E}_i as the APEE $s_{\mathcal{A}}^a(\mathcal{C}_i)$, since the configuration of the normal vectors $\mathbf{n}, \tilde{\mathbf{n}}$ on \mathcal{E}_i is determined by the sub-curve \mathcal{C}_i , as specified by (148), i.e.

$$s_{\mathcal{A}}^a(\mathcal{C}_i) = \frac{1}{4\mu G} \int_{\mathcal{E}_i} d\tau \tilde{\mathbf{n}} \cdot \nabla \mathbf{n} = \frac{1}{4\mu G} \log \left(\frac{(\mathbf{q} - \tilde{\mathbf{q}})|_{H_2} \cdot \mathbf{n}|_{H_2}}{(\mathbf{q} - \tilde{\mathbf{q}})|_{H_1} \cdot \mathbf{n}|_{H_1}} \right), \quad (150)$$

¹⁹For an arbitrary point H on \mathcal{E} , the corresponding modular Hamiltonian slice \mathcal{P}_H is the set of the saddle spacelike geodesics that are normal to \mathcal{E} , hence the geodesic determined by the normal vector $\tilde{\mathbf{n}}|_H$ corresponds to a saddle geodesic which has an intersection point with the boundary.

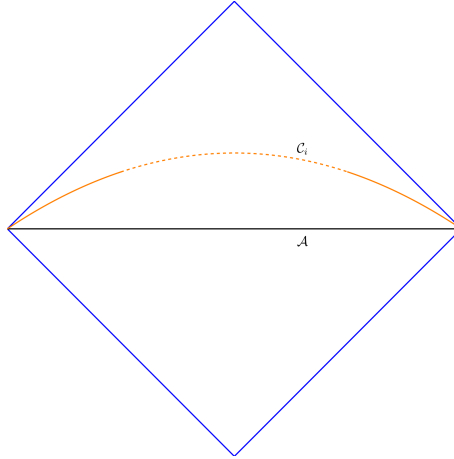


Figure 12: The blue lines represent the boundary of the causal development \mathcal{D}_A . The orange curve \mathcal{C} has the same endpoints with the interval \mathcal{A} , and the dashed part represents a sub-curve \mathcal{C}_i .

where H_1 and H_2 are the partner points of the left and the right endpoints of \mathcal{C}_i on \mathcal{E} , respectively. We find the above expression only depends on the endpoints of \mathcal{C}_i , which suggests us to define a function for the boundary point $P = (U_1, V_1)$ according to the following definition,

$$\bar{\lambda}(P) = \log((\mathbf{q} - \tilde{\mathbf{q}})|_H \cdot \mathbf{n}|_H) = \frac{1}{2} \log \left(\frac{(l_U + 2U_1)(l_V - 2V_1)}{(l_U - 2U_1)(l_V + 2V_1)} \right) = \hat{\tau}_{\hat{H}}, \quad (151)$$

where H and \hat{H} are the partner points of P on \mathcal{E} and on $\hat{\mathcal{E}}$, as specified by (48) and (62), respectively. The reference normal frame $\{\mathbf{q}, \tilde{\mathbf{q}}\}$ is given by (101), and the normal vectors $\mathbf{n}, \tilde{\mathbf{n}}$ are given by (145) and (148). $\hat{\tau}_{\hat{H}}$ is the length parameter of $\hat{\mathcal{E}}$ of the point \hat{H} , which is given by (32). For any sub-interval \mathcal{A}_i whose two endpoints are $P = (U_1, V_1)$ and $Q = (U_2, V_2)$, the APEE $s_{\mathcal{A}}^a(A_i)$ should equal to,

$$\begin{aligned} s_{\mathcal{A}}^a(A_i) &= \frac{1}{4\mu G} \int_{\mathcal{E}_i} d\tau \tilde{\mathbf{n}} \cdot \nabla \mathbf{n} = \frac{\bar{\lambda}(Q) - \bar{\lambda}(P)}{4\mu G} \\ &= \frac{1}{8\mu G} \log \left(\frac{(l_U - 2U_1)(l_V + 2V_1)(l_U + 2U_2)(l_V - 2V_2)}{(l_U + 2U_1)(l_V - 2V_1)(l_U - 2U_2)(l_V + 2V_2)} \right), \end{aligned} \quad (152)$$

where \mathcal{E}_i is the partner geodesic chord of \mathcal{A}_i on \mathcal{E}_i , and the configuration of the normal vectors $\mathbf{n}, \tilde{\mathbf{n}}$ is determined by \mathcal{A}_i , see Fig.13 for an illustration. More importantly, the result aligns exactly with the APEE in the IRT description, based on the fine structure of the extended entanglement wedge, i.e. (76) divided by μ .

Now we turn to the anomalous part $S_{\mathcal{A}}^a$ (149) with the configuration of the normal vectors $\mathbf{n}, \tilde{\mathbf{n}}$ are determined by a boundary curve \mathcal{C} . However, to explicitly calculate $S_{\mathcal{A}}^a$ (149), we need to adopt the holographic regulation $z = \epsilon$, because the metric diverges at the asymptotic boundary. That is, we consider the initial and the final points of the integration in $S_{\mathcal{A}}^a$ to be located on the $z = \epsilon$ surface, which also implies that we simultaneously regulate the boundary curve \mathcal{C} , because the points on \mathcal{C} and those on \mathcal{E} are in one-to-one correspondence. Therefore, we can only focus on the regulation for the boundary curve \mathcal{C} . We denote the regularized curve as \mathcal{C}^{reg} by imposing the regulation for \mathcal{C} at the following boundary points,

$$P_1 = (-l_U/2 + \epsilon_U, -l_V/2 + \epsilon_V), \quad P_2 = (l_U/2 - \epsilon_U, l_V/2 - \epsilon_V), \quad (153)$$

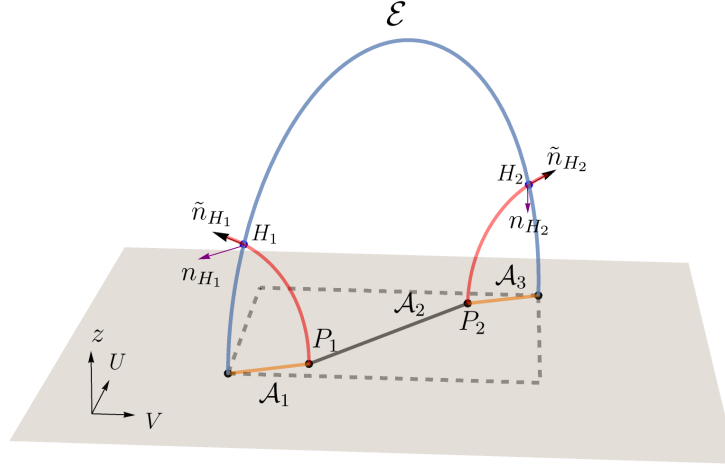


Figure 13: Illustration for the APEE of the sub-interval \mathcal{A}_2 in the twist description. The two red curves are the geodesics normal to the RT surface \mathcal{E} . The two black arrows represent $\tilde{\mathbf{n}}|_{H_1}$ and $\tilde{\mathbf{n}}|_{H_2}$, respectively. The two purple arrows represent $\mathbf{n}|_{H_1}$ and $\mathbf{n}|_{H_2}$, respectively.

which is equivalent to making a holographic regulation at the partner points H_1, H_2 (48) of P_1, P_2 on \mathcal{E} ,

$$\rho_{H_1} = \rho_{H_2} = \frac{1}{2\epsilon_U \epsilon_V}, \Leftrightarrow z_{H_1} = z_{H_2} = 2\sqrt{\epsilon_U \epsilon_V}. \quad (154)$$

And the anomalous part $S_{\mathcal{A}}^a$ (149) is given by the part associated with \mathcal{C}^{reg} ,

$$S_{\mathcal{A}}^a = \frac{1}{4\mu G} \int_{\mathcal{E}^{\text{reg}}} d\tau \tilde{\mathbf{n}} \cdot \nabla n = s_{\mathcal{A}}^a(\mathcal{C}_i) = \frac{1}{4\mu G} \log\left(\frac{l_U \epsilon_V}{l_V \epsilon_U}\right), \quad (155)$$

where \mathcal{E}^{reg} is the partner geodesic chord of \mathcal{C}^{reg} on \mathcal{E} , and we have used (152). And the result aligns exactly with that (108) in the IRT description as we expected. Furthermore, we can also discuss the asymptotic behavior (i.e. the boundary condition) of the normal vector \mathbf{n} . For example, the normal vector $\mathbf{n}|_{H_1}$ for the cutoff point P_1 (153) is given by (145),

$$\mathbf{n}|_{H_1} = -\frac{z_{H_1}}{2} \left(\sqrt{\frac{\epsilon_U}{\epsilon_V}} \partial_U - \sqrt{\frac{\epsilon_V}{\epsilon_U}} \partial_V \right). \quad (156)$$

One can easily verify that $\mathbf{n}|_{H_1}$ is proportional to the vector ∂_t where t is the temporal coordinate of the boundary CFT, only when a special regulation $\epsilon_U = \epsilon_V$ is taken.

7 Summary and discussions

In this work we have studied two relatively independent topics associated to the inner horizon of the Rindler $\widetilde{\text{AdS}}_3$. Firstly, we identify the pre-image of the inner horizon in the original AdS_3 , which coincides with the spacelike geodesic representing the real part of the holographic timelike entanglement entropy. We call it the inner RT surface, and find that it is the set of the fixed points of the bulk modular momentum flow. We also introduce the concept of the extended entanglement wedge by including the region between the RT and IRT surfaces. We identify a timelike geodesic at the boundary of the extended entanglement wedge which reproduces the imaginary part of the holographic timelike entanglement entropy. Nevertheless, the points on

this timelike geodesic are not the fixed points of the modular momentum flow, which makes its role in the analogue replica story [17] of the extended entanglement wedge unclear. We introduce the fine structure of the entanglement wedge and extended entanglement wedge, via slicing them using the modular slices and the modular momentum slices respectively, which gives a partnership between points in the causal development and the points on the RT and IRT surfaces. The (timelike) partial entanglement entropy for sub-intervals in the causal development is then given by the length of the geodesics chord on the RT (IRT) surface, which consists of the partner points of the sub-interval.

Secondly, in the duality between the TMG and the gravitational anomalous CFT_2 , we reproduce the gravitational anomalous correction to the holographic entanglement entropy and the BPE (or reflected entropy) using the length of the geodesic chords on the IRT surface. More interestingly, the geodesic chord that captures the anomalous part of the BPE is also a saddle geodesic connecting different pieces of the IRT surface of the mixed state, which means it can also be understood as an EWCS anchored on the IRT surface, hence captures an optimized quantum information quantity. This is a natural generalization of the observation that, the gravitational anomalous correction to the black hole entropy in TMG is proportional to the area of the inner horizon. Previously the gravitational anomalous correction to the entanglement entropy and the BPE are described by measuring how much the RT surface [40] or the EWCS [41] are twisted after introducing a normal frame configuration on the RT surface. Nevertheless, certain prescription for the normal frame configuration on the RT surface is needed before we can measure the degree of twist, which lacks physical interpretation. We show that, our geometric picture using the geodesic chords on the IRT surfaces is equivalent to the twist description based on the normal frame configurations given in [40, 41].

Unlike the RT surface, the IRT surface extends deep inside the AdS bulk. One can further explore geometry reconstruction using the IRT surface. Also we can define the analogue of the partial entanglement entropy threads [64, 66, 68] using the IRT surfaces, which may be helpful for understanding the geometric reconstruction for covariant or even timelike geometric quantities.

In the context of the AdS/CFT, it was recently pointed out that the twist along the RT surface is also an observable even in pure AdS_3 without gravitational anomaly [83]. From the perspective of operators, the twist commutes with the operator of the area of the RT surface. However, the physical meaning of the twist is still not well understood. In this paper, we find a close relationship between the twist along the RT surface and the IRT surface, hence the twist may have a physical interpretation associated with the timelike entanglement.

Recently, there are some new achievements on the study of the timelike entanglement, see for example [37, 38, 84–87]. In particular, in [87] the authors defined a so-called timelike modular Hamiltonian, which is obtained by analytic continuation for the modular Hamiltonian, to reconstruct the bulk operators, and the timelike geodesic that represents the geometric picture of the imaginary part does not play a similar role in the reconstruction of the bulk operators. It is interesting to re-derive their results in our new context of the timelike entanglement, which does not depend on analytic continuation. Also generalizing our discussion to higher dimensions or other holographic theories is also interesting.

Acknowledgements

We thank Ashish Chandra, Debarshi Basu, Rob Myers and Yiwei Zhong for helpful discussions. QW thanks the “Holographic Duality and Models of Quantum Computation” conference hold at Bali island for helpful discussions with the participants during the conference.

Funding information This work is supported by NSFC Grant No.12447108. HZ is supported by SEU Innovation Capability Enhancement Plan for Doctoral Students (Grant No. CXJH_SEU 24137).

A The IRT surface in the global AdS_3

The CFT_2 on the cylinder is dual to the global AdS_3 ,

$$ds^2 = -(1+r^2)dt^2 + \frac{1}{1+r^2}dr^2 + r^2d\theta^2, \quad (\text{A.1})$$

with the following identifications,

$$\theta \sim \theta + 2\pi, \quad t \sim t + 2\pi. \quad (\text{A.2})$$

Without loss of generality, we consider the static interval A on the $t = 0$ slice with the length ℓ_θ ($\ell_\theta < \pi$). The corresponding Rindler transformation is,

$$\tilde{U} = \frac{1}{T_{\tilde{U}}} \operatorname{arctanh} \left(\frac{\tan\left(\frac{\pi U}{L_U}\right)}{\tan\left(\frac{\pi l_U}{2L_U}\right)} \right), \quad \tilde{V} = \frac{1}{T_{\tilde{V}}} \operatorname{arctanh} \left(\frac{\tan\left(\frac{\pi V}{L_V}\right)}{\tan\left(\frac{\pi l_V}{2L_V}\right)} \right). \quad (\text{A.3})$$

where (U, V) are the light-cone coordinates and are defined as,

$$U = \frac{L_U}{2\pi}(\theta + t), \quad V = \frac{L_V}{2\pi}(\theta - t). \quad (\text{A.4})$$

and the parameters l_U, l_V are given by,

$$l_U = \frac{L_U}{2\pi}\ell_\theta, \quad l_V = \frac{L_V}{2\pi}\ell_\theta. \quad (\text{A.5})$$

Similarly, there are also two modular flows, one is the modular Hamiltonian flow k_t^α and the other one is the modular momentum flow k_t^β ,

$$\begin{aligned} k_t^\alpha &= \frac{\pi}{T_{\tilde{U}}} \partial_{\tilde{U}} - \frac{\pi}{T_{\tilde{V}}} \partial_{\tilde{V}} = \pi \left(\cos t \cos \theta - \cos\left(\frac{\ell_\theta}{2}\right) \right) \csc\left(\frac{\ell_\theta}{4}\right) \sec\left(\frac{\ell_\theta}{4}\right) \partial_t \\ &\quad - 2\pi \csc\left(\frac{\ell_\theta}{2}\right) \sin t \sin \theta \partial_\theta, \\ k_t^\beta &= \frac{\pi}{T_{\tilde{U}}} \partial_{\tilde{U}} + \frac{\pi}{T_{\tilde{V}}} \partial_{\tilde{V}} = -2\pi \csc\left(\frac{\ell_\theta}{2}\right) \sin t \sin \theta \partial_t \\ &\quad + \pi \left(\cos t \cos \theta - \cos\left(\frac{\ell_\theta}{2}\right) \right) \csc\left(\frac{\ell_\theta}{4}\right) \sec\left(\frac{\ell_\theta}{4}\right) \partial_\theta. \end{aligned} \quad (\text{A.6})$$

One can easily verify that the endpoints of A are the fixed points of k_t^α , and those of \widehat{A} are the fixed points of k_t^β , respectively. Here, \widehat{A} is the partner interval that connects the two tips of the causal development \mathcal{D}_A , which is a pure timelike interval with the length ℓ_θ along the θ direction, see Fig.14. The bulk Rindler transformation also maps the original global AdS_3 (A.1) to the Rindler $\widehat{\text{AdS}}_3$ (9), and the radial coordinate transformation is given by,

$$\begin{aligned} \tilde{\rho} &= \frac{T_{\tilde{U}} T_{\tilde{V}}}{4} (2 + (2 + 4r^2) \cos \ell_\theta + 4(1 + r^2) \cos(2t)) \\ &\quad + 8r \cos \theta \left(-2\sqrt{1 + r^2} \cos(\ell_\theta/2) \cos t + r \cos \theta \right) \csc^2(\ell_\theta/2). \end{aligned} \quad (\text{A.7})$$

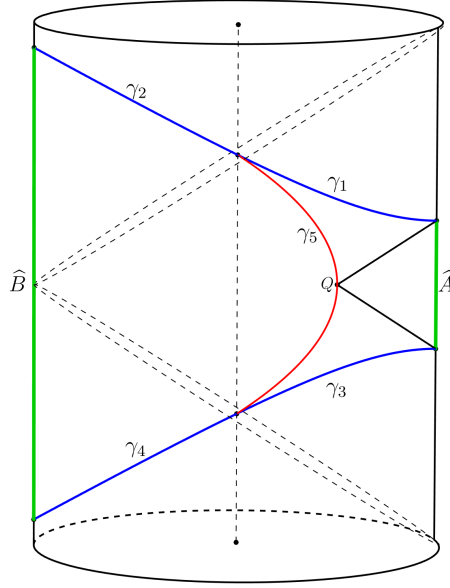


Figure 14: The surfaces enclosed by the dash curve represent the null infinities of the Poincaré patch. The blue curves γ_1 and γ_3 represent the IRT surface of \hat{A} , while the blue curves γ_2 and γ_4 represent the IRT surface of \hat{B} , where B is the complement of A . The black line is the boundary of the entanglement wedge of A on the $\theta = 0$ slice. The red curve γ_5 represents the boundary of the extended entanglement wedge on the $\theta = 0$ slice, which intersects with the RT surface \mathcal{E} at the point Q .

According to the holographic dictionary, the bulk modular flows can be obtained by replacing the boundary global generators in the boundary modular flows with their bulk dual Killing vectors,

$$\begin{aligned}
 k_t^{\alpha,\text{bulk}} &= \frac{\pi \csc\left(\frac{l_\theta}{4}\right) \sec\left(\frac{l_\theta}{4}\right)}{\sqrt{1+r^2}} \left(r \cos t \cos \theta - \sqrt{1+r^2} \cos\left(\frac{l_\theta}{2}\right) \right) \partial_t \\
 &\quad - \frac{2\pi}{r} \sqrt{1+r^2} \csc\left(\frac{l_\theta}{2}\right) \sin t \sin \theta \partial_\theta + 2\pi \sqrt{1+r^2} \cos \theta \csc\left(\frac{l_\theta}{2}\right) \sin t \partial_r, \\
 k_t^{\beta,\text{bulk}} &= -\frac{2\pi r}{\sqrt{1+r^2}} \csc\left(\frac{l_\theta}{2}\right) \sin t \sin \theta \partial_t \\
 &\quad + \frac{\pi \tan\left(\frac{l_\theta}{4}\right)}{r} \left(r - r \cot^2\left(\frac{l_\theta}{4}\right) + \sqrt{1+r^2} \cos t \cos \theta \csc^2\left(\frac{l_\theta}{4}\right) \right) \partial_\theta \\
 &\quad + 2\pi \sqrt{1+r^2} \cos t \csc\left(\frac{l_\theta}{2}\right) \sin \theta.
 \end{aligned} \tag{A.8}$$

As discussed in Sec.2, solving $k_t^{\alpha,\text{bulk}} = 0$ and $k_t^{\beta,\text{bulk}} = 0$ give us the RT surface \mathcal{E} and the IRT

surface $\widehat{\mathcal{E}}$, respectively,

$$\begin{aligned} \mathcal{E}: \quad & r = \frac{\cot\left(\frac{\ell_\theta}{2}\right)}{\sqrt{\cos^2\theta \csc^2\left(\frac{\ell_\theta}{2}\right) - \cot^2\left(\frac{\ell_\theta}{2}\right)}}, \quad t = 0, \\ \widehat{\mathcal{E}}: \quad & \begin{cases} \gamma_1: & t = -\arccos\left(\frac{r \cos(\ell_\theta)}{\sqrt{1+r^2}}\right), \quad \theta = 0 \\ \gamma_2: & t = -\arccos\left(-\frac{r \cos(\ell_\theta/2)}{\sqrt{1+r^2}}\right), \quad \theta = \pi \\ \gamma_3: & t = \arccos\left(\frac{r \cos(\ell_\theta/2)}{\sqrt{1+r^2}}\right), \quad \theta = 0 \\ \gamma_4: & t = \arccos\left(-\frac{r \cos(\ell_\theta/2)}{\sqrt{1+r^2}}\right), \quad \theta = \pi \end{cases} \end{aligned} \quad (\text{A.9})$$

where γ_1 and γ_2 smoothly join together at the null infinity of the Poincaré patch, as do γ_3 and γ_4 . More interestingly, γ_1 intersects the asymptotic boundary at the upper endpoint of \widehat{A} , while γ_2 intersects the asymptotic boundary at the upper endpoint of \widehat{B} , where B is the complement of A , see Fig.14. One can easily verify that the RT surface \mathcal{E} and the IRT surface $\widehat{\mathcal{E}}$ are indeed mapped to the outer and the inner horizons of the Rindler AdS_3 , respectively,

$$\tilde{\rho}|_{\mathcal{E}} = T_{\tilde{U}}T_{\tilde{V}}, \quad \tilde{\rho}|_{\widehat{\mathcal{E}}} = -T_{\tilde{U}}T_{\tilde{V}}. \quad (\text{A.10})$$

On the other hand, we can obtain a timelike geodesic representing the boundary of the intersection surface between the extended entanglement wedge $\widehat{\mathcal{W}}_A$ and the hypersurface $\theta = 0$ by following the derivation of Sec.3.2.2,

$$\gamma_5: \quad r = \cot\left(\frac{\ell_\theta}{2}\right) \cos \tau, \quad t(\tau) = \arctan\left(\sin\left(\frac{\ell_\theta}{2}\right) \tan \tau\right), \quad (\text{A.11})$$

which connects γ_1 and γ_3 at the null infinities of the Poincaré patch. This means γ_2 and γ_4 are not in $\widehat{\mathcal{W}}_A$. Therefore γ_1 and γ_3 should be referred to as the IRT surface of \widehat{A} , while γ_2 and γ_4 should be referred to as the IRT surface of \widehat{B} . And the length of the timelike geodesic γ_5 is also π .

B Spacelike and null geodesics in the Poincaré AdS_3

In this appendix, we list some useful properties of spacelike and null geodesics in the Poincaré AdS_3 . We mainly focus on two types of spacelike geodesics in the Poincaré AdS_3 . One is connected, which we call type I spacelike geodesic, and the other is disconnected, which we call type II spacelike geodesic. The type I spacelike geodesic is,

$$\rho(V) = \frac{2l_V}{l_U(l_V^2 - 4(V - V_0)^2)}, \quad U(V) = \frac{l_U}{l_V}(V - V_0) + U_0, \quad (l_U, l_V > 0), \quad (\text{B.1})$$

which can be referred to as the RT surface of the boundary spatial interval \mathcal{I} ,

$$\mathcal{I}: (-l_U/2 + U_0, -l_V/2 + V_0) \rightarrow (l_U/2 + U_0, l_V/2 + V_0), \quad (\text{B.2})$$

For the type I spacelike geodesic, which connects the two spacelike points (U_1, V_1, ρ_1) and (U_2, V_2, ρ_2) , the parameters (l_U, l_V, V_0, U_0) are,

$$\begin{aligned} l_U &= \frac{X}{2(V_2 - V_1)\rho_1\rho_2}, & l_V &= \frac{X}{2(U_2 - U_1)\rho_1\rho_2}, \\ V_0 &= \frac{\rho_2 + \rho_1(-1 + 2(U_1 - U_2)(V_1 + V_2)\rho_2)}{4(U_1 - U_2)\rho_1\rho_2}, \\ U_0 &= \frac{\rho_2 + \rho_1(-1 + 2(U_1 + U_2)(V_1 - V_2)\rho_2)}{4(V_1 - V_2)\rho_1\rho_2}, \end{aligned} \quad (\text{B.3})$$

where X is,

$$\begin{aligned} X &= \sqrt{\rho_1^2 + 2\rho_1\rho_2(\rho_1 Y - 1) + (\rho_2 + \rho_1\rho_2 Y)^2}, \\ Y &= 2(U_1 - U_2)(V_1 - V_2). \end{aligned} \quad (\text{B.4})$$

Hence the proper distance between (U_1, V_1, ρ_1) and (U_2, V_2, ρ_2) is,

$$L(U_1, V_1, \rho_1, U_2, V_2, \rho_2) = \frac{1}{2} \log \left(\frac{(X + \rho_1 - \rho_2 + Y\rho_1\rho_2)(X + \rho_2 - \rho_1 + Y\rho_1\rho_2)}{(X + \rho_1 - \rho_2 - Y\rho_1\rho_2)(X + \rho_2 - \rho_1 - Y\rho_1\rho_2)} \right). \quad (\text{B.5})$$

Similarly, the equation of the type II spacelike geodesic is,

$$\rho(V) = -\frac{2l_V}{l_U(l_V^2 - 4(V - V_0)^2)}, \quad U(V) = -\frac{l_U}{l_V}(V - V_0) + U_0, \quad (l_U, l_V > 0) \quad (\text{B.6})$$

which has two connected sectors

$$\text{Left sector: } V < V_0 - \frac{l_V}{2}, \quad \text{Right sector: } V > V_0 + \frac{l_V}{2}, \quad (\text{B.7})$$

and can be also referred to as the IRT surface of the interval \mathcal{I} (B.2). The partner interval $\widehat{\mathcal{I}}$ is the timelike interval connecting the two tips of the causal development of \mathcal{I} , i.e.

$$\widehat{\mathcal{I}} : (-l_U/2 + U_0, l_V/2 + V_0) \rightarrow (l_U/2 + U_0, -l_V/2 + V_0) \quad (\text{B.8})$$

For the type II spacelike geodesic, which connects the two spacelike points (U_1, V_1, ρ_1) and (U_2, V_2, ρ_2) , the parameters (l_U, l_V, V_0, U_0) are,

$$\begin{aligned} l_U &= \frac{X}{2(V_2 - V_1)\rho_1\rho_2}, & l_V &= \frac{X}{2(U_1 - U_2)\rho_1\rho_2}, \\ V_0 &= \frac{\rho_2 + \rho_1(-1 + 2(U_1 - U_2)(V_1 + V_2)\rho_2)}{4(U_1 - U_2)\rho_1\rho_2}, \\ U_0 &= \frac{\rho_2 + \rho_1(-1 + 2(U_1 + U_2)(V_1 - V_2)\rho_2)}{4(V_1 - V_2)\rho_1\rho_2}, \end{aligned} \quad (\text{B.9})$$

where X are also (B.4). The proper distance between (U_1, V_1, ρ) and (U_2, V_2, ρ_2) is also given by (B.5) when they are on the same sector of the type II spacelike geodesic (B.6). When they are on the different sectors, for example, (U_1, V_1, ρ_1) is on the Left sector, (U_2, V_2, ρ_2) is on the Right sector, we define the proper distance between them to be,

$$\begin{aligned} L(U_1, V_1, \rho_1, U_2, V_2, \rho_2) &= \int_{-\infty}^{V_1} \sqrt{ds^2} + \int_{V_2}^{\infty} \sqrt{ds^2} \\ &= -\frac{1}{2} \log \left(\frac{(X + \rho_1 - \rho_2 + Y\rho_1\rho_2)(X + \rho_2 - \rho_1 + Y\rho_1\rho_2)}{(X + \rho_1 - \rho_2 - Y\rho_1\rho_2)(X + \rho_2 - \rho_1 - Y\rho_1\rho_2)} \right) \end{aligned} \quad (\text{B.10})$$

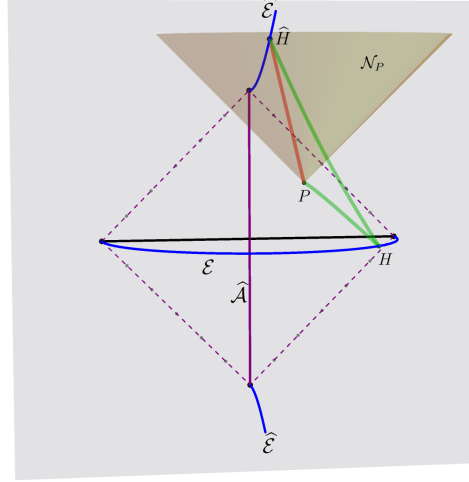


Figure 15: The yellow surface represents the null hypersurface \mathcal{N}_p introduced by P . The two green curves represent the saddle geodesics $\widehat{\gamma}_p^1$ and $\widehat{\gamma}_p^2$, respectively. The partner point \widehat{H} is the intersection point between \mathcal{N}_p and $\widehat{\mathcal{E}}$. And the red curve presents the null geodesic connecting P and \widehat{H} .

where ds^2 is the induced line element on (B.6) and X, Y are (B.4), and the difference between (B.10) with (B.5) is only up to a overall sign.

The null geodesic, which intersects the asymptotic boundary at the boundary point (U_1, V_1) , is given by,

$$\rho(V) = \frac{C^2}{(V_1 - V)^2}, \quad U(V) = U_1 + \frac{V_1 - V}{2C^2}, \quad (\text{B.11})$$

where C is an arbitrary constant. The null hypersurface introduced by the boundary point (U_1, V_1) is,

$$\rho = \frac{1}{2(U - U_1)(V_1 - V)}. \quad (\text{B.12})$$

In particular, the null geodesic (B.11) with the coefficient $C = 1/\sqrt{2}$ is,

$$\rho(V) = \frac{1}{2(V_1 - V)^2}, \quad U(V) = U_1 + V_1 - V. \quad (\text{B.13})$$

C A trick for locating the partner point \widehat{H} on $\widehat{\mathcal{E}}$

Consider a boundary point $P = (U_1, V_1)$ in $\mathcal{D}_{\mathcal{A}}$, and the null hypersurface introduced by P via (B.12), which we denote as \mathcal{N}_p . There is only one intersection point \widehat{H} between \mathcal{N}_p and the IRT surface $\widehat{\mathcal{E}}$ (31), which is given by,

$$\widehat{H} = \mathcal{N}_p \cap \widehat{\mathcal{E}}: \quad V_{\widehat{H}} = -\frac{l_V(l_U l_V - 4U_1 V_1)}{4(l_V U_1 - l_U V_1)}, \quad (\text{C.1})$$

which is exactly the same as the partner point \widehat{H} (62) of P on the IRT surface $\widehat{\mathcal{E}}$. In other words, the partner point \widehat{H} of P is precisely the intersection point between the null hypersurface \mathcal{N}_p and the IRT surface $\widehat{\mathcal{E}}$, see Fig.15 for an illustration.

D Replica trick for the CFT₂ with gravitational anomaly

The generators of the CFT₂ on the plane are given by,

$$L_n = U^{n+1} \partial_U, \quad \bar{L}_n = V^{n+1} \partial_V, \quad (\text{D.1})$$

where L_{\pm}, L_0 and \bar{L}_{\pm}, \bar{L}_0 are the only global generators. The charges $\mathcal{L}_n, \bar{\mathcal{L}}_n$ associated with these generators form the Virasoro algebra which is the central extension of the Witt algebra,

$$\begin{aligned} [\mathcal{L}_n, \mathcal{L}_m] &= (n-m) \mathcal{L}_{n+m} + \frac{c_L}{12} n(n^2-1) \delta_{n+m,0} \\ [\bar{\mathcal{L}}_n, \bar{\mathcal{L}}_m] &= (n-m) \bar{\mathcal{L}}_{n+m} + \frac{c_R}{12} n(n^2-1) \delta_{n+m,0} \end{aligned} \quad (\text{D.2})$$

where c_L and c_R are the left-moving central charge and the right-moving central charge, respectively. For the interval \mathcal{A} (3), the entanglement entropy $S_{\mathcal{A}}$ is defined as the von Neumann entropy $S_{\mathcal{A}} = -\text{Tr} \rho_{\mathcal{A}} \log \rho_{\mathcal{A}}$ of the reduced density matrix $\rho_{\mathcal{A}}$. To calculate the entanglement entropy, we can first consider the n -order Rényi entropy $S_{\mathcal{A}}^{(n)} = \frac{1}{1-n} \log \text{Tr} \rho_{\mathcal{A}}^n$, and then take the limit $n \rightarrow 1$. The replica method [88, 89] proposes the partition function $\mathcal{Z}_n = \text{Tr} \rho_{\mathcal{A}}^n$ of the n -order replica manifold can be calculated by the two-point function of the twist operators, namely

$$\mathcal{Z}_n = \text{Tr} \rho_{\mathcal{A}}^n = \langle \Phi_n(a) \bar{\Phi}_n(b) \rangle = \left(\frac{\epsilon_U}{l_U} \right)^{2h_L} \left(\frac{\epsilon_V}{l_V} \right)^{2h_R} \quad (\text{D.3})$$

where a and b are the left and the right endpoints of the interval \mathcal{A} , respectively. The cutoffs ϵ_U, ϵ_V are introduced to make the action \mathcal{Z}_n dimensionless and ensure the entanglement entropy to vanish in the limit $l_U \rightarrow \epsilon_U, l_V \rightarrow \epsilon_V$. The conformal dimensions of twist operator for the left-moving sector and the right-moving sector are $h_L = \frac{c_L}{24} \left(n - \frac{1}{n} \right)$ and $h_R = \frac{c_R}{24} \left(n - \frac{1}{n} \right)$, which can be determined by the conformal Ward identities. Note that for the CFT₂ with the gravitational anomaly ($c_L \neq c_R$), the twist operator possesses non-zero spin s_n [40],

$$\Delta_n = h_L + h_R = \frac{c_L + c_R}{24} \left(n - \frac{1}{n} \right), \quad s_n = h_L - h_R = \frac{c_L - c_R}{24} \left(n - \frac{1}{n} \right) \quad (\text{D.4})$$

where Δ_n is the scaling dimension of the twist operator. Furthermore, the n -order Rényi entropy is given by,

$$S_{\mathcal{A}}^{(n)} = \frac{n+1}{12n} \left(c_L \log \left(\frac{l_U}{\epsilon_U} \right) + c_R \log \left(\frac{l_V}{\epsilon_V} \right) \right) \quad (\text{D.5})$$

Accordingly, the entanglement entropy $S_{\mathcal{A}}$ is,

$$S_{\mathcal{A}} = \frac{c_L}{6} \log \left(\frac{l_U}{\epsilon_U} \right) + \frac{c_R}{6} \log \left(\frac{l_V}{\epsilon_V} \right). \quad (\text{D.6})$$

E The regulated geodesic chord on the inner RT surface and its flat limit

As discussed in Sec.3.2.2, the regulated interval \mathcal{A}^{reg} corresponds to a geodesic chord on the IRT surface $\hat{\mathcal{E}}$. More explicitly, the partner points on $\hat{\mathcal{E}}$ of the endpoints of \mathcal{A}^{reg} are denoted as the cutoff points Q_1 and Q_2 , respectively, which are given by (62),

$$\begin{aligned} V_{Q_1} &= \frac{l_V(l_V \epsilon_U + (l_U - 2\epsilon_U)\epsilon_V)}{2l_U \epsilon_V - 2l_V \epsilon_U} \sim \frac{l_V(l_V \epsilon_U + l_U \epsilon_V)}{2l_U \epsilon_V - 2l_V \epsilon_U}, \\ V_{Q_2} &= -\frac{l_V(l_V \epsilon_U + (l_U - 2\epsilon_U)\epsilon_V)}{2l_U \epsilon_V - 2l_V \epsilon_U} \sim -\frac{l_V(l_V \epsilon_U + l_U \epsilon_V)}{2l_U \epsilon_V - 2l_V \epsilon_U}, \end{aligned} \quad (\text{E.1})$$

where $V_{Q_1}(V_{Q_2})$ represents the V -coordinate of $Q_1(Q_2)$, and “ \sim ” denotes that we perform a Taylor expansion for the infinitesimal constants ϵ_U and ϵ_V . In particular, if we choose two equal cutoffs, i.e. $\epsilon_U = \epsilon_V = \epsilon$, the corresponding cutoff points Q_1, Q_2 are,

$$V_{Q_1} = \frac{l_V(l_V + l_U)}{2(l_U - l_V)}, \quad V_{Q_2} = -\frac{l_V(l_V + l_U)}{2(l_U - l_V)}. \quad (\text{E.2})$$

We denote the regulated part of $\widehat{\mathcal{E}}$ as γ , which extends from Q_1 to $V = \infty$, and then from $V = -\infty$ to Q_2 ,

$$\gamma = \widehat{\mathcal{E}}^{\text{reg}} : \rho = -\frac{2l_V}{l_U(l_V^2 - 4V^2)}, \quad U = -\frac{l_U}{l_V}V \quad (V < V_{Q_1} \text{ or } V > V_{Q_2}), \quad (\text{E.3})$$

see Fig.16 for an illustration. Therefore, γ represents the partner geodesic chord on $\widehat{\mathcal{E}}$ corresponds to $S_{\mathcal{A}}^a$ (94) with the cutoffs being $\epsilon_U = \epsilon_V = \epsilon$. However, the IRT surface $\widehat{\mathcal{E}}$ is not homologous to \mathcal{A} , such that we can introduce two auxiliary null geodesics γ_-, γ_+ emanating from the endpoints of \mathcal{A} , which are the bulk modular momentum flow lines on \mathcal{M}_{\pm} , to make the composite surface $\gamma_{\mathcal{A}} = \gamma \cup \gamma_- \cup \gamma_+$ homologous to \mathcal{A} , similarly to [16]. We emphasize that γ_{\pm} are not the fixed points of $k_t^{\beta, \text{bulk}}$, hence do not represent the bulk replica symmetry. More explicitly, γ_{\pm} are the bulk modular momentum flow lines connecting $\partial_{\pm}\mathcal{A} = \pm(l_U/2, l_V/2)$ with $Q_1(Q_2)$, which are given by (81),

$$\begin{aligned} \gamma_+ = \widehat{\mathcal{L}}_{Q_2}^+ : \quad \rho(V) &= \frac{2}{(l_V - 2V)^2}, \quad U(V) = \frac{l_U + l_V}{2} - V, \\ \gamma_- = \widehat{\mathcal{L}}_{Q_1}^- : \quad \rho(V) &= \frac{2}{(l_V + 2V)^2}, \quad U(V) = -\frac{l_U + l_V}{2} - V. \end{aligned} \quad (\text{E.4})$$

The anomalous part $S_{\mathcal{A}}^a$ (94) can be given by the total length of $\gamma_{\mathcal{A}}$,

$$\begin{aligned} S_{\mathcal{A}}^a &= \frac{\text{Length}(\gamma_{\mathcal{A}})}{4\mu G} = \frac{\text{Length}(\gamma)}{4\mu G} \\ &= \frac{\widehat{\tau}_{Q_2} - \widehat{\tau}_{Q_1}}{4\mu G} = \frac{1}{4\mu G} \log\left(\frac{l_U}{l_V}\right), \end{aligned} \quad (\text{E.5})$$

where $\widehat{\tau}$ is the length parameter of the IRT surface $\widehat{\mathcal{E}}$. One can see this is very similar to the case in the flat holography. In fact, this is reasonable. The authors in [16] calculated the holographic entanglement entropy by taking the flat limit ($\ell \rightarrow \infty$) for the Rindler method. In the flat limit, the outer horizon of Rindler AdS₃ is pushed to infinity, thus leaving only the inner horizon in the bulk. More interestingly, they find that the flat limit of the area of the inner horizon exactly matches the holographic entanglement entropy in the flat holography. This implies that the holographic entanglement entropy in the flat holography can, to some extent, be referred to as originating from the inner horizon of the Rindler AdS₃, rather than the outer horizon. Now we show that the geometric picture of the holographic entanglement entropy in the flat holography (including the null geodesics), can also be derived by taking the flat limit of our discussions here²⁰.

The infinite-dimensional Bondi-Metzner-Sachs (BMS₃) group [91–95] is the asymptotic symmetry of three-dimensional flat spacetime at the null infinity, hence the Flat/BMS₃ correspondence which we called the flat holography was proposed in [32, 33]. The holographic entanglement entropy, and its geometric picture are given in [16] via the Rindler method,

$$S_{\mathcal{A}}^{\text{BMS}} = \frac{\text{Length}(\gamma^{\text{BMS}})}{4G}, \quad (\text{E.6})$$

²⁰See also [90] for earlier discussions

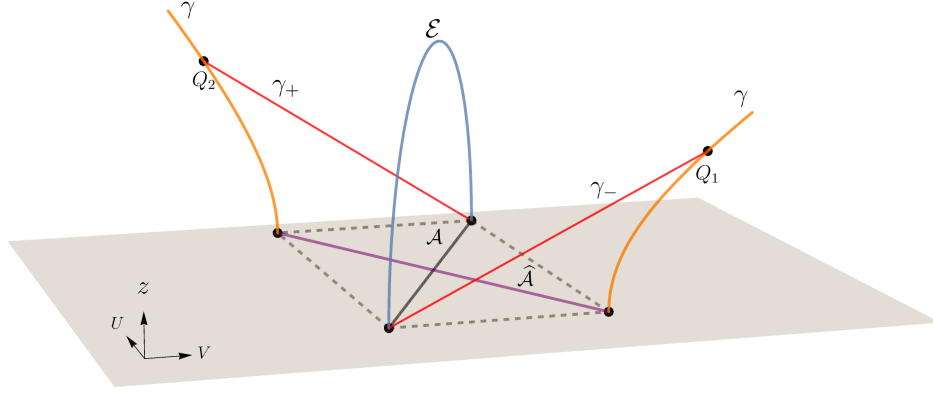


Figure 16: The black and the purple lines represent the interval \mathcal{A} and its partner interval $\widehat{\mathcal{A}}$, respectively. The blue line is the RT surface \mathcal{E} . The orange line is the IRT surface $\widehat{\mathcal{E}}$. The red lines γ_+ and γ_- are two null geodesics emanating from the endpoints of \mathcal{A} , which are introduced to make the composite surface $\gamma_{\mathcal{A}} = \gamma_+ \cup \gamma_- \cup \gamma$ homologous to \mathcal{A} . They intersect $\widehat{\mathcal{E}}$ at the cutoff points Q_1 and Q_2 , and γ is the regulated part of $\widehat{\mathcal{E}}$.

where the superscript ‘‘BMS’’ is used to distinguish it from the AdS/CFT, and γ^{BMS} is the fixed points of the bulk modular flow $k_t^{\text{BMS,bulk}}$ (or bulk replica symmetry). The spacelike geodesic γ is connected to the endpoints of the boundary interval \mathcal{A}^{BMS} on null infinity by two null geodesics $\gamma_{\pm}^{\text{BMS}}$. The null geodesics $\gamma_{\pm}^{\text{BMS}}$ are the orbits of the endpoints $\partial \mathcal{A}^{\text{BMS}}$ under the bulk modular flow $k_t^{\text{BMS,bulk}}$ and they are two r coordinate lines, see (E.11) later. Here we only focus on the null-orbifold whose metric is,

$$ds^2 = -2dudr + r^2d\phi^2, \quad (\text{E.7})$$

which duals to the zero temperature BMSFT on the plane. We consider a boundary interval \mathcal{A}^{BMS} ,

$$\mathcal{A}^{\text{BMS}} : (-l_u/2, -l_\phi/2) \rightarrow (l_u/2, l_\phi/2), \quad (\text{E.8})$$

and the corresponding modular flows k_t^{BMS} and $k_t^{\text{BMS,bulk}}$ are [16],

$$\begin{aligned} k_t^{\text{BMS}} &= -\frac{\pi}{2l_\phi} \left((l_\phi^2 - 4\phi^2) \partial_\phi + \left(l_u l_\phi + 4\frac{l_u}{l_\phi} \phi^2 - 8u\phi \right) \partial_u \right) \\ k_t^{\text{BMS,bulk}} &= -\frac{\pi}{2l_\phi} \left(\left(l_\phi^2 - 4\phi^2 + \frac{8(l_\phi u - l_u \phi)}{l_\phi r} \right) \partial_\phi + \left(l_u l_\phi + 4\frac{l_u}{l_\phi} \phi^2 - 8u\phi \right) \partial_u \right. \\ &\quad \left. + \left(\frac{8l_u}{l_\phi} + 8r\phi \right) \partial_r \right), \end{aligned} \quad (\text{E.9})$$

the spacelike geodesic γ^{BMS} is just the fixed points of $k_t^{\text{BMS,bulk}}$, i.e.

$$k_t^{\text{BMS,bulk}}|_{\gamma^{\text{BMS}}} = 0, \quad (\text{E.10})$$

and $\gamma_{\pm}^{\text{BMS}}$ are two r coordinate lines passing the endpoints of \mathcal{A}^{BMS} ,

$$\gamma_+^{\text{BMS}} : u = \frac{l_u}{2}, \phi = \frac{l_\phi}{2}, \quad \gamma_-^{\text{BMS}} : u = -\frac{l_u}{2}, \phi = -\frac{l_\phi}{2}. \quad (\text{E.11})$$

Now we return to consider the flat limit of the geometric picture of the anomalous part $S_{\mathcal{A}}^a$. We recover the AdS radius ℓ such that the metric of Poincaré AdS₃ is,

$$ds^2 = \ell^2 \left(2\rho dUdV + \frac{d\rho^2}{4\rho^2} \right), \quad (\text{E.12})$$

which is the solution of the Einstein-Hilbert action plus the cosmological constant term,

$$S = \frac{1}{16\pi G} \int d^3x \sqrt{-g} (R - 2\Lambda), \quad (\text{E.13})$$

where the cosmological constant $\Lambda = -1/\ell^2$. The cosmological constant Λ will vanish in the limit $\ell \rightarrow \infty$, which we called the flat limit of the AdS/CFT. When the cosmological constant vanishes, there is only the Einstein-Hilbert term, whose solution is just the flat spacetime. In order to consider the flat limit properly, we rewritten the metric (E.12) in the BMS gauge [96],

$$ds^2 = r^2 \left(d\phi^2 - \frac{du^2}{\ell^2} \right) - 2dudr, \quad (\text{E.14})$$

by the following coordinate transformation,

$$U = \frac{1}{2} \left(\ell\phi + u - \frac{\ell^2}{r} \right), \quad V = \frac{1}{2} \left(\ell\phi - u + \frac{\ell^2}{r} \right), \quad \rho = \frac{2r^2}{\ell^4}. \quad (\text{E.15})$$

One can easily verify that the Poincaré-BMS metric (E.14) will reduce to the null-orbifold (E.7) in the flat limit. According to the coordinate transformation (E.15), the parameters l_U, l_V can be written in terms of l_u, l_ϕ ,

$$l_U = \frac{\ell l_\phi + l_u}{2}, \quad l_V = \frac{\ell l_\phi - l_u}{2}. \quad (\text{E.16})$$

According to the coordinate transformation (E.15) and the parameters (E.16), we can rewrite the modular momentum flow vectors k_t^β (28) and $k_t^{\beta, \text{bulk}}$ (26) in the Poincaré-BMS coordinate (u, ϕ, r) ,

$$\begin{aligned} k_t^\beta &= \frac{\pi}{2(l_u^2 - \ell^2 l_\phi^2)} \left((l_u^3 + 8l_\phi u \ell^2 \phi - l_u(4u^2 + \ell^2(l_\phi^2 + 4\phi^2))) \partial_u \right. \\ &\quad \left. + (l_u^2 l_\phi - l_\phi^3 \ell^2 - 8l_u u \phi + 4l_\phi(u^2 + \ell^2 \phi^2)) \partial_\phi \right) \\ k_t^{\beta, \text{bulk}} &= \frac{\pi}{2(l_u^2 - \ell^2 l_\phi^2)} \left((l_u^3 - l_u(\ell^2(l_\phi^2 + 4\phi^2) + 4u^2) + 8\ell^2 l_\phi u \phi) \partial_u \right. \\ &\quad \left. + (l_u^2 l_\phi r + 8l_u \phi(\ell^2 - ru) + l_\phi(-\ell^2 r(l_\phi^2 - 4\phi^2) + 4ru^2 - 8\ell^2 u)) \partial_\phi \right. \\ &\quad \left. - 8((l_u(\ell^2 - ru) + \ell^2 l_\phi r \phi)) \partial_r \right). \end{aligned}$$

After taking the flat limit, the only difference between $k_t^\beta, k_t^{\beta, \text{bulk}}$ and $k_t^{\text{BMS}}, k_t^{\text{BMS}, \text{bulk}}$ is an overall coefficient negative sign, which does not change the physical essence. Therefore, in the flat limit, the spacelike geodesic γ , which is the set of the fixed points of $k_t^{\beta, \text{bulk}}$, will reduce to γ^{BMS} , the fixed point of $k_t^{\text{BMS}, \text{bulk}}$. Similarly, we can also rewrite the null geodesics γ_\pm (E.4) in the Poincaré-BMS coordinate (u, ϕ, r) ,

$$\gamma_+ : u = \frac{l_u}{2}, \quad \phi = \frac{l_\phi}{2}, \quad \gamma_- : u = -\frac{l_u}{2}, \quad \phi = -\frac{l_\phi}{2}, \quad (\text{E.17})$$

which exactly match the null geodesics $\gamma_{\pm}^{\text{BMS}}$ (E.11) even without taking the flat limit. Therefore, the geometric picture of the holographic entanglement entropy in the flat holography can be obtained by taking the flat limit for the geometric picture of the anomalous part $S_{\mathcal{A}}^a$ in the AdS/CFT with gravitational anomaly.

Interestingly, all the null geodesics (B.13) are the r coordinate lines even without taking the flat limit. More explicitly, the parameters (U_1, V_1) which characterize the null geodesics (B.13) can be rewritten in terms of the parameters in the Poincaré-BMS coordinate according to the coordinate transformation (E.15),

$$U_1 = \frac{1}{2}(\ell\phi_1 + u_1), \quad V_1 = \frac{1}{2}(\ell\phi_1 - u_1). \quad (\text{E.18})$$

According to (E.15), the null geodesics (B.13) can be rewritten in the Poincaré-BMS coordinate,

$$u = u_1, \quad \phi = \phi_1, \quad (\text{E.19})$$

which are the r coordinate lines in the BMS gauge.

F The equality between the two sides of (120)

In this appendix, we demonstrate the equality between the two sides of equation (120) by showing that the right-hand side of (120) indeed evaluates the APEE $s_{A_1'AA_2'}^a(A)$, and thus equals to the left-hand side. Consider the configuration of $A_1'AA_2'$ described by (123) and (131). The RT surfaces \mathcal{E}_1 and \mathcal{E}_2 can be also understood as the saddle spacelike geodesics $\widehat{\gamma}_{P_1}^1$ and $\widehat{\gamma}_{P_2}^1$ corresponding to the left and the right endpoints of A for the interval $A_1'AA_2'$, where P_1 and P_2 are the endpoints of A . This is because \mathcal{E}_1 and \mathcal{E}_2 are both normal to the EWCS Σ_{AB} , as shown in Fig.10. Therefore, the endpoints H_1 and H_2 (described by (127)) of Σ_{AB} are the partner points of the left and the right endpoints of A on the RT surface $\mathcal{E}_{A_1'AA_2'}$, respectively. For (120), the authors in [41] chose the following boundary condition of the spacelike normal vectors $\tilde{\mathbf{n}}_i$ and $\tilde{\mathbf{n}}_f$ for the EWCS Σ_{AB} ,

$$\tilde{\mathbf{n}}_i = v_{\widehat{\gamma}_{P_1}^1}|_{H_1}, \quad \tilde{\mathbf{n}}_f = v_{\widehat{\gamma}_{P_2}^1}|_{H_2}, \quad (\text{F.1})$$

where $v_{\widehat{\gamma}_{P_1}^1}|_{H_1}$ and $v_{\widehat{\gamma}_{P_2}^1}|_{H_2}$ represent the normalized tangent vectors of \mathcal{E}_1 and \mathcal{E}_2 at the endpoints H_1 and H_2 of Σ_{AB} , respectively. According to the discussion in Sec.6, the above equation also implies the boundary condition of the timelike normal vectors \mathbf{n}_i and \mathbf{n}_f ,

$$\mathbf{n}_i = v_{\widehat{\gamma}_{P_1}^2}|_{H_1}, \quad \mathbf{n}_f = v_{\widehat{\gamma}_{P_2}^2}|_{H_2}, \quad (\text{F.2})$$

where $\widehat{\gamma}_{P_1}^2$ and $\widehat{\gamma}_{P_2}^2$ are the saddle timelike geodesics corresponding to the two endpoints of A for the interval $A_1'AA_2'$. Therefore, \mathbf{n}_i and \mathbf{n}_f are given by (145) up to a translation $(U_1, V_1) \rightarrow (U_1 - U_0, V_1 - V_0)$ and a variable replacement $l_U, l_V \rightarrow \widetilde{l}_U, \widetilde{l}_V$, where $(\widetilde{l}_U, \widetilde{l}_V, U_0, V_0)$ are specified by (130). In fact, this choice can also ensure that the term inside the logarithm in (120) is positive, see (151). According to (151), the right-hand side of (120) is given by,

$$\text{RHS} = \frac{\widehat{\tau}_{\widehat{H}_2} - \widehat{\tau}_{\widehat{H}_1}}{4\mu G} = s_{A_1'AA_2'}^a(A), \quad (\text{F.3})$$

where \widehat{H}_1 and \widehat{H}_2 are the partner points of the endpoints P_1 and P_2 of A , respectively. Therefore, the two sides of (120) are equal.

References

- [1] J. D. Bekenstein, *Black holes and the second law*, Lett. Nuovo Cim. **4**, 737 (1972), doi:[10.1007/BF02757029](https://doi.org/10.1007/BF02757029).
- [2] J. M. Bardeen, B. Carter and S. W. Hawking, *The Four laws of black hole mechanics*, Commun. Math. Phys. **31**, 161 (1973), doi:[10.1007/BF01645742](https://doi.org/10.1007/BF01645742).
- [3] S. W. Hawking, *Particle Creation by Black Holes*, Commun. Math. Phys. **43**, 199 (1975), doi:[10.1007/BF02345020](https://doi.org/10.1007/BF02345020), [Erratum: Commun.Math.Phys. 46, 206 (1976)].
- [4] A. Strominger and C. Vafa, *Microscopic origin of the Bekenstein-Hawking entropy*, Phys. Lett. B **379**, 99 (1996), doi:[10.1016/0370-2693\(96\)00345-0](https://doi.org/10.1016/0370-2693(96)00345-0), [hep-th/9601029](https://arxiv.org/abs/hep-th/9601029).
- [5] A. Sen, *Extremal black holes and elementary string states*, Mod. Phys. Lett. A **10**, 2081 (1995), doi:[10.1142/S0217732395002234](https://doi.org/10.1142/S0217732395002234), [hep-th/9504147](https://arxiv.org/abs/hep-th/9504147).
- [6] A. Strominger, *Black hole entropy from near horizon microstates*, JHEP **02**, 009 (1998), doi:[10.1088/1126-6708/1998/02/009](https://doi.org/10.1088/1126-6708/1998/02/009), [hep-th/9712251](https://arxiv.org/abs/hep-th/9712251).
- [7] J. M. Maldacena, *The Large N limit of superconformal field theories and supergravity*, Adv. Theor. Math. Phys. **2**, 231 (1998), doi:[10.4310/ATMP1998.v2.n2.a1](https://doi.org/10.4310/ATMP1998.v2.n2.a1), [hep-th/9711200](https://arxiv.org/abs/hep-th/9711200).
- [8] S. S. Gubser, I. R. Klebanov and A. M. Polyakov, *Gauge theory correlators from noncritical string theory*, Phys. Lett. B **428**, 105 (1998), doi:[10.1016/S0370-2693\(98\)00377-3](https://doi.org/10.1016/S0370-2693(98)00377-3), [hep-th/9802109](https://arxiv.org/abs/hep-th/9802109).
- [9] E. Witten, *Anti-de Sitter space and holography*, Adv. Theor. Math. Phys. **2**, 253 (1998), doi:[10.4310/ATMP1998.v2.n2.a2](https://doi.org/10.4310/ATMP1998.v2.n2.a2), [hep-th/9802150](https://arxiv.org/abs/hep-th/9802150).
- [10] S. Ryu and T. Takayanagi, *Holographic derivation of entanglement entropy from AdS/CFT*, Phys. Rev. Lett. **96**, 181602 (2006), doi:[10.1103/PhysRevLett.96.181602](https://doi.org/10.1103/PhysRevLett.96.181602), [hep-th/0603001](https://arxiv.org/abs/hep-th/0603001).
- [11] S. Ryu and T. Takayanagi, *Aspects of Holographic Entanglement Entropy*, JHEP **08**, 045 (2006), doi:[10.1088/1126-6708/2006/08/045](https://doi.org/10.1088/1126-6708/2006/08/045), [hep-th/0605073](https://arxiv.org/abs/hep-th/0605073).
- [12] V. E. Hubeny, M. Rangamani and T. Takayanagi, *A Covariant holographic entanglement entropy proposal*, JHEP **07**, 062 (2007), doi:[10.1088/1126-6708/2007/07/062](https://doi.org/10.1088/1126-6708/2007/07/062), [0705.0016](https://arxiv.org/abs/0705.0016).
- [13] H. Casini, M. Huerta and R. C. Myers, *Towards a derivation of holographic entanglement entropy*, JHEP **05**, 036 (2011), doi:[10.1007/JHEP05\(2011\)036](https://doi.org/10.1007/JHEP05(2011)036), [1102.0440](https://arxiv.org/abs/1102.0440).
- [14] A. Castro, D. M. Hofman and N. Iqbal, *Entanglement Entropy in Warped Conformal Field Theories*, JHEP **02**, 033 (2016), doi:[10.1007/JHEP02\(2016\)033](https://doi.org/10.1007/JHEP02(2016)033), [1511.00707](https://arxiv.org/abs/1511.00707).
- [15] W. Song, Q. Wen and J. Xu, *Modifications to Holographic Entanglement Entropy in Warped CFT*, JHEP **02**, 067 (2017), doi:[10.1007/JHEP02\(2017\)067](https://doi.org/10.1007/JHEP02(2017)067), [1610.00727](https://arxiv.org/abs/1610.00727).
- [16] H. Jiang, W. Song and Q. Wen, *Entanglement Entropy in Flat Holography*, JHEP **07**, 142 (2017), doi:[10.1007/JHEP07\(2017\)142](https://doi.org/10.1007/JHEP07(2017)142), [1706.07552](https://arxiv.org/abs/1706.07552).
- [17] A. Lewkowycz and J. Maldacena, *Generalized gravitational entropy*, JHEP **08**, 090 (2013), doi:[10.1007/JHEP08\(2013\)090](https://doi.org/10.1007/JHEP08(2013)090), [1304.4926](https://arxiv.org/abs/1304.4926).

- [18] A. Castro and M. J. Rodriguez, *Universal properties and the first law of black hole inner mechanics*, Phys. Rev. D **86**, 024008 (2012), doi:[10.1103/PhysRevD.86.024008](https://doi.org/10.1103/PhysRevD.86.024008), [1204.1284](#).
- [19] M. Cvetič and F. Larsen, *Grey body factors for rotating black holes in four-dimensions*, Nucl. Phys. B **506**, 107 (1997), doi:[10.1016/S0550-3213\(97\)00541-5](https://doi.org/10.1016/S0550-3213(97)00541-5), [hep-th/9706071](#).
- [20] M. Cvetič and F. Larsen, *General rotating black holes in string theory: Grey body factors and event horizons*, Phys. Rev. D **56**, 4994 (1997), doi:[10.1103/PhysRevD.56.4994](https://doi.org/10.1103/PhysRevD.56.4994), [hep-th/9705192](#).
- [21] M. Cvetič, G. W. Gibbons and C. N. Pope, *Universal Area Product Formulae for Rotating and Charged Black Holes in Four and Higher Dimensions*, Phys. Rev. Lett. **106**, 121301 (2011), doi:[10.1103/PhysRevLett.106.121301](https://doi.org/10.1103/PhysRevLett.106.121301), [1011.0008](#).
- [22] A. Castro and F. Larsen, *Near Extremal Kerr Entropy from AdS(2) Quantum Gravity*, JHEP **12**, 037 (2009), doi:[10.1088/1126-6708/2009/12/037](https://doi.org/10.1088/1126-6708/2009/12/037), [0908.1121](#).
- [23] M. Ansorg and J. Hennig, *The Inner Cauchy horizon of axisymmetric and stationary black holes with surrounding matter*, Class. Quant. Grav. **25**, 222001 (2008), doi:[10.1088/0264-9381/25/22/222001](https://doi.org/10.1088/0264-9381/25/22/222001), [0810.3998](#).
- [24] M. Ansorg and J. Hennig, *The Inner Cauchy horizon of axisymmetric and stationary black holes with surrounding matter in Einstein-Maxwell theory*, Phys. Rev. Lett. **102**, 221102 (2009), doi:[10.1103/PhysRevLett.102.221102](https://doi.org/10.1103/PhysRevLett.102.221102), [0903.5405](#).
- [25] S. Detournay, *Inner Mechanics of 3d Black Holes*, Phys. Rev. Lett. **109**, 031101 (2012), doi:[10.1103/PhysRevLett.109.031101](https://doi.org/10.1103/PhysRevLett.109.031101), [1204.6088](#).
- [26] S. Deser, R. Jackiw and S. Templeton, *Topologically Massive Gauge Theories*, Annals Phys. **140**, 372 (1982), doi:[10.1016/0003-4916\(82\)90164-6](https://doi.org/10.1016/0003-4916(82)90164-6), [Erratum: Annals Phys. **185**, 406 (1988)].
- [27] S. Deser, R. Jackiw and S. Templeton, *Three-Dimensional Massive Gauge Theories*, Phys. Rev. Lett. **48**, 975 (1982), doi:[10.1103/PhysRevLett.48.975](https://doi.org/10.1103/PhysRevLett.48.975).
- [28] S. N. Solodukhin, *Holography with gravitational Chern-Simons*, Phys. Rev. D **74**, 024015 (2006), doi:[10.1103/PhysRevD.74.024015](https://doi.org/10.1103/PhysRevD.74.024015), [hep-th/0509148](#).
- [29] M.-I. Park, *BTZ black hole with gravitational Chern-Simons: Thermodynamics and statistical entropy*, Phys. Rev. D **77**, 026011 (2008), doi:[10.1103/PhysRevD.77.026011](https://doi.org/10.1103/PhysRevD.77.026011), [hep-th/0608165](#).
- [30] B. Sahoo and A. Sen, *BTZ black hole with Chern-Simons and higher derivative terms*, JHEP **07**, 008 (2006), doi:[10.1088/1126-6708/2006/07/008](https://doi.org/10.1088/1126-6708/2006/07/008), [hep-th/0601228](#).
- [31] Y. Tachikawa, *Black hole entropy in the presence of Chern-Simons terms*, Class. Quant. Grav. **24**, 737 (2007), doi:[10.1088/0264-9381/24/3/014](https://doi.org/10.1088/0264-9381/24/3/014), [hep-th/0611141](#).
- [32] A. Bagchi, *Correspondence between asymptotically flat spacetimes and non-relativistic conformal field theories*, Phys. Rev. Lett. **105**, 171601 (2010), doi:[10.1103/PhysRevLett.105.171601](https://doi.org/10.1103/PhysRevLett.105.171601).
- [33] A. Bagchi and R. Fareghbal, *BMS/GCA Redux: Towards Flatspace Holography from Non-Relativistic Symmetries*, JHEP **10**, 092 (2012), doi:[10.1007/JHEP10\(2012\)092](https://doi.org/10.1007/JHEP10(2012)092), [1203.5795](#).

- [34] A. Bagchi, S. Detournay, R. Fareghbal and J. Simón, *Holography of 3D Flat Cosmological Horizons*, Phys. Rev. Lett. **110**(14), 141302 (2013), doi:[10.1103/PhysRevLett.110.141302](https://doi.org/10.1103/PhysRevLett.110.141302), [1208.4372](https://arxiv.org/abs/1208.4372).
- [35] G. Barnich, *Entropy of three-dimensional asymptotically flat cosmological solutions*, JHEP **10**, 095 (2012), doi:[10.1007/JHEP10\(2012\)095](https://doi.org/10.1007/JHEP10(2012)095), [1208.4371](https://arxiv.org/abs/1208.4371).
- [36] A. Bagchi, R. Basu, D. Grumiller and M. Riegler, *Entanglement entropy in Galilean conformal field theories and flat holography*, Phys. Rev. Lett. **114**(11), 111602 (2015), doi:[10.1103/PhysRevLett.114.111602](https://doi.org/10.1103/PhysRevLett.114.111602), [1410.4089](https://arxiv.org/abs/1410.4089).
- [37] K. Doi, J. Harper, A. Mollabashi, T. Takayanagi and Y. Taki, *Timelike entanglement entropy*, JHEP **05**, 052 (2023), doi:[10.1007/JHEP05\(2023\)052](https://doi.org/10.1007/JHEP05(2023)052), [2302.11695](https://arxiv.org/abs/2302.11695).
- [38] K. Doi, J. Harper, A. Mollabashi, T. Takayanagi and Y. Taki, *Pseudoentropy in dS/CFT and Timelike Entanglement Entropy*, Phys. Rev. Lett. **130**(3), 031601 (2023), doi:[10.1103/PhysRevLett.130.031601](https://doi.org/10.1103/PhysRevLett.130.031601), [2210.09457](https://arxiv.org/abs/2210.09457).
- [39] D. G. Boulware and S. Deser, *String Generated Gravity Models*, Phys. Rev. Lett. **55**, 2656 (1985), doi:[10.1103/PhysRevLett.55.2656](https://doi.org/10.1103/PhysRevLett.55.2656).
- [40] A. Castro, S. Detournay, N. Iqbal and E. Perlmutter, *Holographic entanglement entropy and gravitational anomalies*, JHEP **07**, 114 (2014), doi:[10.1007/JHEP07\(2014\)114](https://doi.org/10.1007/JHEP07(2014)114), [1405.2792](https://arxiv.org/abs/1405.2792).
- [41] Q. Wen and H. Zhong, *Covariant entanglement wedge cross-section, balanced partial entanglement and gravitational anomalies*, SciPost Physics **13**(3), 056 (2022), doi:[10.21468/SciPostPhys.13.3.056](https://doi.org/10.21468/SciPostPhys.13.3.056), [2205.10858](https://arxiv.org/abs/2205.10858).
- [42] Q. Wen, *Towards the generalized gravitational entropy for spacetimes with non-Lorentz invariant duals*, JHEP **01**, 220 (2019), doi:[10.1007/JHEP01\(2019\)220](https://doi.org/10.1007/JHEP01(2019)220), [1810.11756](https://arxiv.org/abs/1810.11756).
- [43] L. Apolo, H. Jiang, W. Song and Y. Zhong, *Swing surfaces and holographic entanglement beyond AdS/CFT*, JHEP **12**, 064 (2020), doi:[10.1007/JHEP12\(2020\)064](https://doi.org/10.1007/JHEP12(2020)064), [2006.10740](https://arxiv.org/abs/2006.10740).
- [44] J. L. Cardy, *Operator Content of Two-Dimensional Conformally Invariant Theories*, Nucl. Phys. B **270**, 186 (1986), doi:[10.1016/0550-3213\(86\)90552-3](https://doi.org/10.1016/0550-3213(86)90552-3).
- [45] T. Hartman, C. A. Keller and B. Stoica, *Universal Spectrum of 2d Conformal Field Theory in the Large c Limit*, JHEP **09**, 118 (2014), doi:[10.1007/JHEP09\(2014\)118](https://doi.org/10.1007/JHEP09(2014)118), [1405.5137](https://arxiv.org/abs/1405.5137).
- [46] Q. Wen, *Fine structure in holographic entanglement and entanglement contour*, Phys. Rev. D **98**(10), 106004 (2018), doi:[10.1103/PhysRevD.98.106004](https://doi.org/10.1103/PhysRevD.98.106004), [1803.05552](https://arxiv.org/abs/1803.05552).
- [47] B. Czech, J. L. Karczmarek, F. Nogueira and M. Van Raamsdonk, *The Gravity Dual of a Density Matrix*, Class. Quant. Grav. **29**, 155009 (2012), doi:[10.1088/0264-9381/29/15/155009](https://doi.org/10.1088/0264-9381/29/15/155009), [1204.1330](https://arxiv.org/abs/1204.1330).
- [48] Z. Li, Z.-Q. Xiao and R.-Q. Yang, *On holographic time-like entanglement entropy*, JHEP **04**, 004 (2023), doi:[10.1007/JHEP04\(2023\)004](https://doi.org/10.1007/JHEP04(2023)004), [2211.14883](https://arxiv.org/abs/2211.14883).
- [49] M. Afrasiar, J. K. Basak and D. Giataganas, *Timelike entanglement entropy and phase transitions in non-conformal theories*, JHEP **07**, 243 (2024), doi:[10.1007/JHEP07\(2024\)243](https://doi.org/10.1007/JHEP07(2024)243), [2404.01393](https://arxiv.org/abs/2404.01393).
- [50] M. P. Heller, F. Ori and A. Serantes, *Geometric interpretation of timelike entanglement entropy* (2024), [2408.15752](https://arxiv.org/abs/2408.15752).

- [51] G. Vidal and Y. Chen, *Entanglement contour*, J. Stat. Mech. **2014**(10), P10011 (2014), doi:[10.1088/1742-5468/2014/10/P10011](https://doi.org/10.1088/1742-5468/2014/10/P10011), [1406.1471](https://arxiv.org/abs/1406.1471).
- [52] Q. Wen, *Formulas for Partial Entanglement Entropy*, Phys. Rev. Res. **2**(2), 023170 (2020), doi:[10.1103/PhysRevResearch.2.023170](https://doi.org/10.1103/PhysRevResearch.2.023170), [1910.10978](https://arxiv.org/abs/1910.10978).
- [53] Q. Wen, *Entanglement contour and modular flow from subset entanglement entropies*, JHEP **05**, 018 (2020), doi:[10.1007/JHEP05\(2020\)018](https://doi.org/10.1007/JHEP05(2020)018), [1902.06905](https://arxiv.org/abs/1902.06905).
- [54] M. Han and Q. Wen, *Entanglement entropy from entanglement contour: higher dimensions*, SciPost Phys. Core **5**, 020 (2022), doi:[10.21468/SciPostPhysCore.5.2.020](https://doi.org/10.21468/SciPostPhysCore.5.2.020), [1905.05522](https://arxiv.org/abs/1905.05522).
- [55] M. Han and Q. Wen, *First law and quantum correction for holographic entanglement contour*, SciPost Physics **11**(3), 058 (2021), doi:[10.21468/SciPostPhys.11.3.058](https://doi.org/10.21468/SciPostPhys.11.3.058), [2106.12397](https://arxiv.org/abs/2106.12397).
- [56] J. Kudler-Flam, I. MacCormack and S. Ryu, *Holographic entanglement contour, bit threads, and the entanglement tsunami*, Journal of Physics A Mathematical General **52**(32), 325401 (2019), doi:[10.1088/1751-8121/ab2dae](https://doi.org/10.1088/1751-8121/ab2dae), [1902.04654](https://arxiv.org/abs/1902.04654).
- [57] D. Basu, J. Lin, Y. Lu and Q. Wen, *Ownerless island and partial entanglement entropy in island phases*, SciPost Physics **15**(6), 227 (2023), doi:[10.21468/SciPostPhys.15.6.227](https://doi.org/10.21468/SciPostPhys.15.6.227), [2305.04259](https://arxiv.org/abs/2305.04259).
- [58] A. Rolph, *Local measures of entanglement in black holes and CFTs*, SciPost Physics **12**(3), 079 (2022), doi:[10.21468/SciPostPhys.12.3.079](https://doi.org/10.21468/SciPostPhys.12.3.079), [2107.11385](https://arxiv.org/abs/2107.11385).
- [59] Y.-Y. Lin, J.-R. Sun, Y. Sun and J.-C. Jin, *The PEE aspects of entanglement islands from bit threads*, JHEP **07**, 009 (2022), doi:[10.1007/JHEP07\(2022\)009](https://doi.org/10.1007/JHEP07(2022)009), [2203.03111](https://arxiv.org/abs/2203.03111).
- [60] Y.-Y. Lin, *Distilled density matrices of holographic partial entanglement entropy from thread-state correspondence*, Phys. Rev. D **108**(10), 106010 (2023), doi:[10.1103/PhysRevD.108.106010](https://doi.org/10.1103/PhysRevD.108.106010), [2305.02895](https://arxiv.org/abs/2305.02895).
- [61] Q. Wen, *Balanced Partial Entanglement and the Entanglement Wedge Cross Section*, JHEP **04**, 301 (2021), doi:[10.1007/JHEP04\(2021\)301](https://doi.org/10.1007/JHEP04(2021)301), [2103.00415](https://arxiv.org/abs/2103.00415).
- [62] H. A. Camargo, P. Nandy, Q. Wen and H. Zhong, *Balanced partial entanglement and mixed state correlations*, SciPost Physics **12**(4), 137 (2022), doi:[10.21468/SciPostPhys.12.4.137](https://doi.org/10.21468/SciPostPhys.12.4.137), [2201.13362](https://arxiv.org/abs/2201.13362).
- [63] D. S. Ageev, *Shaping contours of entanglement islands in BCFT*, JHEP **03**, 033 (2022), doi:[10.1007/JHEP03\(2022\)033](https://doi.org/10.1007/JHEP03(2022)033), [2107.09083](https://arxiv.org/abs/2107.09083).
- [64] Q. Wen, M. Xu and H. Zhong, *Partial entanglement entropy threads in island phase* (2024), [2408.13535](https://arxiv.org/abs/2408.13535).
- [65] A. Chandra, Z. Li and Q. Wen, *Entanglement islands and cutoff branes from path-integral optimization*, JHEP **07**, 069 (2024), doi:[10.1007/JHEP07\(2024\)069](https://doi.org/10.1007/JHEP07(2024)069), [2402.15836](https://arxiv.org/abs/2402.15836).
- [66] J. Lin, Y. Lu, Q. Wen and Y. Zhong, *Weaving the (AdS) spaces with partial entanglement entropy threads* (2024), [2401.07471](https://arxiv.org/abs/2401.07471).
- [67] J. Lin, Y. Lu and Q. Wen, *Cutoff brane vs the Karch-Randall brane: the fluctuating case*, JHEP **06**, 017 (2024), doi:[10.1007/JHEP06\(2024\)017](https://doi.org/10.1007/JHEP06(2024)017), [2312.03531](https://arxiv.org/abs/2312.03531).

- [68] J. Lin, Y. Lu and Q. Wen, *Geometrizing the partial entanglement entropy: from PEE threads to bit threads*, JHEP **2024**(02), 191 (2024), doi:[10.1007/JHEP02\(2024\)191](https://doi.org/10.1007/JHEP02(2024)191), [2311.02301](https://arxiv.org/abs/2311.02301).
- [69] J. Kudler-Flam, H. Shapourian and S. Ryu, *The negativity contour: a quasi-local measure of entanglement for mixed states*, SciPost Physics **8**(4), 063 (2020), doi:[10.21468/SciPostPhys.8.4.063](https://doi.org/10.21468/SciPostPhys.8.4.063), [1908.07540](https://arxiv.org/abs/1908.07540).
- [70] L. Alvarez-Gaume and E. Witten, *Gravitational Anomalies*, Nucl. Phys. B **234**, 269 (1984), doi:[10.1016/0550-3213\(84\)90066-X](https://doi.org/10.1016/0550-3213(84)90066-X).
- [71] S. Deser, R. Jackiw and S. Templeton, *Topologically massive gauge theories*, Annals of Physics **140**(2), 372 (1982), doi:[https://doi.org/10.1016/0003-4916\(82\)90164-6](https://doi.org/10.1016/0003-4916(82)90164-6).
- [72] P. Kraus and F. Larsen, *Holographic gravitational anomalies*, JHEP **01**, 022 (2006), doi:[10.1088/1126-6708/2006/01/022](https://doi.org/10.1088/1126-6708/2006/01/022), [hep-th/0508218](https://arxiv.org/abs/hep-th/0508218).
- [73] K. A. Moussa, G. Clement and C. Leygnac, *The Black holes of topologically massive gravity*, Class. Quant. Grav. **20**, L277 (2003), doi:[10.1088/0264-9381/20/24/L01](https://doi.org/10.1088/0264-9381/20/24/L01), [gr-qc/0303042](https://arxiv.org/abs/gr-qc/0303042).
- [74] R. M. Wald, *Black hole entropy is the Noether charge*, Phys. Rev. D **48**(8), R3427 (1993), doi:[10.1103/PhysRevD.48.R3427](https://doi.org/10.1103/PhysRevD.48.R3427), [gr-qc/9307038](https://arxiv.org/abs/gr-qc/9307038).
- [75] T. Jacobson, G. Kang and R. C. Myers, *On black hole entropy*, Phys. Rev. D **49**, 6587 (1994), doi:[10.1103/PhysRevD.49.6587](https://doi.org/10.1103/PhysRevD.49.6587), [gr-qc/9312023](https://arxiv.org/abs/gr-qc/9312023).
- [76] V. Iyer and R. M. Wald, *Some properties of Noether charge and a proposal for dynamical black hole entropy*, Phys. Rev. D **50**, 846 (1994), doi:[10.1103/PhysRevD.50.846](https://doi.org/10.1103/PhysRevD.50.846), [gr-qc/9403028](https://arxiv.org/abs/gr-qc/9403028).
- [77] H. Jiang, *Anomalous Gravitation and its Positivity from Entanglement*, JHEP **10**, 283 (2019), doi:[10.1007/JHEP10\(2019\)283](https://doi.org/10.1007/JHEP10(2019)283), [1906.04142](https://arxiv.org/abs/1906.04142).
- [78] B. Gao and J. Xu, *Holographic entanglement entropy in AdS₃/WCFT*, Phys. Lett. B **822**, 136647 (2021), doi:[10.1016/j.physletb.2021.136647](https://doi.org/10.1016/j.physletb.2021.136647), [1912.00562](https://arxiv.org/abs/1912.00562).
- [79] L. Cheng, L.-Y. Hung, S.-N. Liu and H.-Z. Zhou, *First law of entanglement entropy in topologically massive gravity*, Phys. Rev. D **94**(6), 064063 (2016), doi:[10.1103/PhysRevD.94.064063](https://doi.org/10.1103/PhysRevD.94.064063), [1511.03844](https://arxiv.org/abs/1511.03844).
- [80] D. Basu, *Balanced Partial Entanglement in Flat Holography* (2022), [2203.05491](https://arxiv.org/abs/2203.05491).
- [81] S. Dutta and T. Faulkner, *A canonical purification for the entanglement wedge cross-section*, JHEP **03**, 178 (2021), doi:[10.1007/JHEP03\(2021\)178](https://doi.org/10.1007/JHEP03(2021)178), [1905.00577](https://arxiv.org/abs/1905.00577).
- [82] D. Basu, H. Parihar, V. Raj and G. Sengupta, *Entanglement negativity, reflected entropy, and anomalous gravitation*, Phys. Rev. D **105**(8), 086013 (2022), doi:[10.1103/PhysRevD.105.086013](https://doi.org/10.1103/PhysRevD.105.086013), [Erratum: Phys.Rev.D 105, 129902 (2022)], [2202.00683](https://arxiv.org/abs/2202.00683).
- [83] X.-S. Wang and J.-q. Wu, *An observable in Classical Pure AdS₃ Gravity: the twist along a geodesic*, JHEP **05**, 111 (2024), doi:[10.1007/JHEP05\(2024\)111](https://doi.org/10.1007/JHEP05(2024)111), [2312.10751](https://arxiv.org/abs/2312.10751).
- [84] T. Anegawa and K. Tamaoka, *Black hole singularity and timelike entanglement*, JHEP **10**, 182 (2024), doi:[10.1007/JHEP10\(2024\)182](https://doi.org/10.1007/JHEP10(2024)182), [2406.10968](https://arxiv.org/abs/2406.10968).

- [85] M. Nath, S. Sahoo and D. Sarkar, *Revisiting subregion holography using OPE blocks* (2024), [2406.09027](#).
- [86] S. Griener, K. Ikeda and D. E. Kharzeev, *Temporal entanglement entropy as a probe of renormalization group flow*, *JHEP* **05**, 030 (2024), doi:[10.1007/JHEP05\(2024\)030](#), [2312.08534](#).
- [87] A. Das, S. Sachdeva and D. Sarkar, *Bulk reconstruction using timelike entanglement in (A)dS*, *Phys. Rev. D* **109**(6), 066007 (2024), doi:[10.1103/PhysRevD.109.066007](#), [2312.16056](#).
- [88] P. Calabrese and J. L. Cardy, *Entanglement entropy and quantum field theory*, *J. Stat. Mech.* **0406**, P06002 (2004), doi:[10.1088/1742-5468/2004/06/P06002](#), [hep-th/0405152](#).
- [89] P. Calabrese and J. Cardy, *Entanglement entropy and conformal field theory*, *J. Phys. A* **42**, 504005 (2009), doi:[10.1088/1751-8113/42/50/504005](#), [0905.4013](#).
- [90] R. Fareghbal, M. Hakami Shalamzari and P. Karimi, *Flat-space limit of extremal curves*, *Phys. Rev. D* **102**(6), 066002 (2020), doi:[10.1103/PhysRevD.102.066002](#), [2006.16122](#).
- [91] G. Barnich and G. Compere, *Classical central extension for asymptotic symmetries at null infinity in three spacetime dimensions*, *Class. Quant. Grav.* **24**, F15 (2007), doi:[10.1088/0264-9381/24/5/F01](#), [gr-qc/0610130](#).
- [92] A. Ashtekar, J. Bicak and B. G. Schmidt, *Asymptotic structure of symmetry reduced general relativity*, *Phys. Rev. D* **55**, 669 (1997), doi:[10.1103/PhysRevD.55.669](#), [gr-qc/9608042](#).
- [93] G. Barnich and C. Troessaert, *Aspects of the BMS/CFT correspondence*, *JHEP* **05**, 062 (2010), doi:[10.1007/JHEP05\(2010\)062](#), [1001.1541](#).
- [94] R. K. Sachs, *Gravitational waves in general relativity. 8. Waves in asymptotically flat spacetimes*, *Proc. Roy. Soc. Lond. A* **270**, 103 (1962), doi:[10.1098/rspa.1962.0206](#).
- [95] H. Bondi, M. G. J. van der Burg and A. W. K. Metzner, *Gravitational waves in general relativity. 7. Waves from axisymmetric isolated systems*, *Proc. Roy. Soc. Lond. A* **269**, 21 (1962), doi:[10.1098/rspa.1962.0161](#).
- [96] G. Barnich, A. Gomberoff and H. A. Gonzalez, *The Flat limit of three dimensional asymptotically anti-de Sitter spacetimes*, *Phys. Rev. D* **86**, 024020 (2012), doi:[10.1103/PhysRevD.86.024020](#), [1204.3288](#).